2

NASA CR 114310
(Available to the public)

STUDY OF THE EFFECT OF SPACECRAFT WINDOW CONFIGURATION ON LINES OF SIGHT

By David M. Kelley

JANUARY 1971

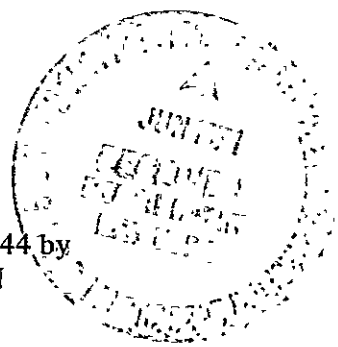

Prepared under Contract No. NAS2-5044 by
PHILCO-FORD CORPORATION
WDL DIVISION
For
NATIONAL AERONAUTICS AND SPACE ADMINISTRATION
AMES RESEARCH CENTER
MOFFETT FIELD, CALIFORNIA

NASA CR 114310
(Available to the public)

STUDY OF THE EFFECT OF SPACECRAFT WINDOW CONFIGURATION ON LINES OF SIGHT

By David M. Kelley

JANUARY 1971

Prepared Under Contract No. NAS2-5044
by
PHILCO-FORD CORPORATION
WESTERN DEVELOPMENT LABORATORIES DIVISION
for
NATIONAL AERONAUTICS AND SPACE ADMINISTRATION
AMES RESEARCH CENTER
MOFFETT FIELD, CALIFORNIA

FOREWORD

This report was prepared by Philco-Ford, Western Development Laboratories' personnel, under NASA Contract No. NAS2-5044. Work was administered under the direction of the Manned Systems Research Branch, Ames Research Center, Moffett Field, California. The Technical Monitor for the contract was Mr. Kenneth C. White.

This report covers work conducted between June 1968 and January 1971. The manuscript was released by the author for publication as a NASA technical report in January 1971.

ABSTRACT

This report describes the results of a study of pressure deformations of spacecraft windows and the angular line-of-sight deviations of light rays passing through the windows which result from these deformations. The results of a computer survey of line-of-sight deviations associated with various design parameters are presented. Information on the retrieval of the design data from microfilms and computer tapes is given.

Window panes are assumed to be originally flat and of uniform thickness. Elliptical, rectangular, and trapezoidal window planforms are considered. Window deformations due to uniform pressure loadings are summarized for clamped and simply supported edge conditions. Rays entering at mesh points of a one-inch grid on the undeformed window surface are traced and line-of-sight deviations are calculated for elliptical, rectangular, and trapezoidal planforms. Plots of mean and root mean square deviations of light rays for various incidence angles and incidence planes are included.

This document reports contours of window deformations (constant deflection and constant maximum slope) for circular, square, and trapezoidal planforms as well as contour plots of constant line-of-sight deviations.

Studies of single-pane configuration light ray deviations are presented. These studies show the effects of varying the pane shape, pressure differential, dimensional scale, pane thickness, edge support condition and incidence angle. Results of the studies indicate that small pressure differentials, small dimensional scales, large pane

thicknesses, clamped edge conditions, and low incidence angles all result in smaller LOS deviations. The trapezoid is the best planform shape for the single-pane configurations.

Studies of double-pane configuration light ray deviations are also presented. These studies show the effects of varying the pane shape, pressure environment, pane spacing, edge support conditions, incidence angle, and the theory used in prediction of deformations. Results of these studies indicate the pressure environment, pane spacing, and edge support conditions giving the smallest LOS deviations for the circle and square are different than those for the trapezoid. Low incidence angles result in better characteristics for all configurations. Considering large deflection effects results in smaller deviations while including shear deformations has no significant effect. The circle has the best characteristics of double-pane configurations.

TABLE OF CONTENTS

LIST OF ILLUSTRATIONS

LIST OF ILLUSTRATIONS (Cont'd)

LIST OF ILLUSTRATIONS (Cont'd)

LIST OF ILLUSTRATIONS (Cont'd)

LIST OF ILLUSTRATIONS (Cont'd)

LIST OF TABLES

Section 1

INTRODUCTION

Celestial navigation sightings taken through spacecraft windows deformed by pressure differentials are subject to errors. One source of these errors is window induced line-of-sight deviations caused by window deformations. The purpose of this study is to provide the pressure deformation characteristics and line-of-sight deviations for a variety of window shapes and loadings. The data are intended to assist in developing and evaluating various window designs by defining the magnitudes of the line-of-sight errors associated with window deformations.

This study involves the analytical determination of spacecraft window surface deformations and line-of-sight deviations due to in-flight pressure environments for eight different window planforms with clamped or simply supported edge conditions. Both single and double pane window configurations are analyzed. Planform geometry, number of panes, pane thickness and spacing, pressure differentials, and edge fixity are parametric variables in the study.

Section 2 of this document describes the technical approach to development of the design data. It defines the problem, the assumptions employed, the method of solution, and the analysis plan. The third section summarizes the design data obtained. The fourth section presents results of studies of the design data. The last section gives concluding remarks.

Section 2

TECHNICAL APPROACH

The ability to predict the deviations of lines-of-sight regardless of which area of the window surface is used is of primary importance in correcting observations made through window systems. A good window system (outside of one having no deviations) is the one for which corrections to the line-of-sight observations are small and constant over the surface of the window. Thus, if the deviation values for individual points of the window system differ very little from the mean deviation value (as measured by the rms deviation value) and if the mean deviation value is fairly constant over the surface of the window system, the window can be considered to have good optical qualities when used for navigation sightings.

The analyses to determine window deformations and line-of-sight deviations are performed for a variety of window configurations, pressure differentials, and line-of-sight orientations. It is assumed that the surfaces of the glass panes are flat and parallel prior to imposing pressure differentials. The window glass for all configurations is Corning Glass, Code Number 7940, fused silica.

The windows of this study involve eight planforms: three elliptical, three rectangular, and two trapezoidal. The planforms are shown in Figure 1. Hereafter, individual planforms will be referenced by their respective titles in this figure (e.g., circle a, trapezoid g, etc.).

The numerical results required are the information to determine surface deformations and deviations of the rays traced through the glass and pressure media. The deformation quantities required at specified

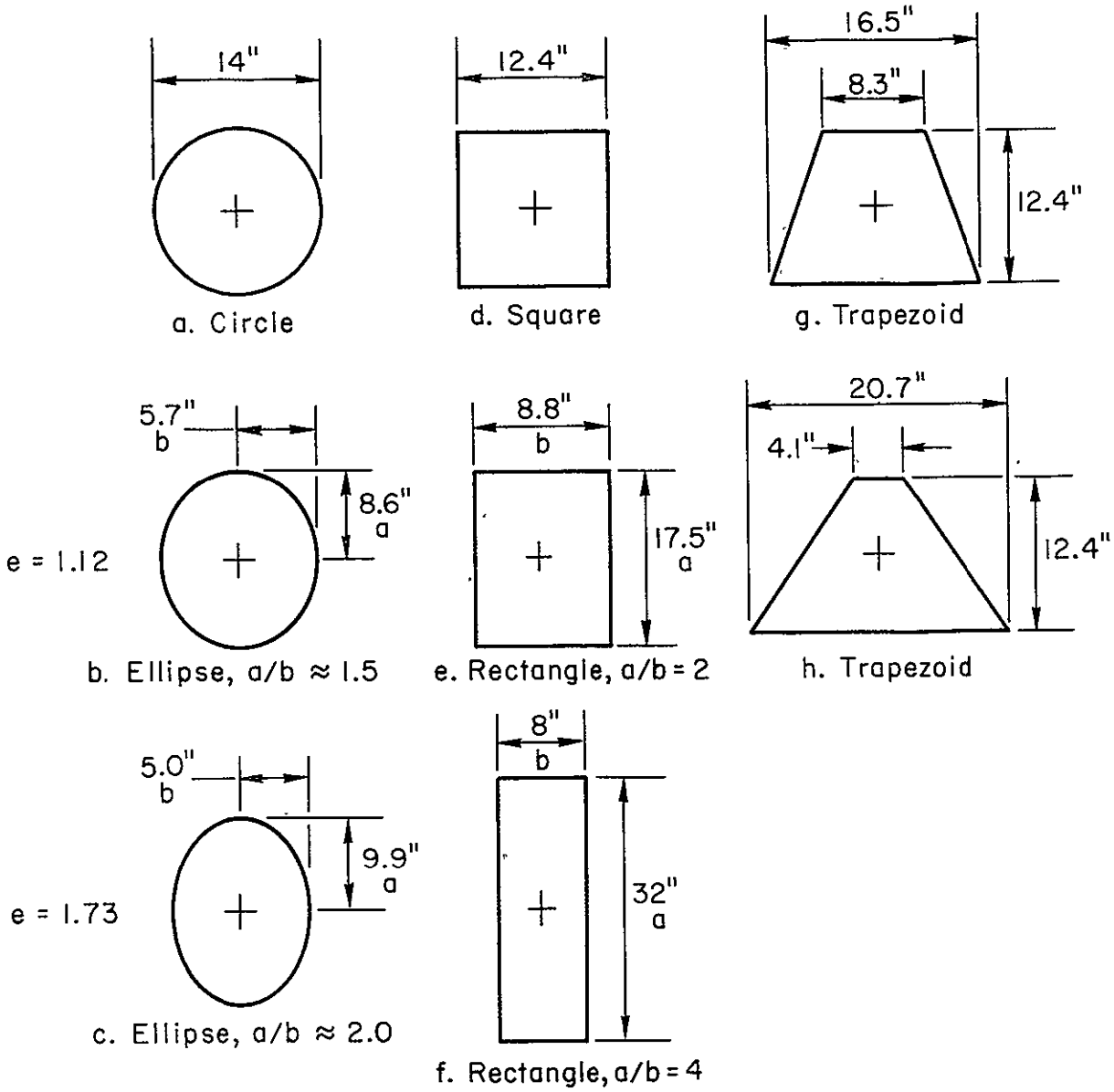

Figure 1. Window Planforms Investigated

locations on the window surface are defined in Figure 2. These quantities are the displacement, ΔZ, and the components of the slope in the XZ and YZ planes, the angles γ_{XZ} and γ_{YZ} respectively. These quantities are developed using two computer programs. Small deflection deformations for the elliptical and rectangular planforms are calculated by exact solutions employing thin plate theory and using the computer program described in Ref. 1. This computer program also quantifies the large deflections and shear deformations of rectangular plates using approximate solutions. Deformations for trapezoidal shapes are found using the Structural Analysis and Matrix Interpretative System (SAMIS).[2,3,4]* SAMIS employs the finite element approach in obtaining solutions.

As rays of light pass through the pane(s) of glass and the surrounding media, they are refracted. The amount of refraction is a function of the indices of refraction of the media and the incidence angle of the ray in each media interface. White and Gradeberg[5,6] give the details of the equations necessary to determine the path of the refracted light ray. Exact solutions of these equations are obtained by tracing the ray geometry through the window system. These equations are particularized and solved by the computer program as described in Ref. 1.

The ray trace data required of this study consist of identifying the position and orientation of the incident ray, the location of the exiting (deviated) ray, the difference in the orientation of the incident and deviated rays, the angle, Θ , between these two rays, and the orthogonal components of the angle between the two rays.

* Numbers in parentheses indicate references at end of report.

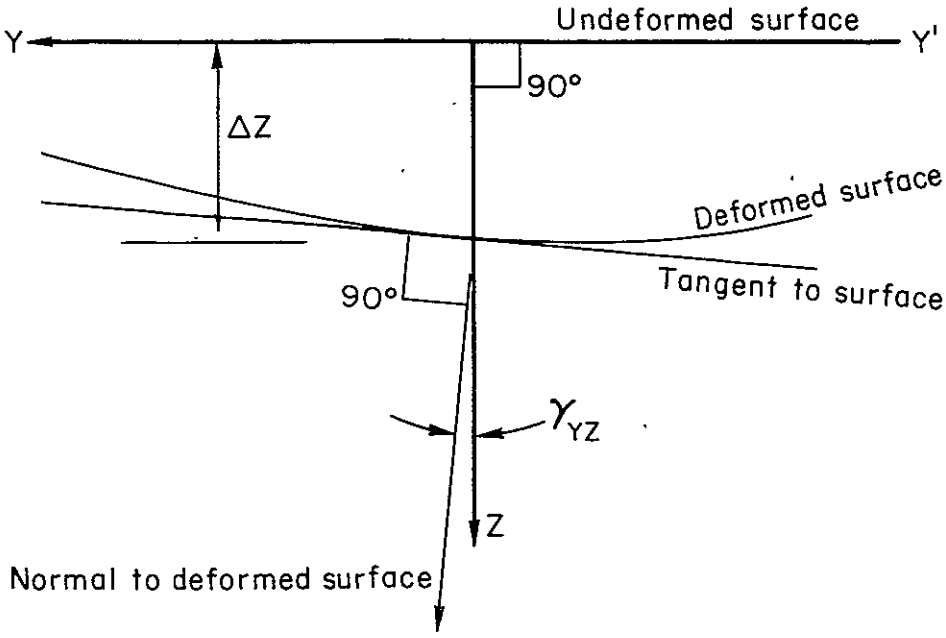

(a) Sketch of deformed surface in YZ plane

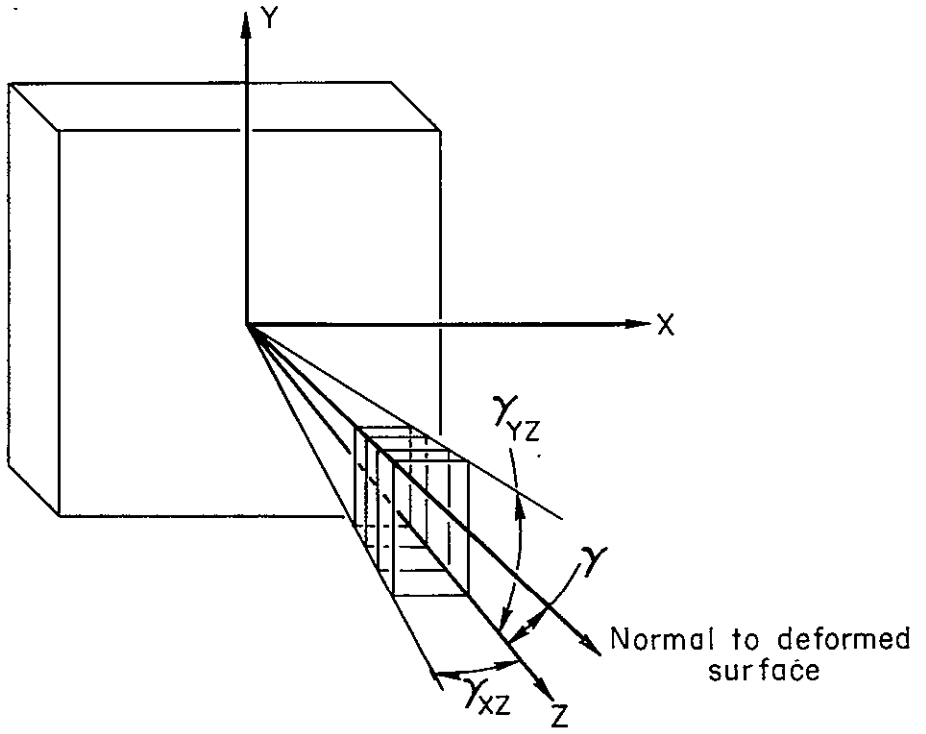

(b) Sketch showing angular components defining slope of deformed surface

Figure 2. Definition and Orientation of Surface Deformation Quantities

Two groups of window configurations are examined in the study. The first group consists of single-pane window configurations. The second group consists of double-pane window configurations.

Each configuration of both groups is analyzed for line-of-sight deviation due to refraction. The incidence angles, incidence planes, and locations on the interior surface of the window configuration are specified in the following paragraphs.

(1) In Figure 3, the orientation of the plane of incidence and the angle of incidence is shown. Each ray is traced for six incidence angles (0°, 15°, 30°, 45°, 60°, and 75°) in each of eight planes of incidence (0°, 45°, 90°, 135°, 180°, 225°, 270°, and 315°).

(2) Line-of-sight deviations are determined for light rays incident on the interior window surface at the intersections of a one-inch grid network parallel to the X and Y axes of Figure 3.

For both groups of window configurations, surface deformations and line-of-sight deviations are obtained for two window frame edge conditions: clamped and simply supported. The clamped edge condition assumes the window frame has no distortion due to the pressure differential and the slope of the glass surface at the window frame edge is unchanged from its original undeformed value. The simply supported edge condition simulates support of the window pane by a knife edge which permits rotation but no lateral deflection due to the pressure differential. Thus, the slope of the glass pane at the edge is a function of the structural characteristics of the glass and the pressure loading. When analyzing the double-pane configurations, the edge condition is the same for both panes.

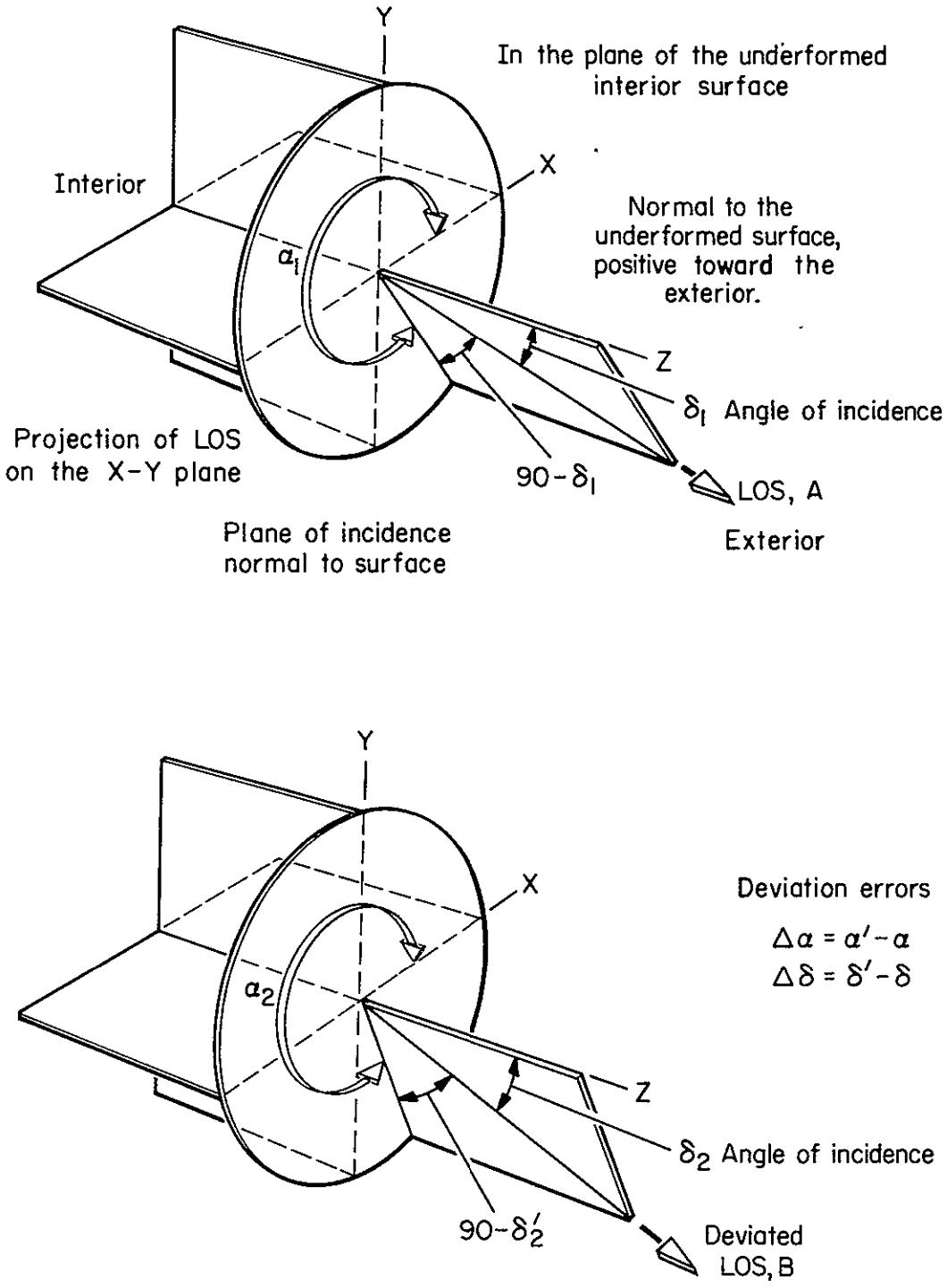

Figure 3. Lines-of-Sight and Axes Orientations

Table 1 summarizes the parameters for the single-pane configuration group. Each planform in a set of brackets of the first column of the table is analyzed for every combination of parameters in the brackets on the same line of the table. Thus, each planform from the first set of brackets is analyzed in 6 configurations; those from the second and third set of brackets in 12 configurations. Therefore, there are a total of 120 configurations in the group of single-pane window configurations. The values in the column labeled "Dimensional Scales" are the factors by which the dimensions of the planforms of Figure 1 are multiplied to change the size of the window planform. For each of these configurations, the surface deformations and line-of-sight deviations are determined.

Figure 4 shows the arrangement of the glass panes in the group of double-pane window configurations. This group of configurations introduces the pane spacing dimension, W, as a design parameter. Study of the double-pane window systems also includes evaluation of the effect of changes of the theory used to predict deformation.

Table 2 summarizes the study parameters for the double-pane configurations. These configurations are analyzed for an interior pressure, P_1, of 5.2 psia and exterior pressure, P_3, of zero psia. The interstitial pressure, P_2, is specified in the table. Surface deformations and line-of-sight deviations are determined for each of the 180 configurations involving double-pane windows.

In addition to the above, analyses are made on single-pane window configurations of circle a, square d, and trapezoid g (of Fig. 1), with pane thicknesses of 0.3 inch. This yields data for constant maximum slope contour plots. Analyses are also made on double-pane configurations

Table 1

Single-Pane Configurations

Planforms	Dimensional Scales	Pane Thicknesses	Edge Conditions	Pressure Differentials	Total Number of Configurations
8 { Circle a; Ellipses b, c; Square d; Rectangles e, f; Trapezoids g, h }	1 { 1.0 }	1 { .3" }	2 { Clamped; Simply Supported }	3 { ΔP = 5 psia; ΔP = 10 psia; ΔP = 15 psia }	48
3 { Circle a; Square d; Trapezoid g }	2 { .75; 1.5 }	1 { .3" }	2 { Clamped; Simply Supported }	3 { ΔP = 5 psia; ΔP = 10 psia; ΔP = 15 psia }	36
3 { Circle a; Square d; Trapezoid g }	1 { 1.0 }	2 { .6"; 1.2" }	2 { Clamped; Simply Supported }	3 { ΔP = 5 psia; ΔP = 10 psia; ΔP = 15 psia }	36

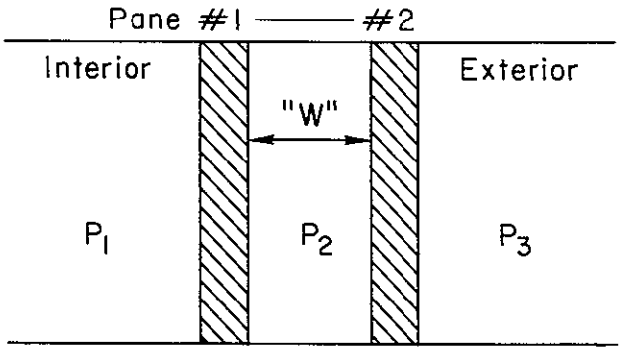

Figure 4. Schematic Sketch of Double-Pane Configuration

Table 2

Double-Pane Configurations

Planforms	Dimensional Scales	Pane Thicknesses	Pane Spacings	Edge Conditions	Pressure Environment	Deformation Theory	Total Number of Configurations
3 { Circle a, Square d, Trapezoid g }	1 { 1.0 }	1 { .3" }	4 { .25", .5", 1.0", 2.0" }	2 { Clamped, Simply Supported }	3 { P_2 = 7.5 psia, P_2 = 10 psia, P_2 = 15 psia }	Small	72
3 { Square d, Rectangle e, Rectangle f }	3 { .75, 1.0, 1.5 }	1 { .3" }	1 { 1.0" }	2 { Clamped, Simply Supported }	3 { P_2 = 7.5 psia, P_2 = 10 psia, P_2 = 15 psia }	Large	54
3 { Square d, Rectangle e, Rectangle f }	1 { 1.0 }	3 { .3", .6", 1.2" }	1 { 1.0" }	2 { Clamped, Simply Supported }	3 { P_2 = 7.5 psia, P_2 = 10 psia, P_2 = 15 psia }	Shear	54

of square d and rectangles e and f for small deflection theory. These data are used for comparison with large deflection and shear deformation data.

Section 3

DATA SUMMARY

The data obtained from the analyses described in the previous section are divided into two categories: pressure deformations and line-of-sight deviations. Pressure deformation data are developed to provide information on the deformed window for determining the line-of-sight deviations. The line-of-sight deviations are classified by the number of panes as single-pane or double-pane configuration deviations. There are a total of 300 different configurations: 120 single-pane and 180 double-pane.

The line-of-sight deviations generated by the ray trace analyses of the window configurations described amount to a vast accumulation of data. There are from 25 to 175 points on the interior window surface of each configuration for which line-of-sight deviations are determined. Since there are 300 configurations and each ray is traced for six incidence angles and eight orientations of the incidence plane, the data for approximately 1.5 million ray traces are generated.

The resulting data are stored on computer magnetic tape and on microfilm cartridges. Each of the configurations is assigned an identifying "retrieval number." The number appears in the upper left-hand corner of each frame of microfilm and at appropriate locations on the computer tape to enable retrieval of the data. Table 3 shows the retrieval number assignment, the microfilm cartridge number, and the computer magnetic tape number for the window configurations of this study. For completeness, the table also contains a breakdown of the parameters of the study.

Table 3

Configuration Analyses Performed

Retrival Number	Planform	Dimensional Scale	Number of Panes	Pane Thickness	Pane Spacing	Edge Fixity	Pressure Environment	Deformation Theory	Microfilm Cartridge Number	Computer Magnetic Tape Number
1-6	Ellipse b	1.0	1	.3	NA	Both	5,10,15	Small	003	00053
7-12	Ellipse c	1.0	1	.3	NA	Both	5,10,15	Small	003	00053
13-18	Rectangle e	1.0	1	.3	NA	Both	5,10,15	Small	003	00053
19-24	Rectangle f	1.0	1	.3	NA	Both	5,10,15	Small	004	01584
25-30	Trapezoid h	1.0	1	.3	NA	Both	5,10,15	Small	004	01584
31-48	Circle a	.75,1.0,1.5	1	.3	NA	Both	5,10,15	Small	005	00091
49-66	Square d	.75,1.0,1.5	1	.3	NA	Both	5,10,15	Small	006	01583
67-84	Trapezoid g	.75,1.0,1.5	1	.3	NA	Both	5,10,15	Small	007-008	03414
85-90	Circle a	1.0	1	.6	NA	Both	5,10,15	Small	009	02369
91-96	Square d	1.0	1	.6	NA	Both	5,10,15	Small	009	02369
97-102	Trapezoid g	1.0	1	.6	NA	Both	5,10,15	Small	010	01584
103-108	Circle a	1.0	1	1.2	NA	Both	5,10,15	Small	009	02369
109-114	Square d	1.0	1	1.2	NA	Both	5,10,15	Small	009	02369
115-120	Trapezoid g	1.0	1	1.2	NA	Both	5,10,15	Small	010	01584
121-144	Circle a	1.0	2	.3	.25,.5,1.0,2.0	Both	7.5,10,15	Small	011	02711
145-168	Square d	1.0	2	.3	.25,.5,1.0,2.0	Both	7.5,10,15	Small	012	02818
169-192	Trapezoid g	1.0	2	.3	.25,.5,1.0,2.0	Both	7.5,10,15	Small	013-014	03431
193	Circle a	1.0	1	.3	NA	Clamped	10	Max/Min	015	00262
194	Square d	1.0	1	.3	NA	Clamped	10	Max/Min	015	00262
195	Trapezoid g	1.0	1	.3	NA	Clamped	10	Max/Min	015	00262
196-213	Square d	.75,1.0,1.5	2	.3	1.0	Both	7.5,10,15	Large	016-017	14229
214-231	Rectangle e	.75,1.0,1.5	2	.3	1.0	Both	7.5,10,15	Large	018-019	02587
232-249	Rectangle f	.75,1.0,1.5	2	.3	1.0	Both	7.5,10,15	Large	020-021	02571
250-267	Square d	1.0	2	.3,.6,1.2	1.0	Both	7.5,10,15	Shear	022	02723
268-285	Rectangle e	1.0	2	.3,.6,1.2	1.0	Both	7.5,10,15	Shear	023	04010
286-303	Rectangle f	1.0	2	.3,.6,1.2	1.0	Both	7.5,10,15	Shear	024-025	09147
304	Not used									
305	Square d	1.5	2	.3	1.0	Clamped	10	Small	015	00262
306	Rectangle e	1.5	2	.3	1.0	Clamped	10	Small	015	00262
307	Rectangle f	1.5	2	.3	1.0	Clamped	10	Small	015	00262
308	Square d	1.0	2	1.2	1.0	Clamped	10	Small	015	00262
309	Rectangle e	1.0	2	1.2	1.0	Clamped	10	Small	015	00262
310	Rectangle f	1.0	2	1.2	1.0	Clamped	10	Small	015	00262

The mean and root mean square (rms) of the line-of-sight (LOS) deviations for all points on the window surface except those within one inch of the window boundary are also calculated by the computer program of Ref. 1. The mean and rms deviations are obtained for each incidence angle and orientation of the incidence plane (hereafter termed the plane angle). These summation data are used to characterize the optical effects of the various window configurations.

The pressure deformation data for all the configurations are contained on microfilm cartridge number 001. The summation data are contained on cartridge number 002. Neither the pressure deformation data nor the summation data were stored on computer magnetic tape.

The microfilmed data and information on the retrieval of data from the computer tapes are available for review at the NASA Ames Research Center, Moffett Field, California.

Section 4

RESULTS

This section of the report reviews deformation and light ray deviation data from the analyses of selected window configurations. These reviews were performed to evaluate the optical performance of various window configurations as a function of the study variables. The data presented in this section deal primarily with the mean and rms deviation values and how the mean deviation value varies as a function of the plane angle.

More detailed information concerning the line-of-sight deviations of the windows is available in the microfilmed data and the data stored on computer tapes.

In the following subsections, characteristics of the deformations of certain window configurations are presented. Subsequent subsections present parametric studies for the single-pane and the double-pane configurations.

Pressure Deformation Data

The pressure deformation data presented in the first portion of this subsection results from analyses performed on single-pane configurations of circle a, square d, and trapezoid g. In the latter portion, deformation data for double-pane configurations of square d and rectangle f are presented. These data show large deflections and shear deformation effects for the plan forms.

The parameter values used in the single-pane configuration analyses were a pressure differential of 10.0 psia, a dimensional scale of 1.0, a pane thickness of 0.3 inch and clamped edge conditions.

Contours of constant deflection are shown in Figs. 5, 6, and 7 for circle a, square d, and trapezoid g, respectively. Each of these figures demonstrates the regularity of the deflection contours of each of the planforms. Near the center of the planforms, the surface deforms into spherical shape (exactly spherical for circle a). Proceeding outward toward the boundaries, the contours begin to assume the shapes of the boundaries.

To use these data for other pressure loadings and different window parameters, scaling may be used. Thus, to find the magnitude of the deflection for a pressure loading other than 10.0 psia, simply multiply the deflections given by the ratio of the new pressure to 10.0 psia. To determine the deflections for windows of other thicknesses, multiply the given deflections by the cube of the ratio 0.3 to the new thickness measured in inches. To determine the deflections of windows of the same shapes but different sizes multiply the deflections by the fourth power of the ratio of the new size to the current size. To determine the deflections of the windows when the glass has elastic properties different from the fused silica glass, multiply the deflections by the ratio of $10.776 \cdot 10^6$ to $E/(1-\nu^2)$ (where E is Young's modulus of elasticity measured in psi and ν is Poisson's ratio) of the new glass.

More meaningful information to aid in interpreting the line-of-sight deviation data is provided by contours of constant maximum and minimum slopes. Constant maximum slope contours are plotted in Figs. 8, 9, and 10 for the three window shapes. The parameters used in obtaining the data for these figures are the same as for the constant deflection contour plots. The slopes are measured in radians.

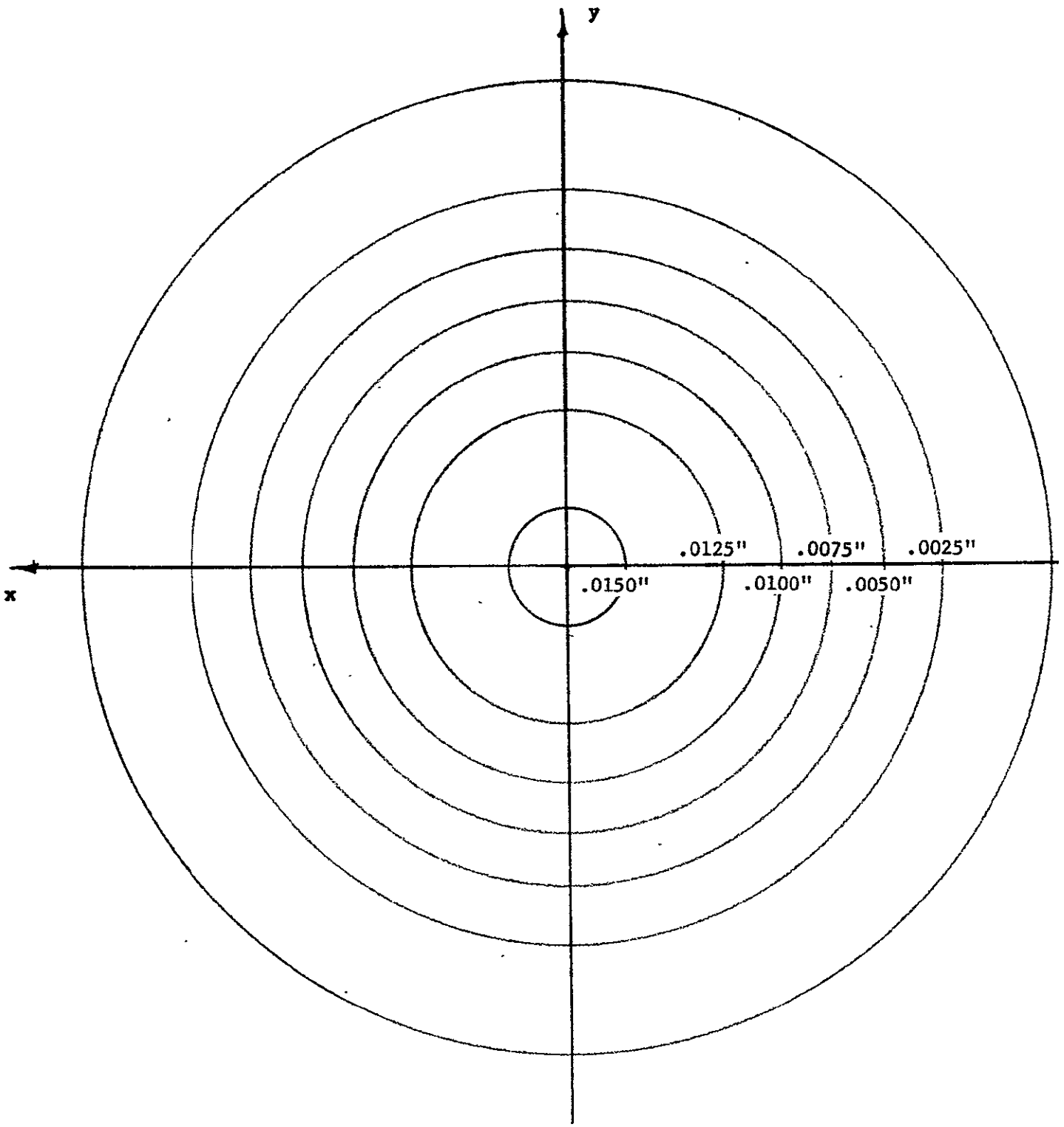

Figure 5. Contours of Constant Deflection - Circle a

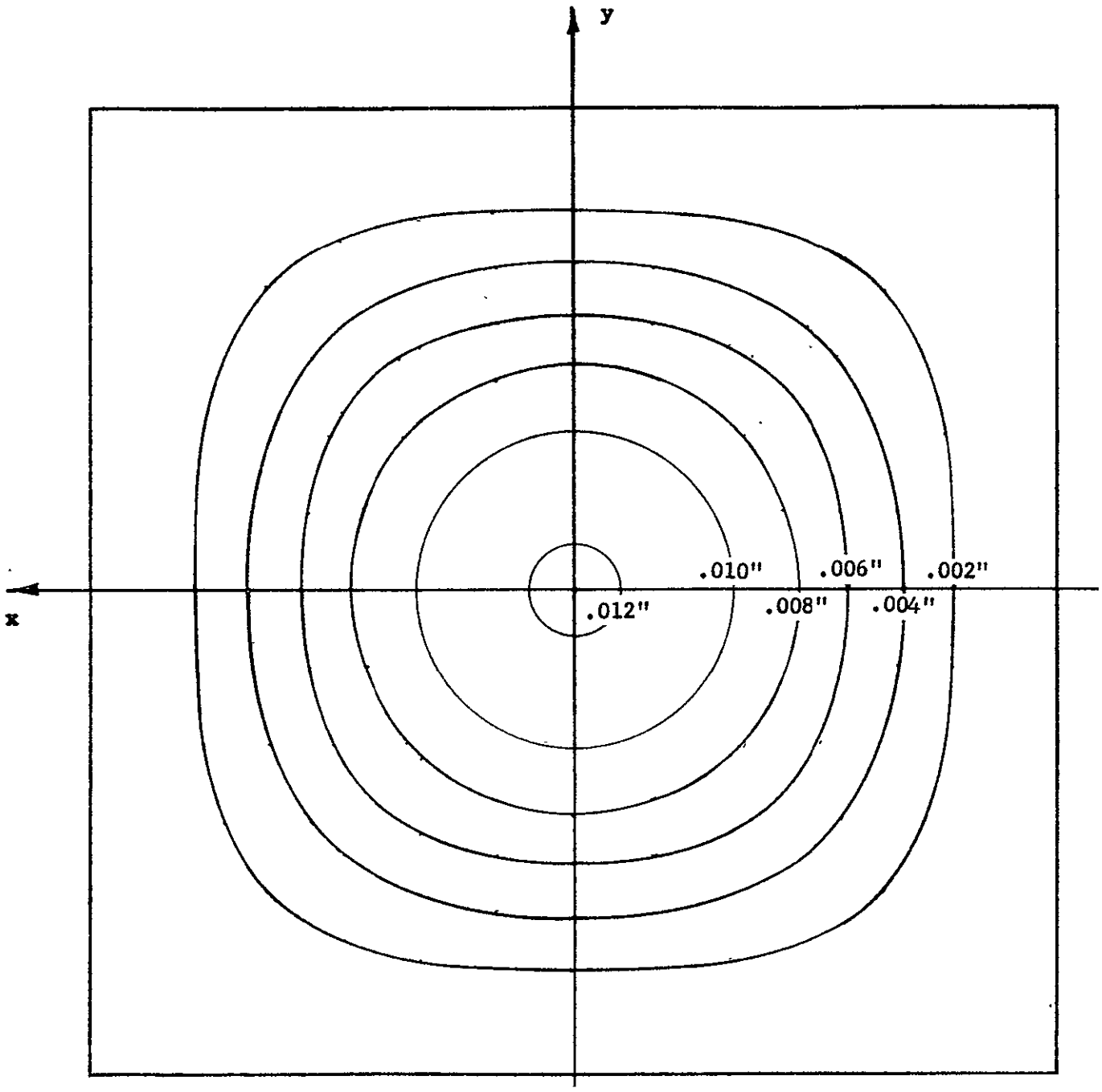

Figure 6. Contours of Constant Deflection - Square d

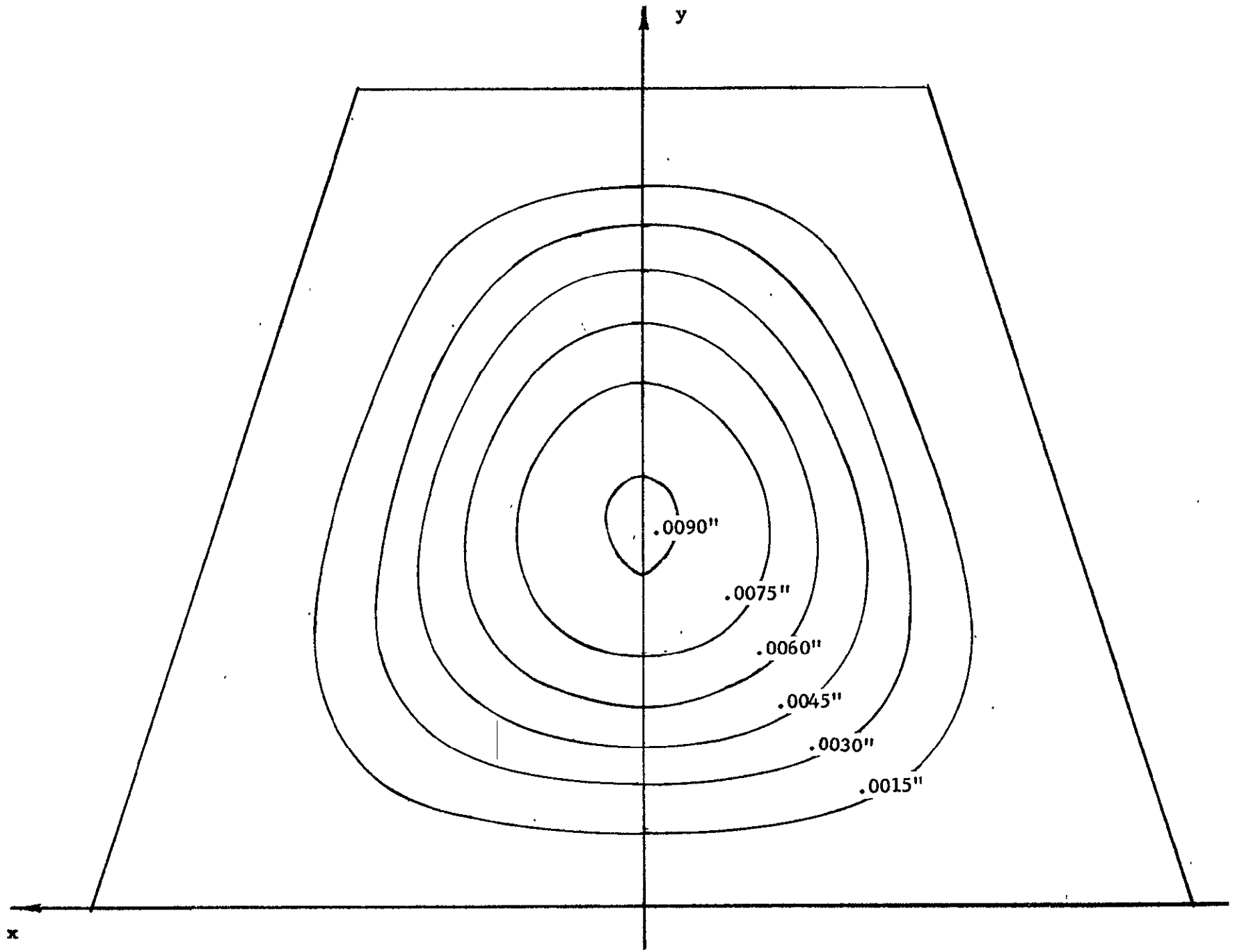

Figure 7. Contours of Constant Deflection - Trapezoid g

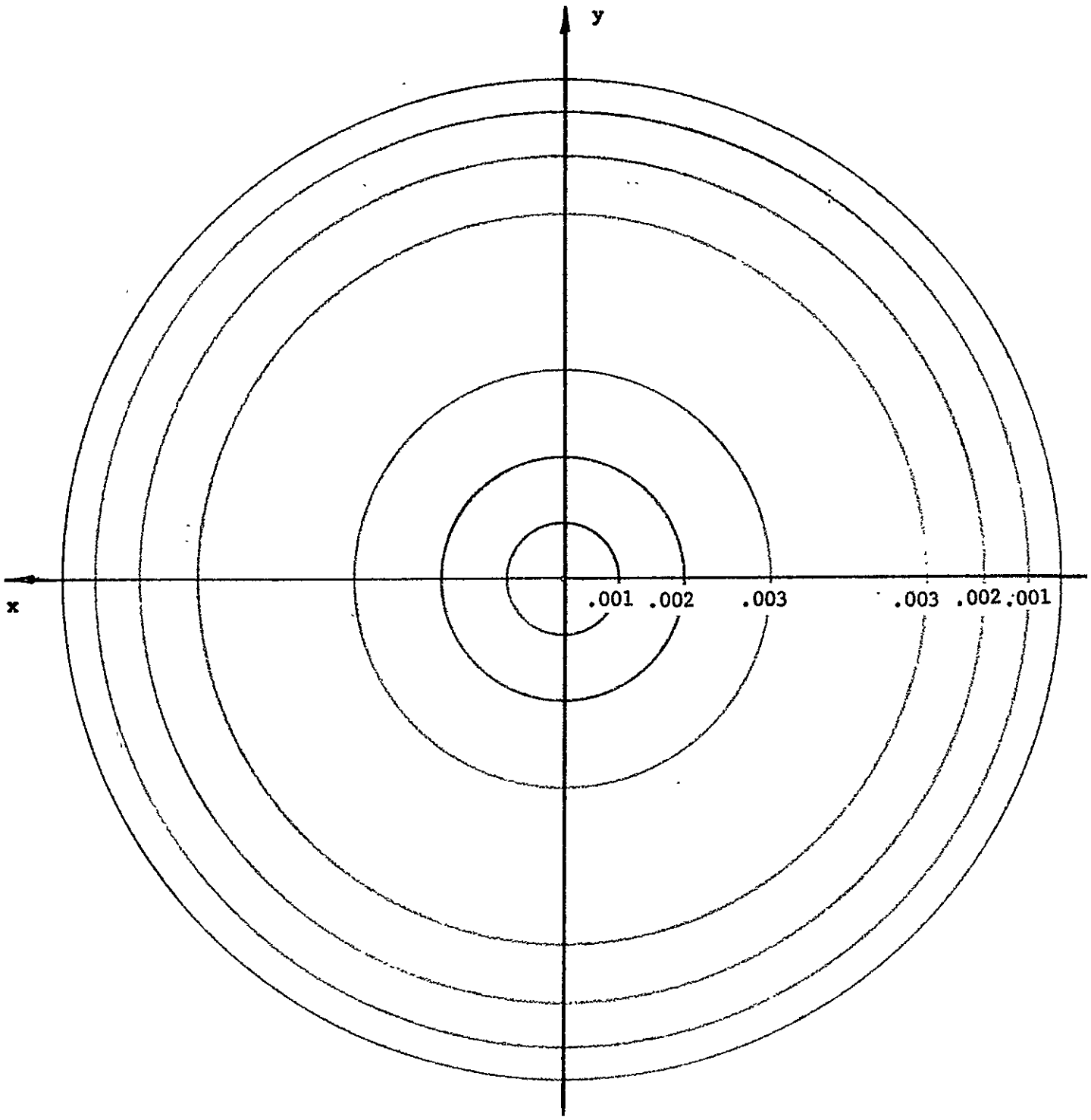

Figure 8. Contours of Constant Maximum Slope - Circle a

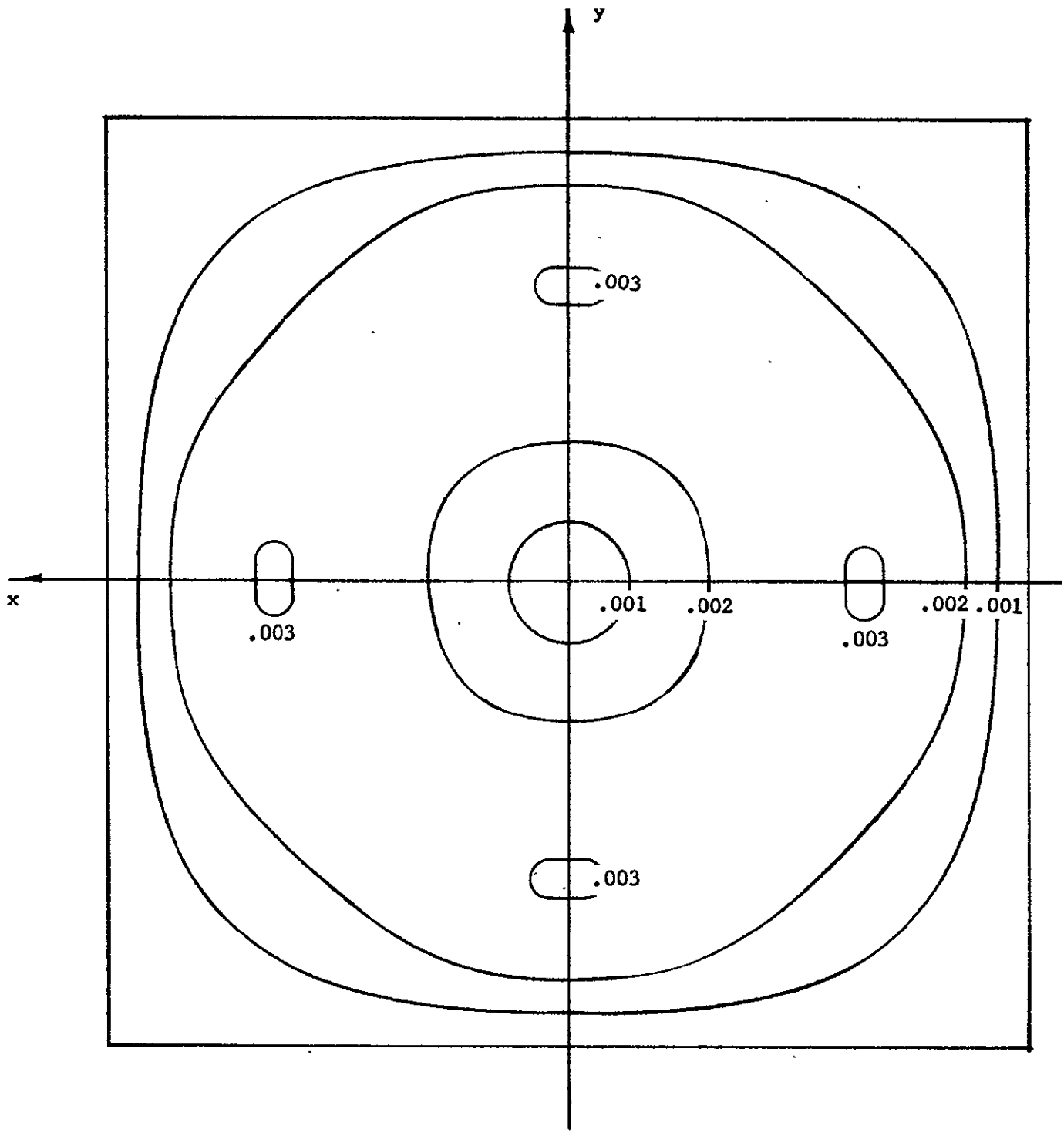

Figure 9. Contours of Constant Maximum Slope - Square d

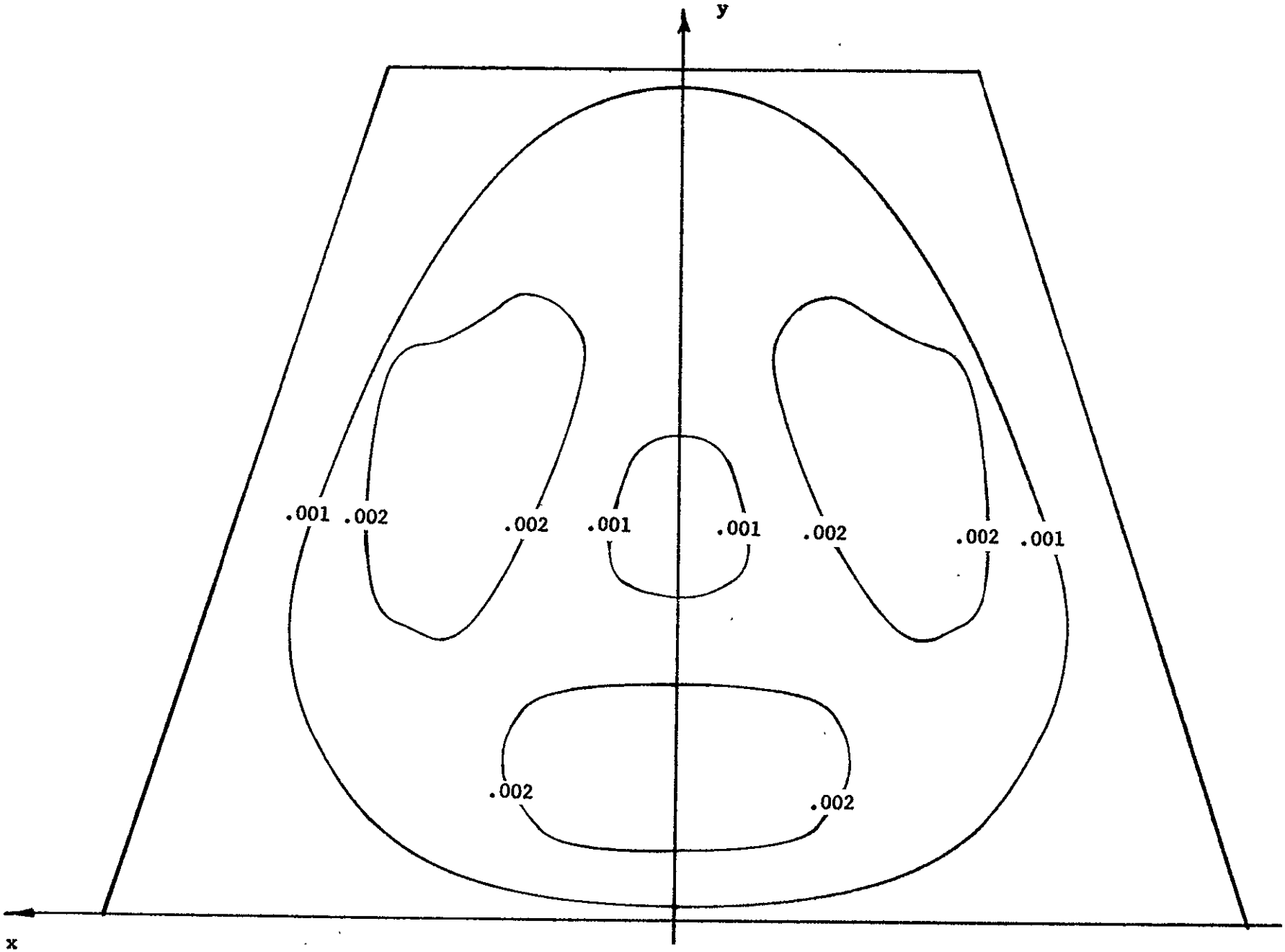

Figure 10. Contours of Constant Maximum Slope - Trapezoid g

The maximum slopes occur at angles orthogonal to the contours of equal deflection (since these are the directions of the largest gradients). The minimum slopes occur at angles orthogonal to the maximum slopes[7] and are thus parallel to the contours of equal deflection. Therefore, the minimum slopes are zero everywhere. Consequently, contours of constant minimum slope are not presented.

Figure 8 indicates that the areas of least maximum slope (and, hence, least LOS deviations) occur near the center and edges of circle a. Figures 9 and 10 indicate similar areas for square d and trapezoid g. The closed contours of Figs. 9 and 10 which do not enclose other contours (or the center) would "grow together" to form two closed contours if the pressure differentials on the window panes were increased.

These last three figures indicate that the areas of smallest angular change (through which sightings can be made) for circle a, square d, and trapezoid g are the areas surrounding the center of the planforms.

Figures 11 and 12 present deflection curves predicted using large deflection theory for square d and rectangle f in double-pane configurations. The values of the parameters used in the analyses were an interior pressure of 5.2 psia, an interstitial pressure of 10.0 psia, an exterior pressure of zero psia, a dimensional scale of 1.5, plane thicknesses of 0.3 inch, a pane separation distance of 1.0 inch, and clamped edge conditions. The deflection curves shown in the figures are those of the outer panes. The deflections are plotted as functions of the x-coordinate for constant values of the y-coordinate. Three such curves are presented in each figure. Both figures indicate

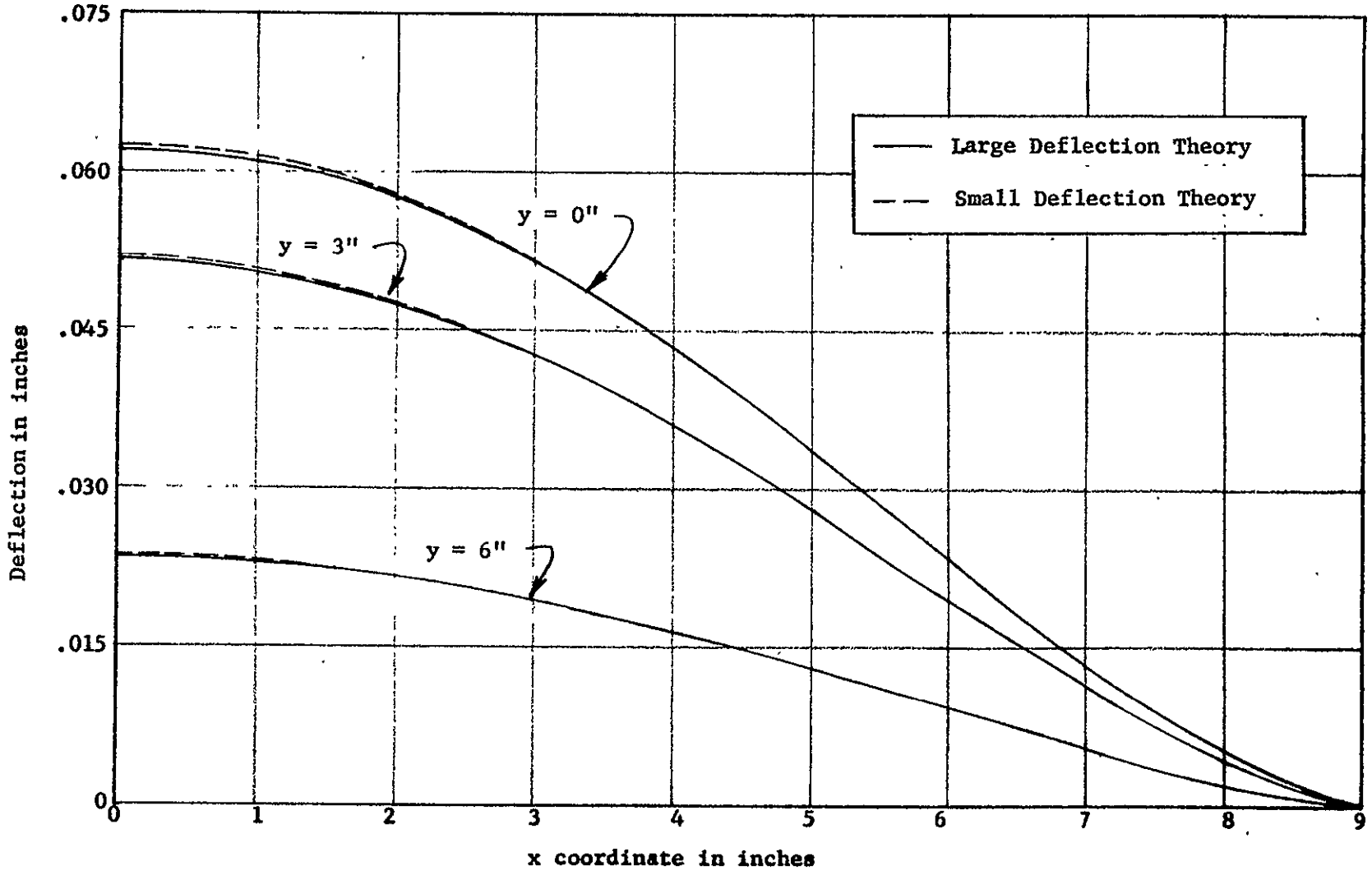

Figure 11. Large Deflection Curves for Square d

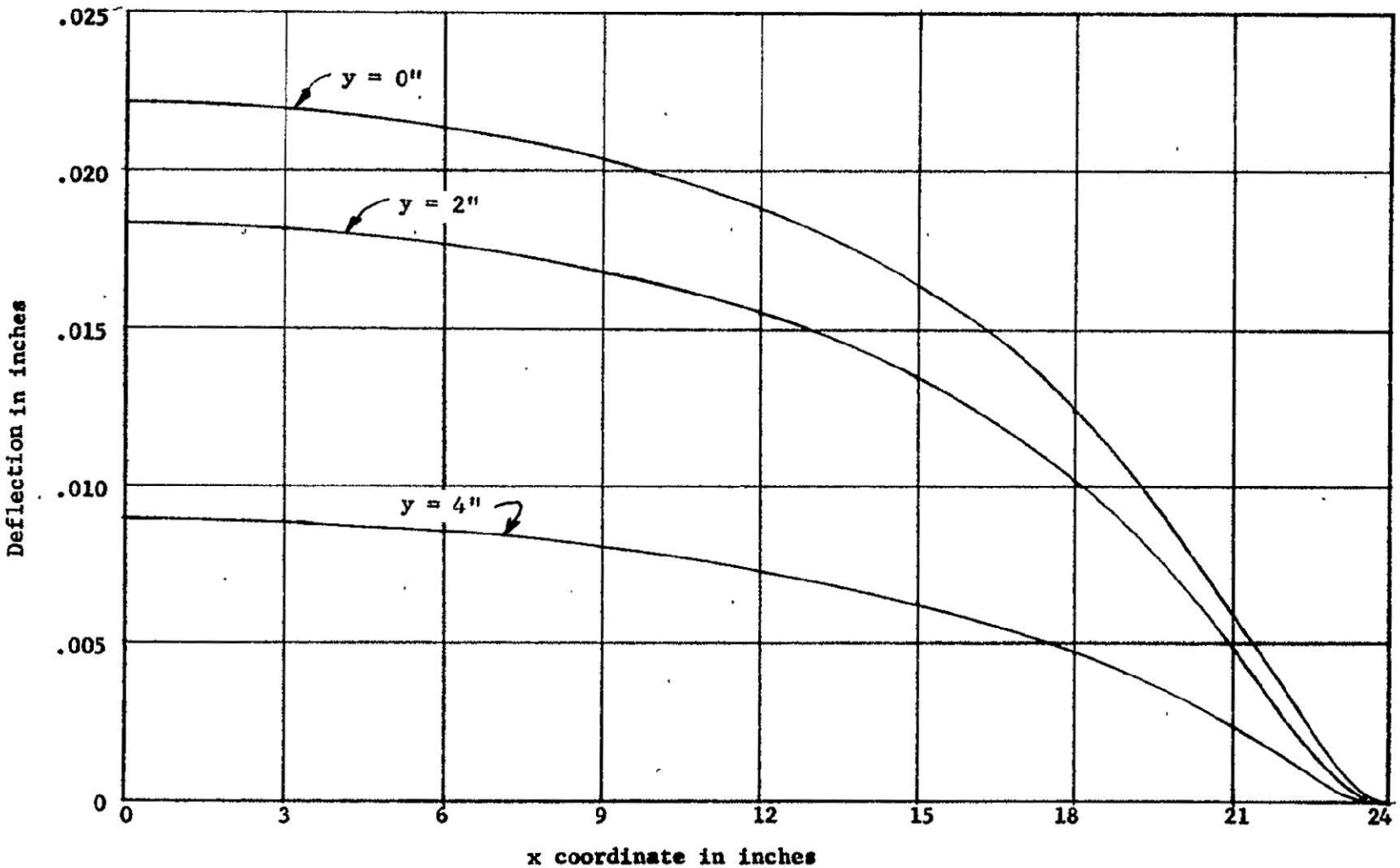

Figure 12. Large Deflection Curves for Rectangle f

that the maximum deflection occurs at the center of the window with a monotonic decrease in magnitude with an increase in either of the two coordinates.

Also plotted on Fig. 11 are the deflection curves obtained using small deflection theory. These curves indicate that the resulting deflections are slightly larger than the deflections obtained using large deflection theory. The difference in the two curves is not very large and can only be observed over the area of largest deflections (due to plotting limitations). Similar results can be anticipated for the deflections of rectangle f.

Figures 13 and 14 present deflection curves predicted taking into account shear deformations for square d and rectangle f in double-pane configurations. The values of the parameters used in the analyses were an interior pressure of 5.2 psia, an interstitial pressure of 10.0 psia, an exterior pressure of zero psia, a dimensional scale of 1.0, pane thicknesses of 1.2 inches, a pane separation distance of 1.0 inch, and clamped edge conditions. The deflection curves shown in the figures are those of the outer panes. The deflections are plotted as functions of the x-coordinate for constant values of the y-coordinate. Three such curves are presented in each figure. Both figures indicate that the maximum deflection occurs at the center of the window with a monotonic decrease in magnitude with an increase in either of the two coordinates.

For these particular configurations, the difference in deflections with and without shear deformations is so small that the two curves coincide when plotted. Thus, it is concluded that the inclusion of

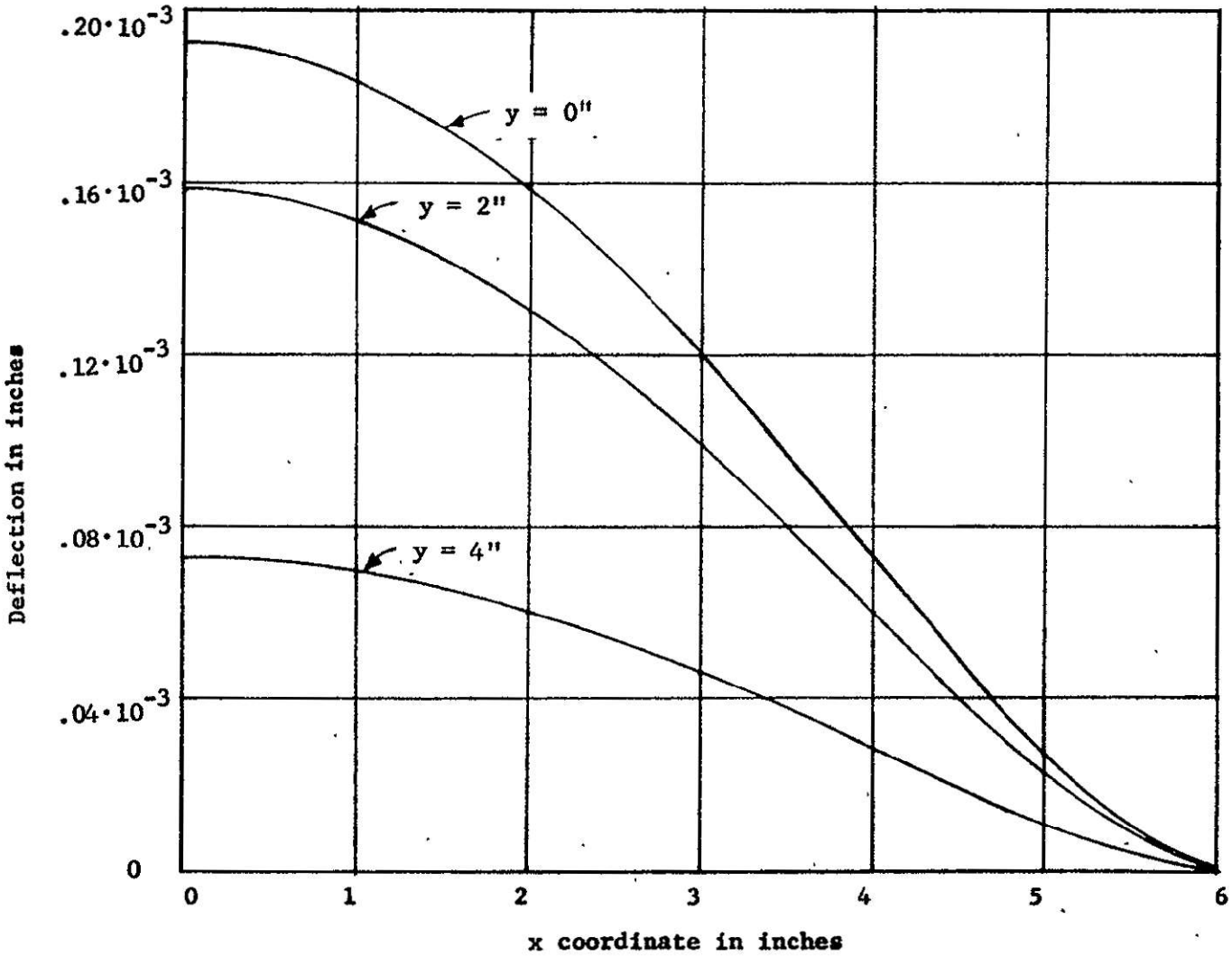

Figure 13. Deformation Curves for Square d with Shear Deformation Included

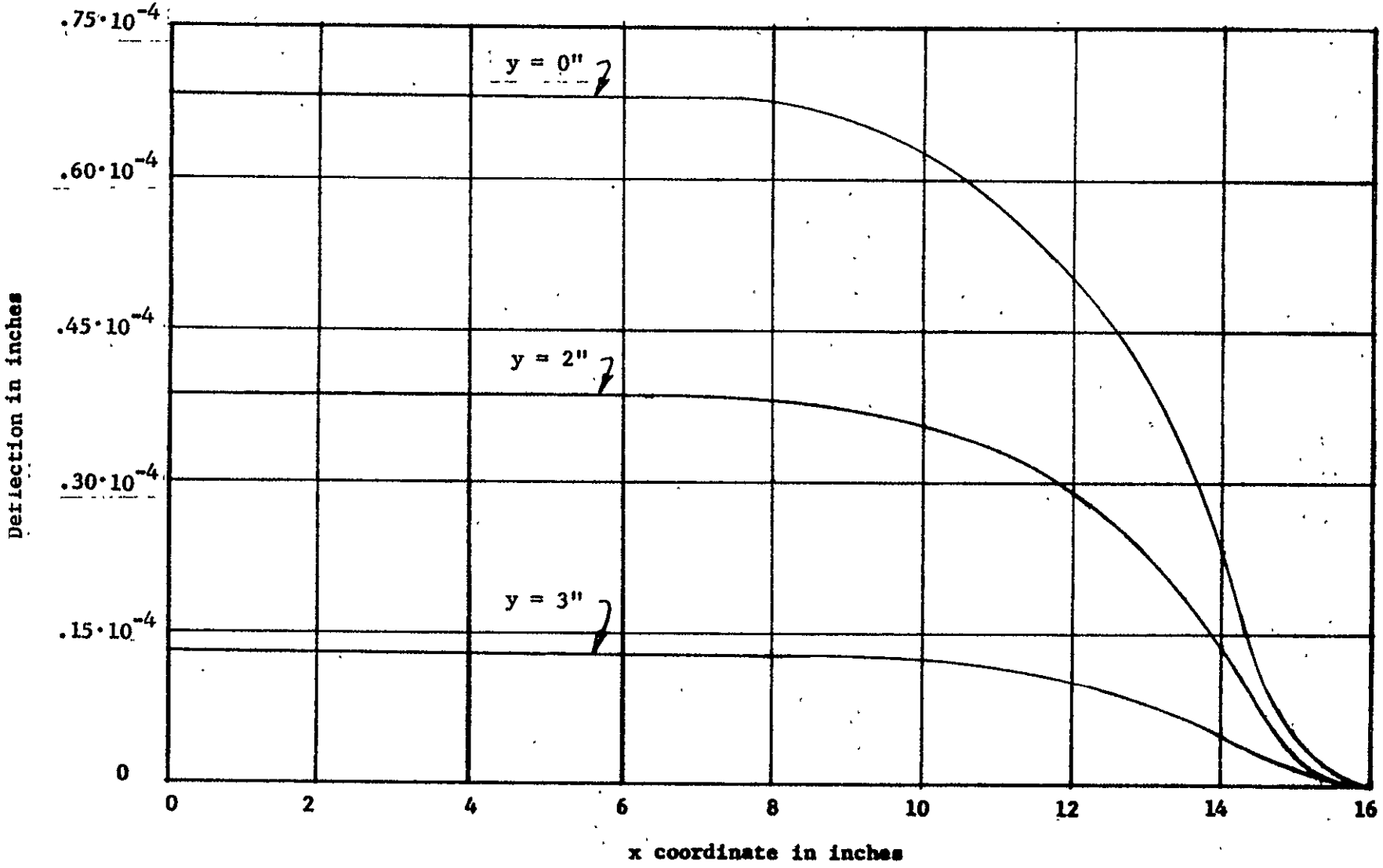

Figure 14. Deformation Curves for Rectangle f with Shear Deformation Included

shear deformation terms in the prediction of deformations has a negligible effect on the magnitude of the deformations.

LOS Deviation Data

Single-Pane Configurations.- The ray trace data in this subsection present the effects of various parameters on LOS deviations. The parameters to be varied are given in Table 1. For a given window planform nominal values of the parameters are a dimensional scale of 1.0, a pane thickness of 0.3 inch, a pressure differential of 10.0 psia, incidence angles of 30° and 60°, and clamped edge conditions.

For each of the parametric studies of single-pane configurations, the data for each parameter are presented in the form of mean and rms deviation curves as a function of the plane angle (i.e., the orientation of the plane in which the incidence angle is measured). These curves are presented for incidence angles of 30° and 60°, except in the study of incidence angle variation. For this study, the curves are presented for incidence angles of 15°, 30°, 45°, 60°, and 75°. In general, these curves are symmetric about either one or three plane angles depending on the number of axes of symmetry in the window planform studied. The curves for elliptical and rectangular planforms are symmetric about plane angles of 90°, 180°, and 270°. Those of the trapezoidal shape are symmetric only about a plane angle of 180°.

In addition, the parameter variations investigated are ranked in three categories: mean deviation values, rms deviation values, and how the mean deviation values vary over the range of plane angles (mean value variation). By summing the rankings in the three categories, an overall measure of the window system's effect on LOS deviations is obtained. Low

values for this window ranking indicate better window systems. Since the rms deviation values and the mean value variation are more important, their rankings are weighted by a factor of two in the sum.

The effect of varying the shape of the window pane in a single-pane configuration is determined by studying the data presented in Figs. 15 through 22. The data resulting from analyses of circle a, square d, and trapezoid g with the nominal parameter values are shown in Figs. 15 and 16. Figures 17 and 18 present the data for similar analyses of circle a and ellipses b and c, Figs. 19 and 20 data for square d and rectangles e and f, and Figs. 21 and 22 data for trapezoids g and h.

The results of studying the curves of these figures are summarized in Table 4. This table gives the rankings for the eight planforms studied. This table indicates that trapezoid h has the best ranking of the eight. Even though it has almost the highest mean deviation values, the variance of the deviations is the least and it also has one of the lowest variations in the mean deviation values over the range of plane angles.

The effect of variations in the pressure differential across the window pane is determined by a study of Figs. 23 through 28. The analyses to obtain the data presented in these figures were performed for the nominal values of the parameters and additional pressure differentials of 5.0 and 15.0 psia. Figures 23 and 24 present the data for square d, and Figs. 27 and 28 the data for trapezoid g.

The curves of these figures show that the mean and rms deviation values and the mean variations over the plane angle all increase with an increase in the magnitude of the pressure differential. Thus, it is

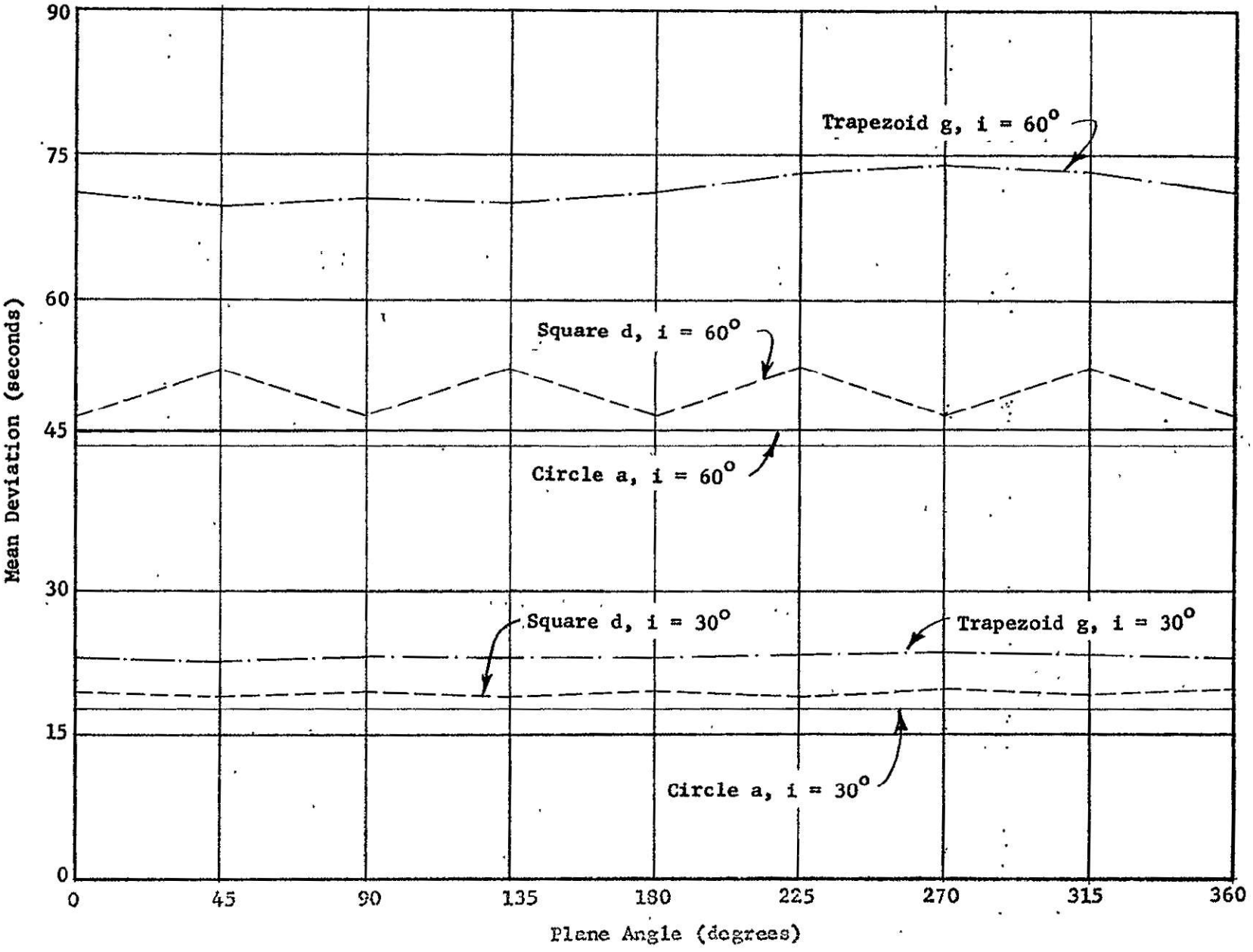

Figure 15. Mean of LOS Deviations - Variation of Pane Shape

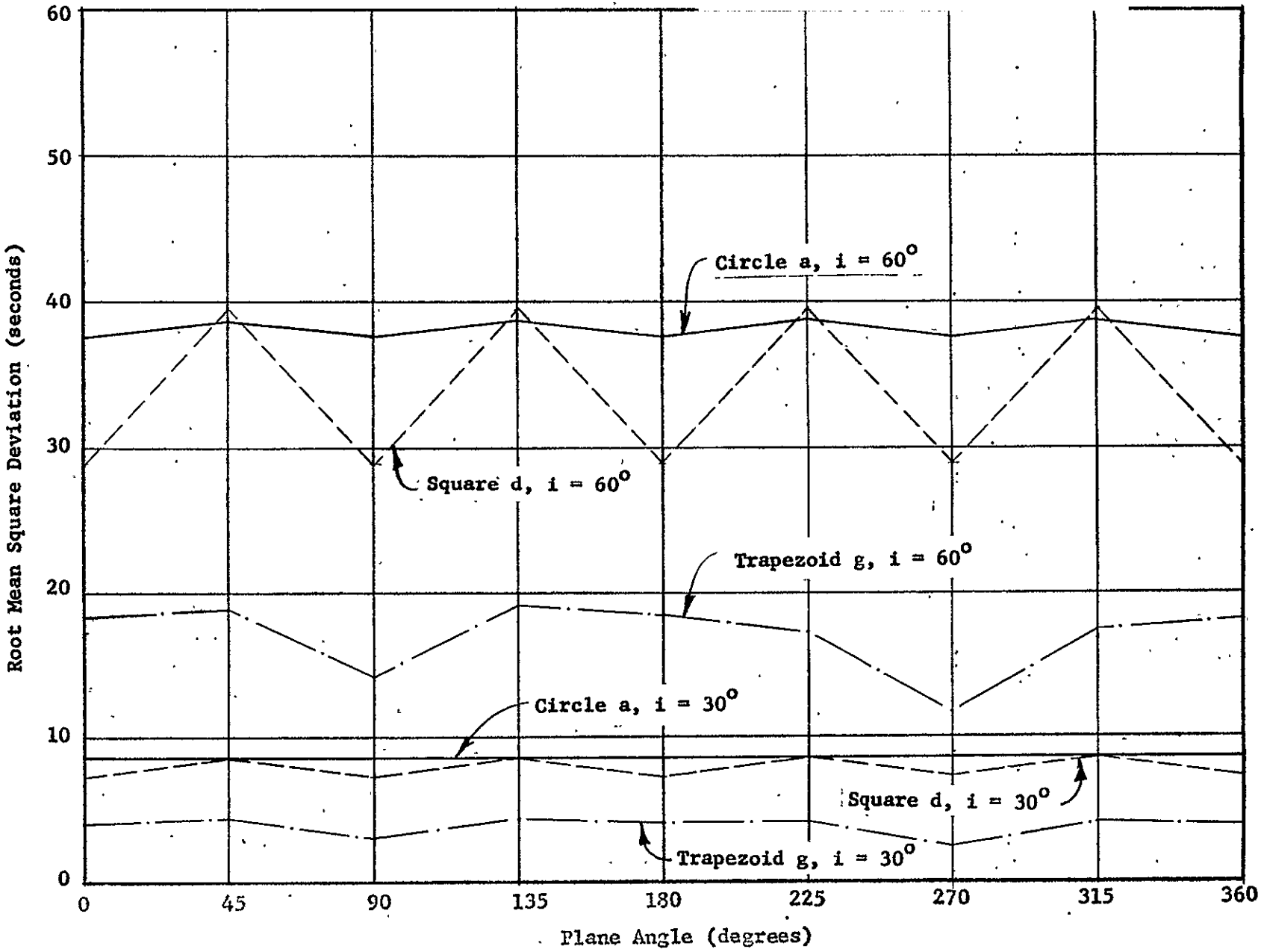

Figure 16. RMS of LOS Deviations - Variation of Pane Shape

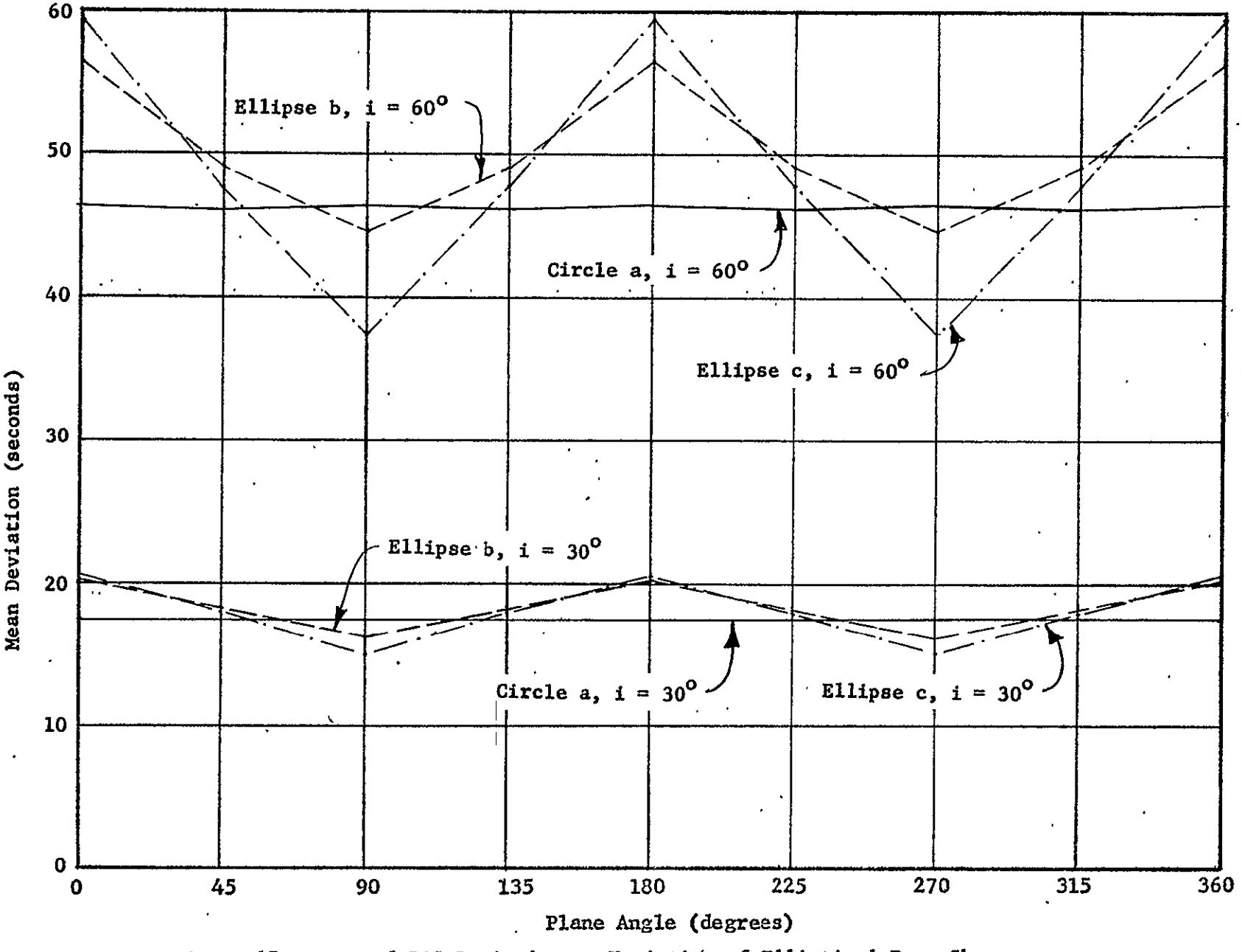

Figure 17. Mean of LOS Deviations - Variation of Elliptical Pane Shape

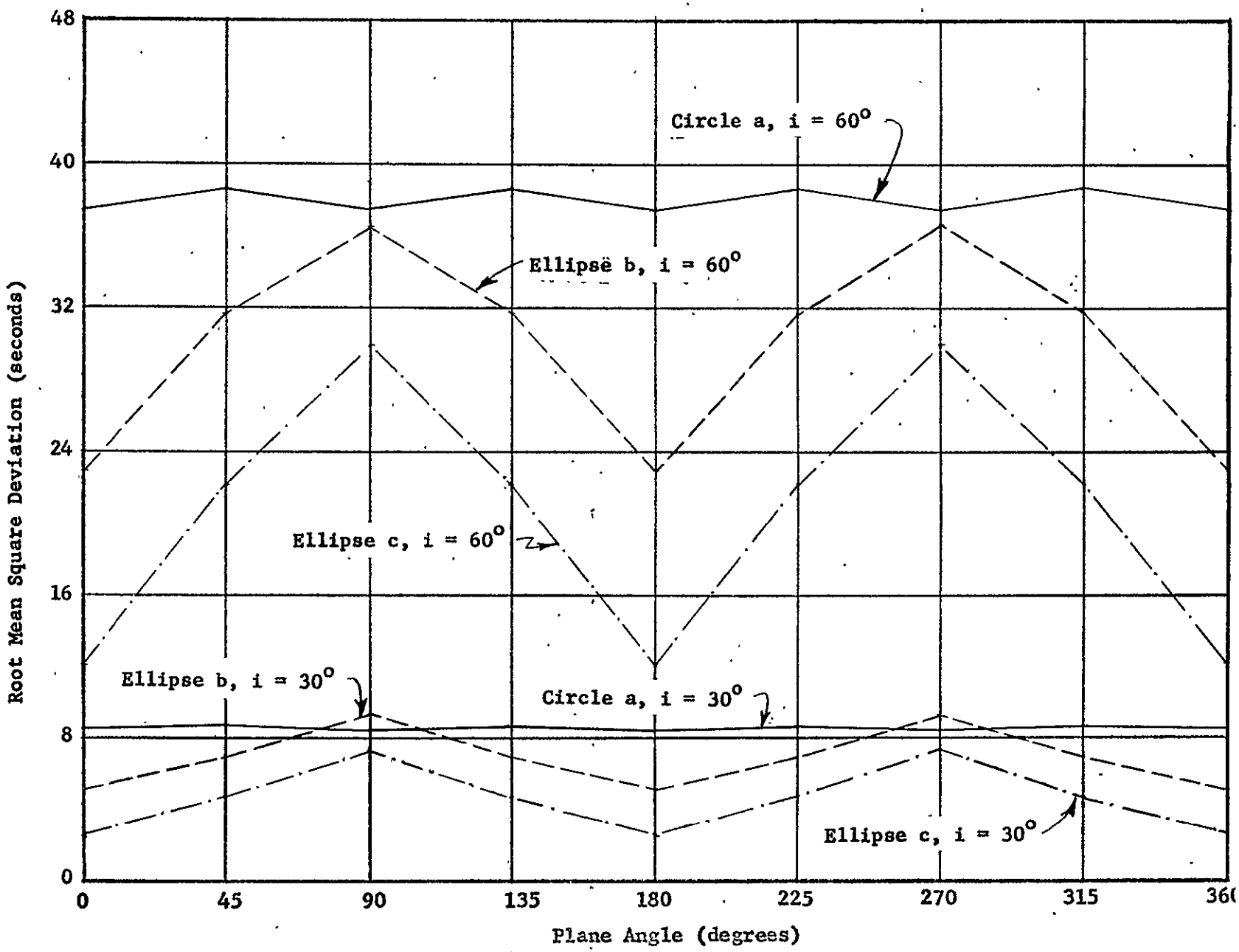

Figure 18. RMS of LOS Deviations - Variation of Elliptical Pane Shape

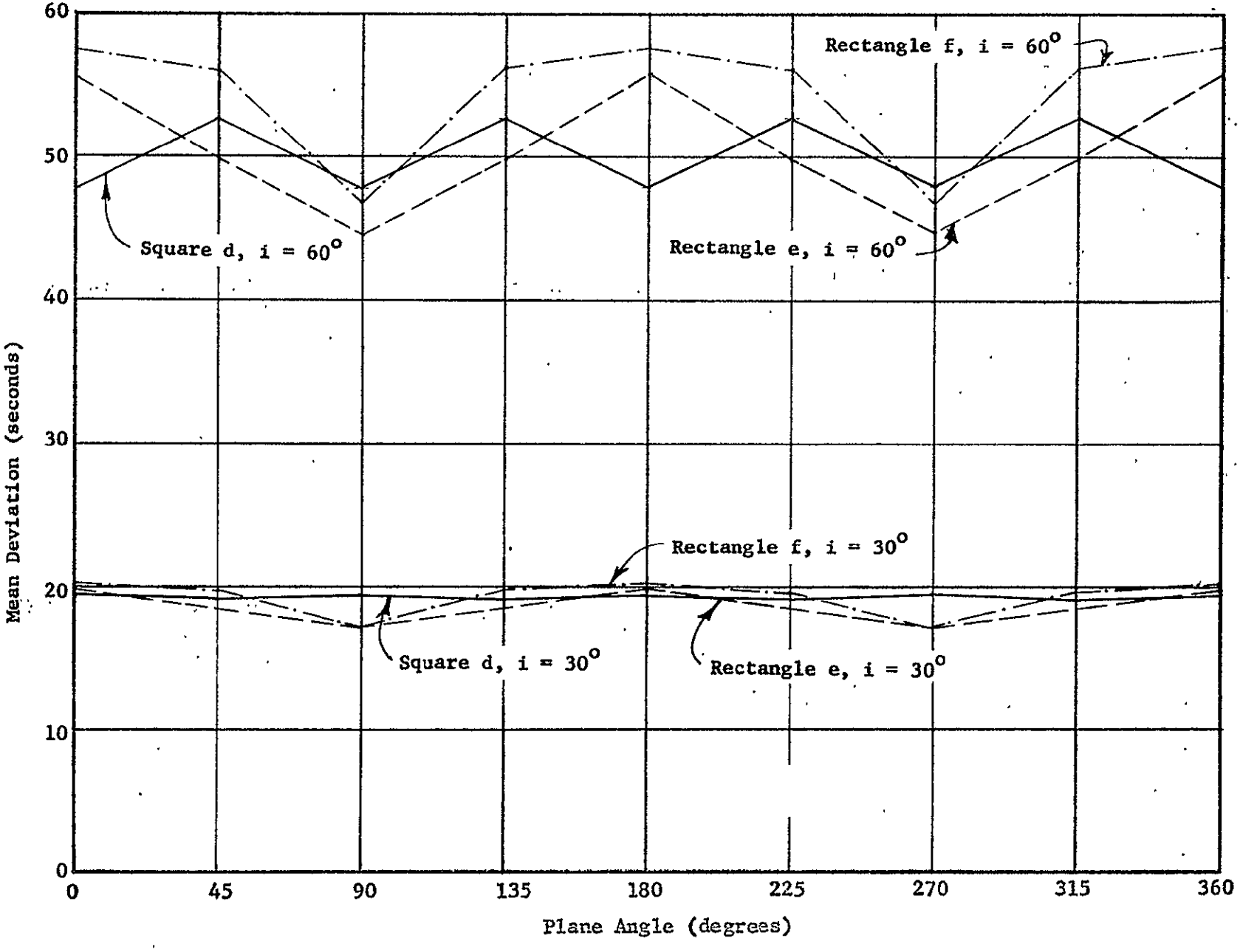

Figure 19. Mean of LOS Deviations - Variation of Rectangular Pane Shape

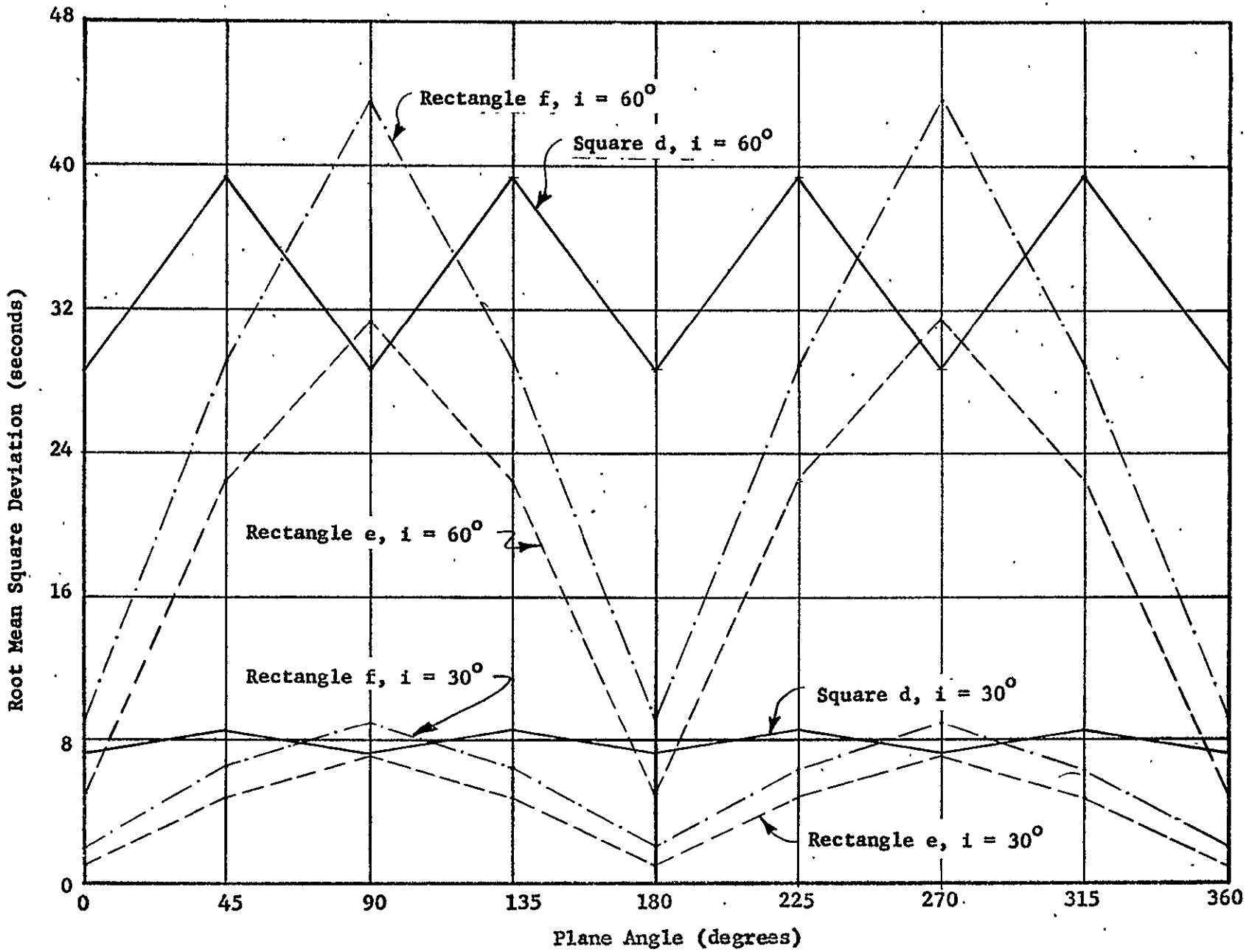

Figure 20. RMS of LOS Deviations - Variation of Rectangular Pane Shape

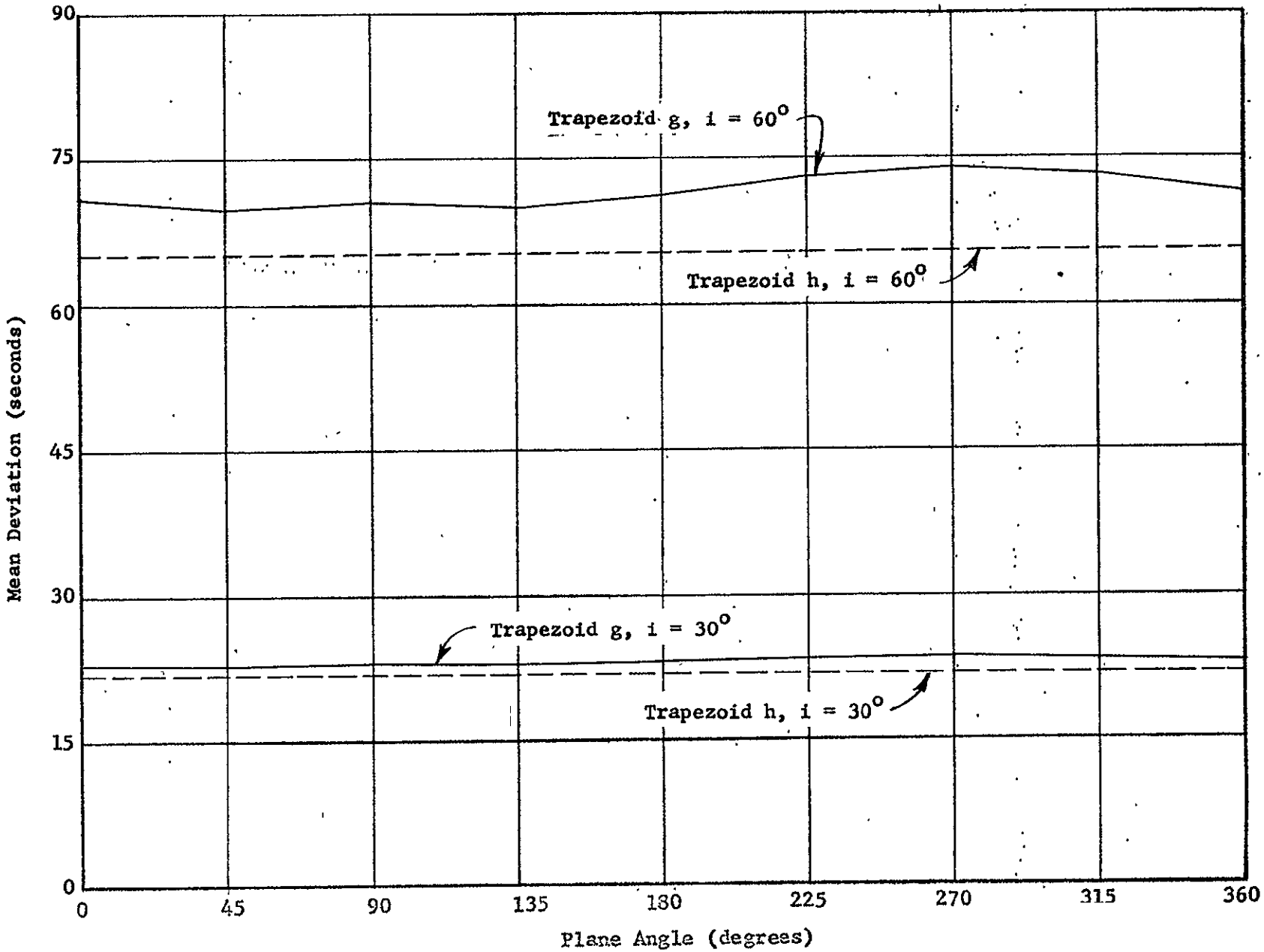

Figure 21. Mean of LOS Deviations - Variation of Trapezoidal Pane Shape

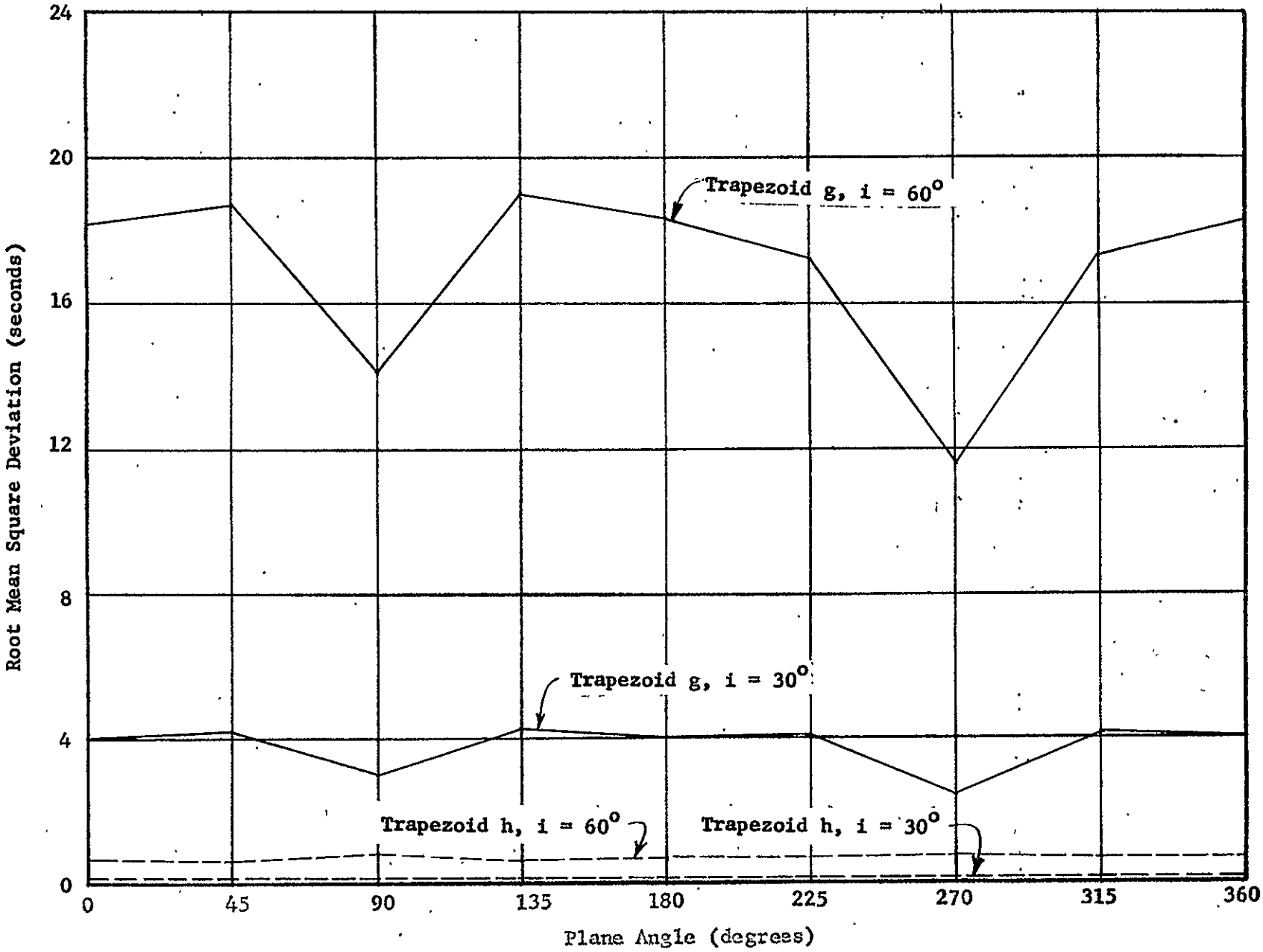

Figure 22. RMS of LOS Deviations - Variation of Trapezoidal Pane Shape

Table 4

Rankings for Variation of Pane Shape

Shape	Mean Value	RMS Value	Mean Value Variation	Overall Ranking
Circle a	1	16	2	19
Ellipse b	3	12	14	29
Ellipse c	2	8	16	26
Square d	5	14	8	27
Rectangle e	4	6	10	20
Rectangle f	6	10	12	28
Trapezoid g	8	4	6	18
Trapezoid h	7	2	4	13

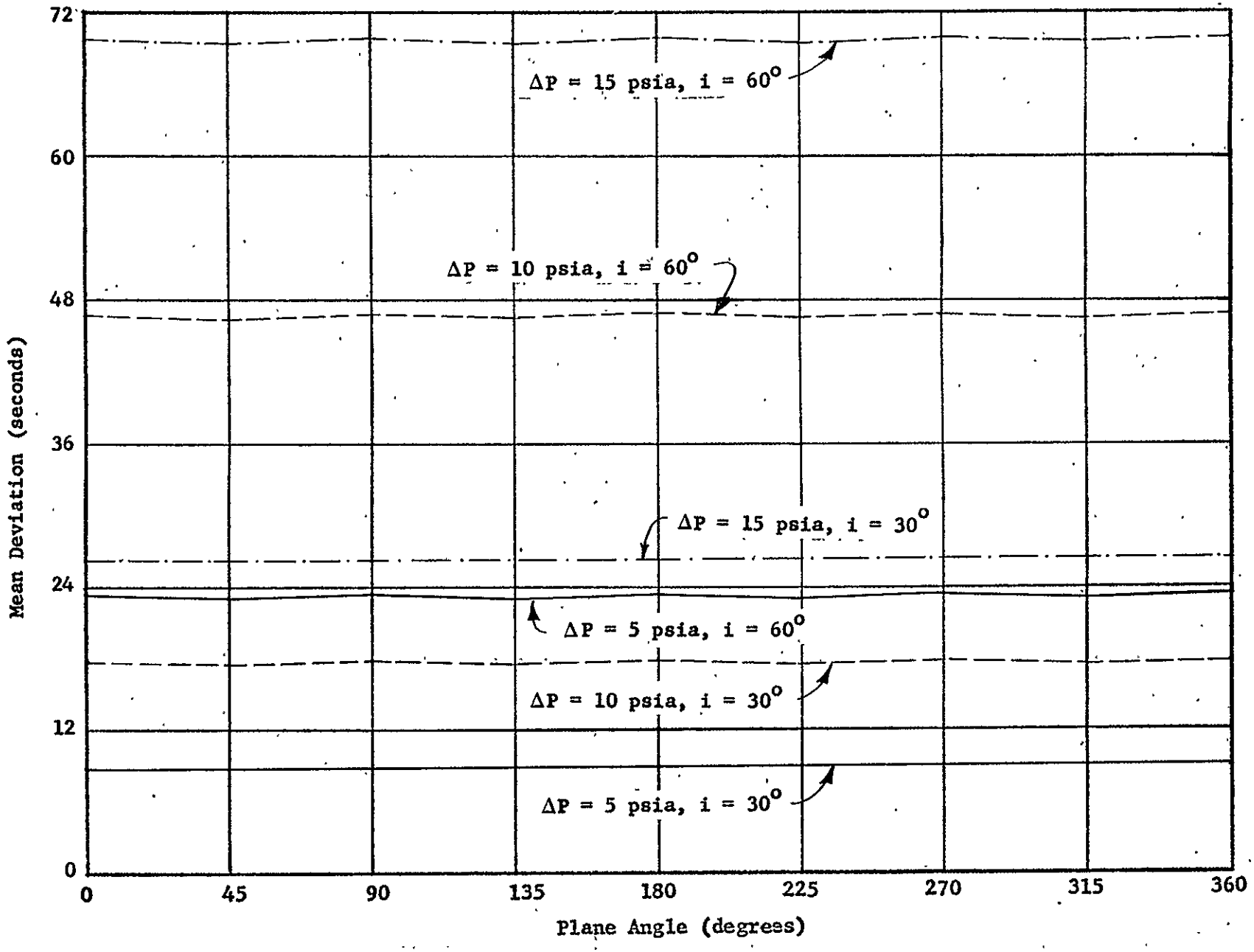

Figure 23. Mean of LOS Deviations - Variation of Pressure Differential (Circle a)

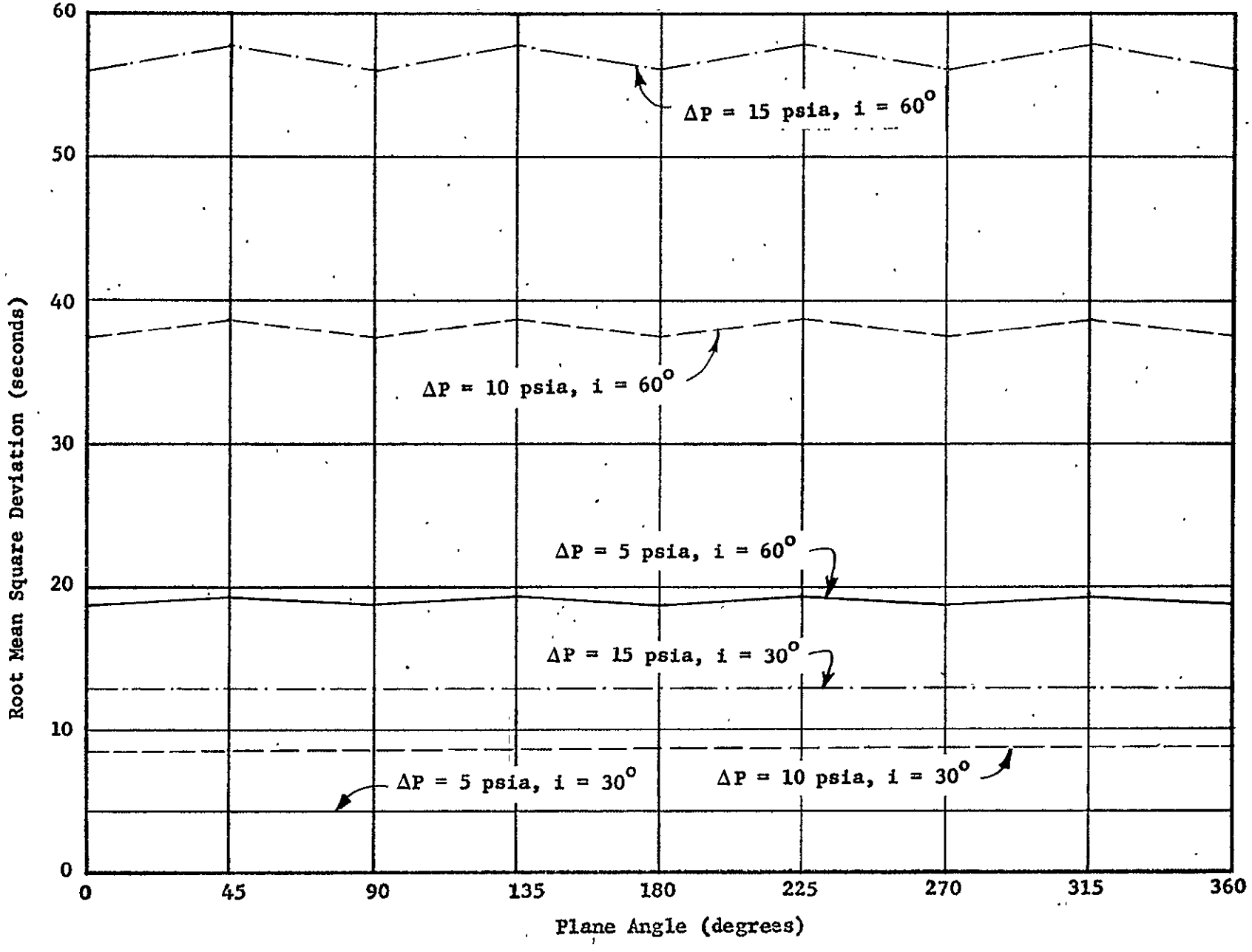

Figure 24. RMS of LOS Deviations - Variation of Pressure Differential (Circle a)

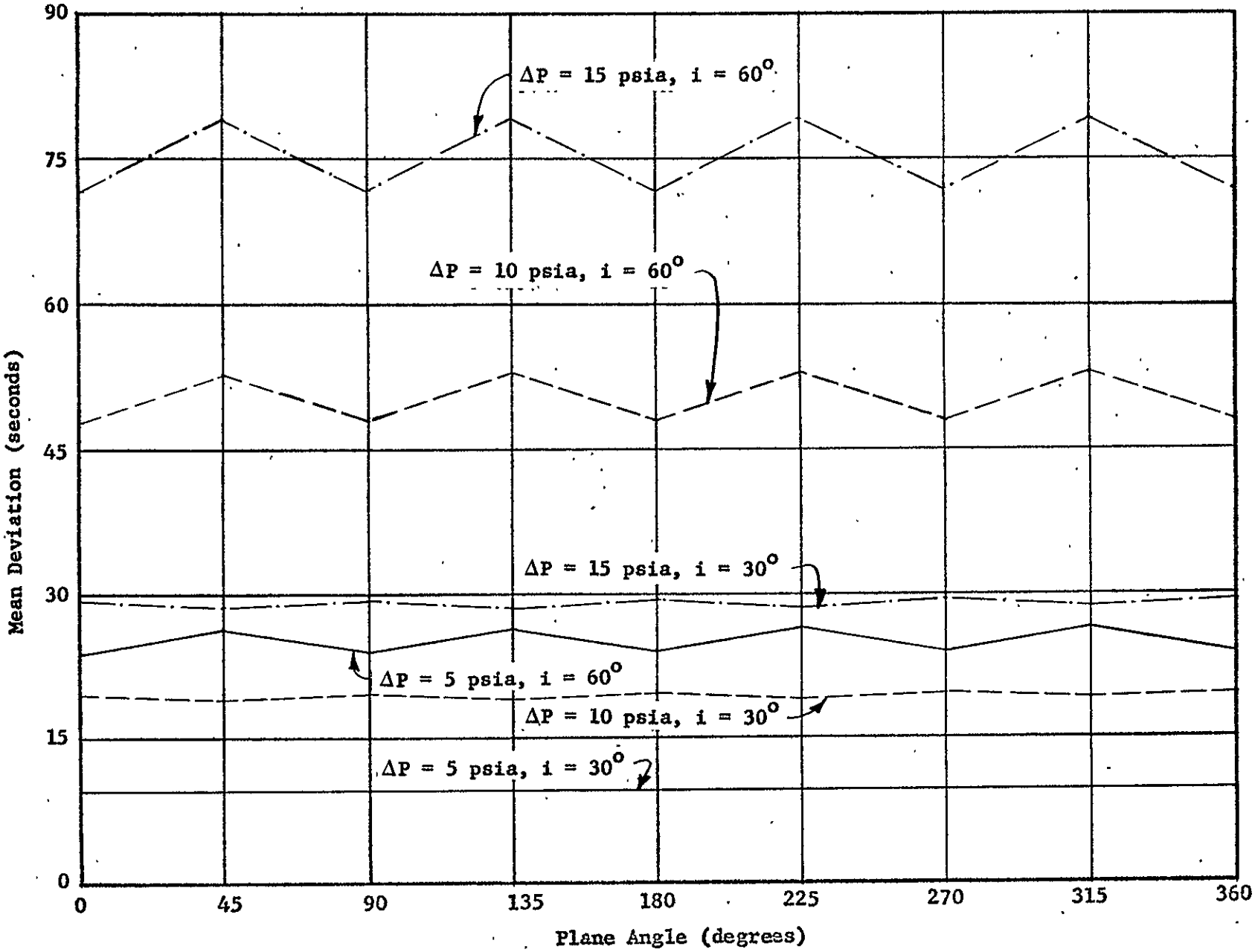

Figure 25. Mean of LOS Deviations - Variation of Pressure Differential (Square d)

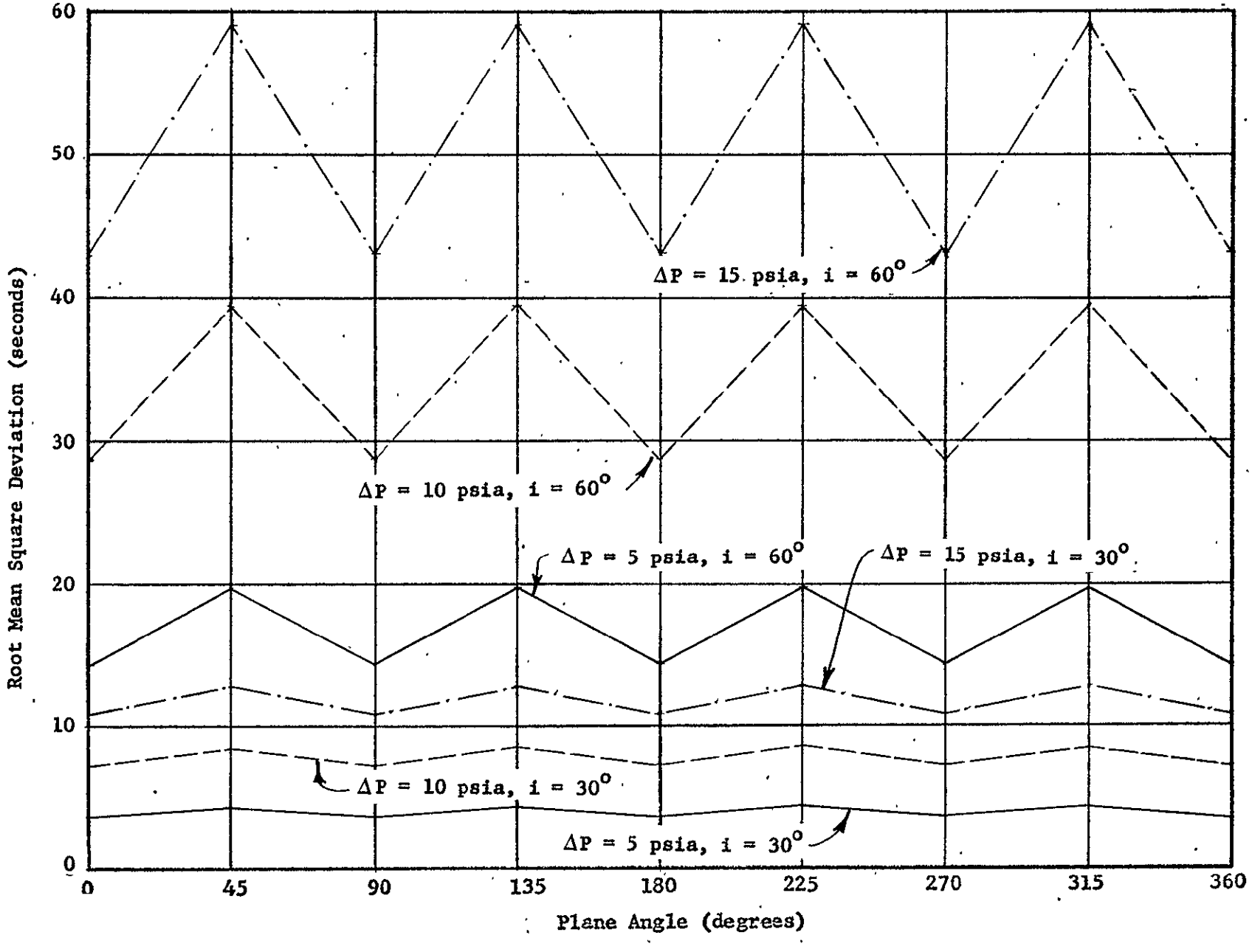

Figure 26. RMS of LOS Deviations - Variation of Pressure Differential (Square d)

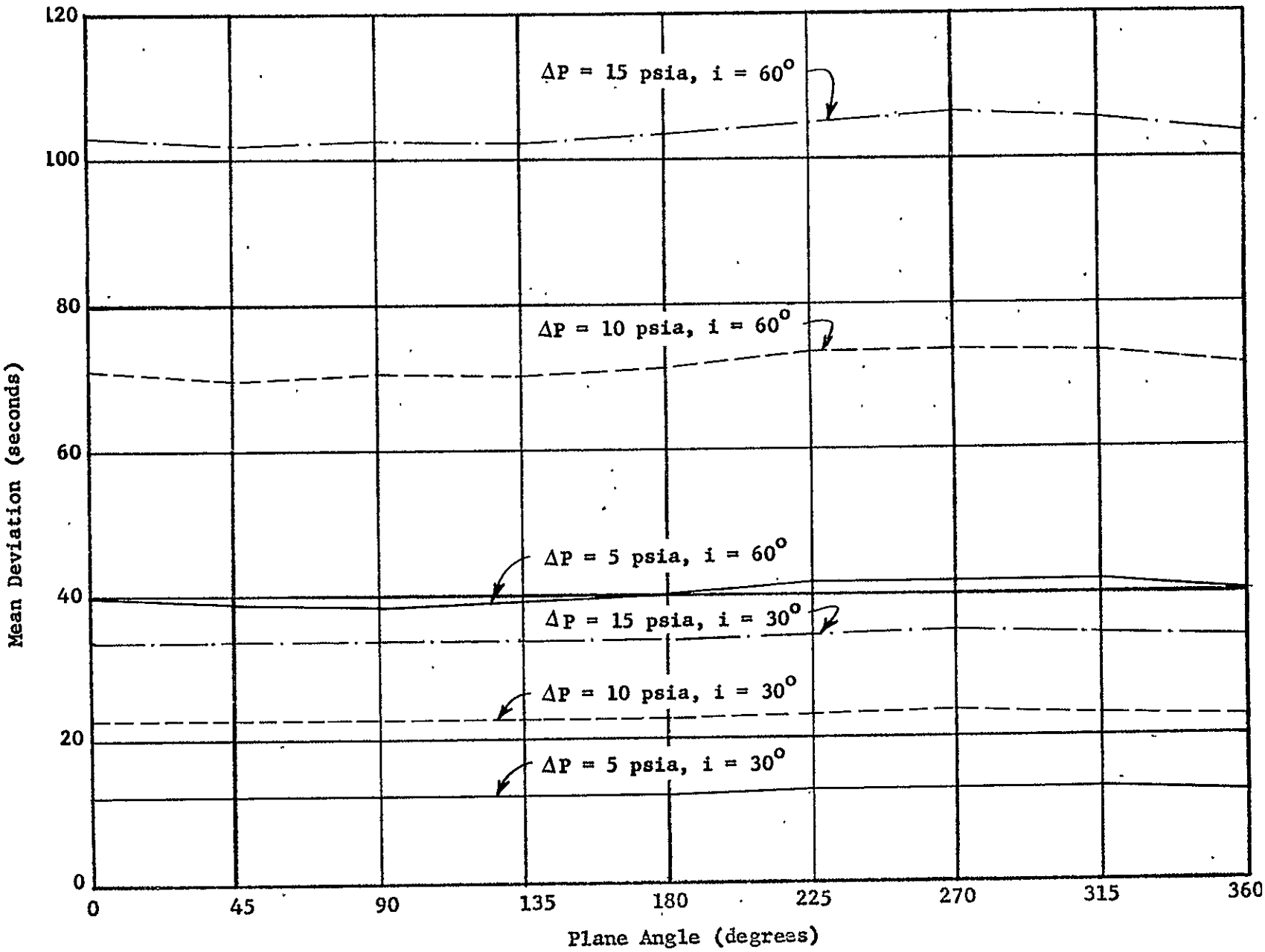

Figure 27. Mean of LOS Deviations - Variation of Pressure Differential (Trapezoid g)

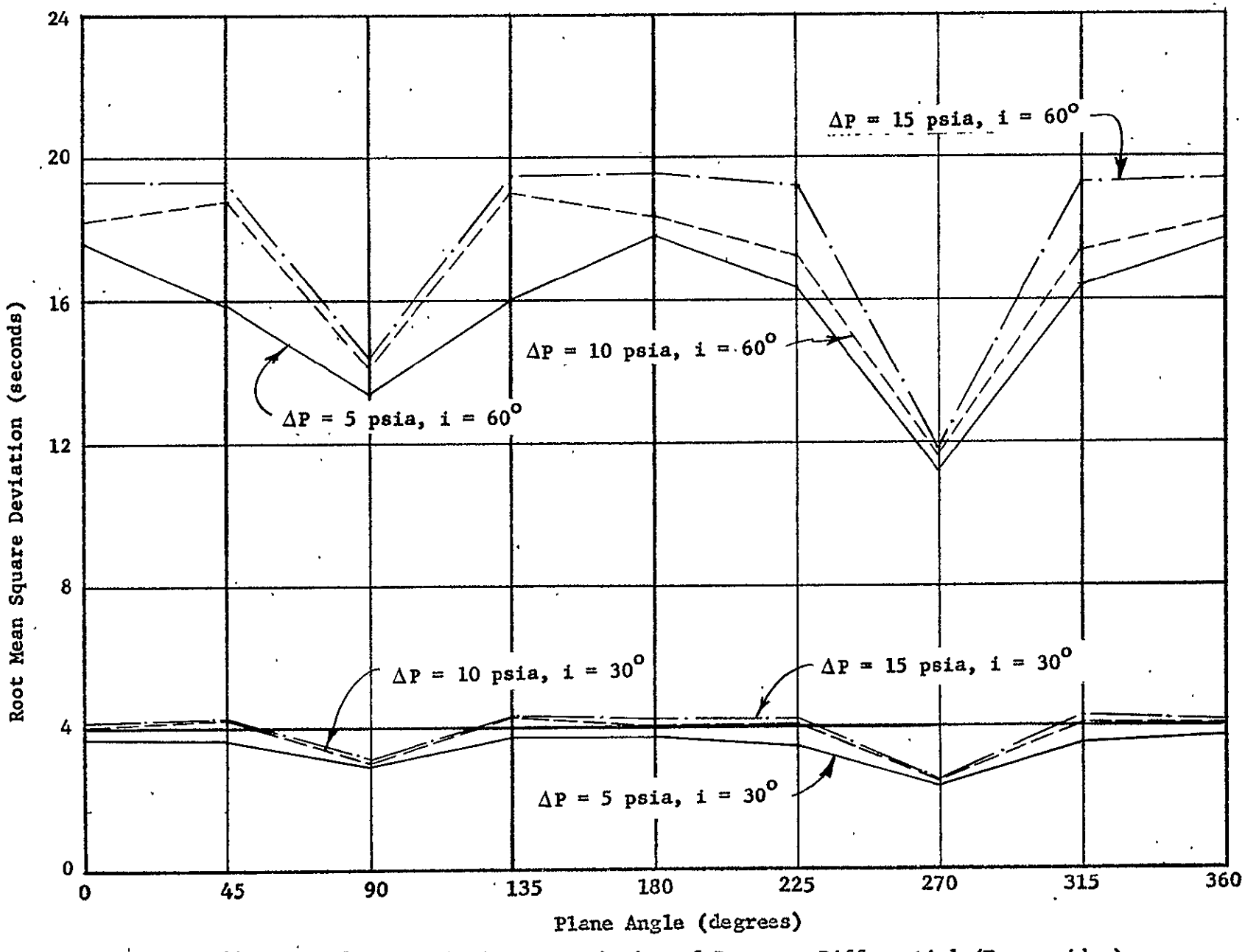

Figure 28. RMS of LOS Deviations - Variation of Pressure Differential (Trapezoid g)

concluded that the smallest pressure differential will result in smaller LOS deviations for the single-pane window configurations studied. This is because the smaller pressure differentials result in smaller deflections and thus less variation in the slope of the window surface.

Variations in the dimensional scale (i.e., the size of the window planforms of Fig. 1) are studied using the data shown in Figs. 29 through 34. In addition to the nominal parameter values, the analyses performed to obtain the data for these figures used dimensional scales of 0.75 and 1.5. Figures 29 and 30 present the data for circle a, Figs. 31 and 32 the data for square d, and Figs. 33 and 34 the data for trapezoid g.

Rankings for the nine sizes of planforms investigated in this study are given in Table 5. The overall rankings indicate that square d with a dimensionsl scale of 0.75 (i.e., a square 9.3 inches on a side) has the best characteristics. This square has the second lowest mean deviation values and mean value variations over the range of plane angles and the third lowest rms deviation values.

The effect of variations in the pane thickness is presented in Figs. 35 through 40. The analyses leading to the data in these figures were performed for pane thicknesses of 0.6 and 1.2 inches, in addition to the nominal parameter values. Figures 35 and 36 present the data for circle a, Figs. 37 and 38 the data for square d, and Figs. 39 and 40 the data for trapezoid g.

Rankings for the nine configurations investigated in this study are given in Table 6. The overall rankings indicate that square d with a pane thickness of 1.2 inches has the best characteristics. This square

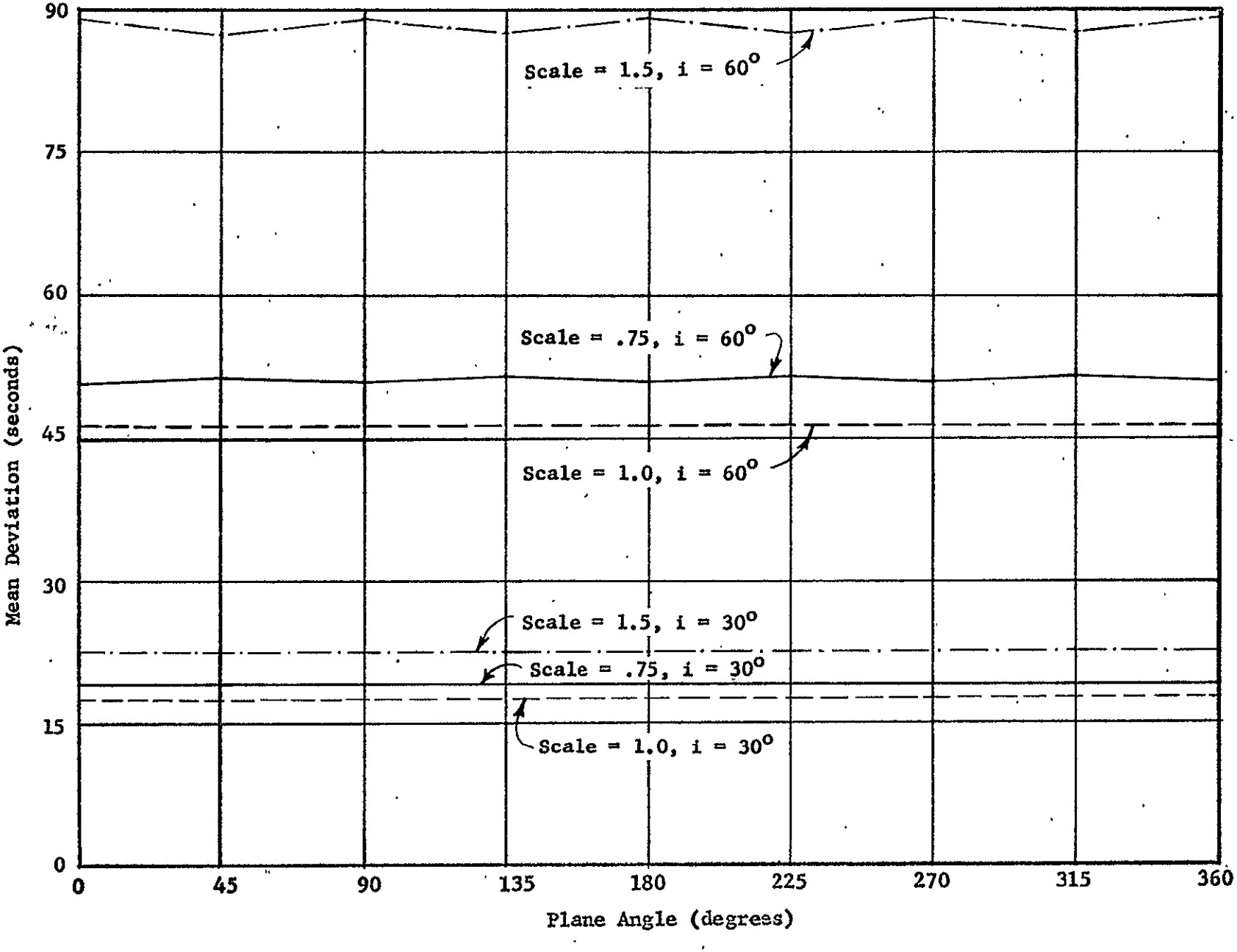

Figure 29. Mean of LOS Deviations - Variation of Dimensional Scale (Circle a)

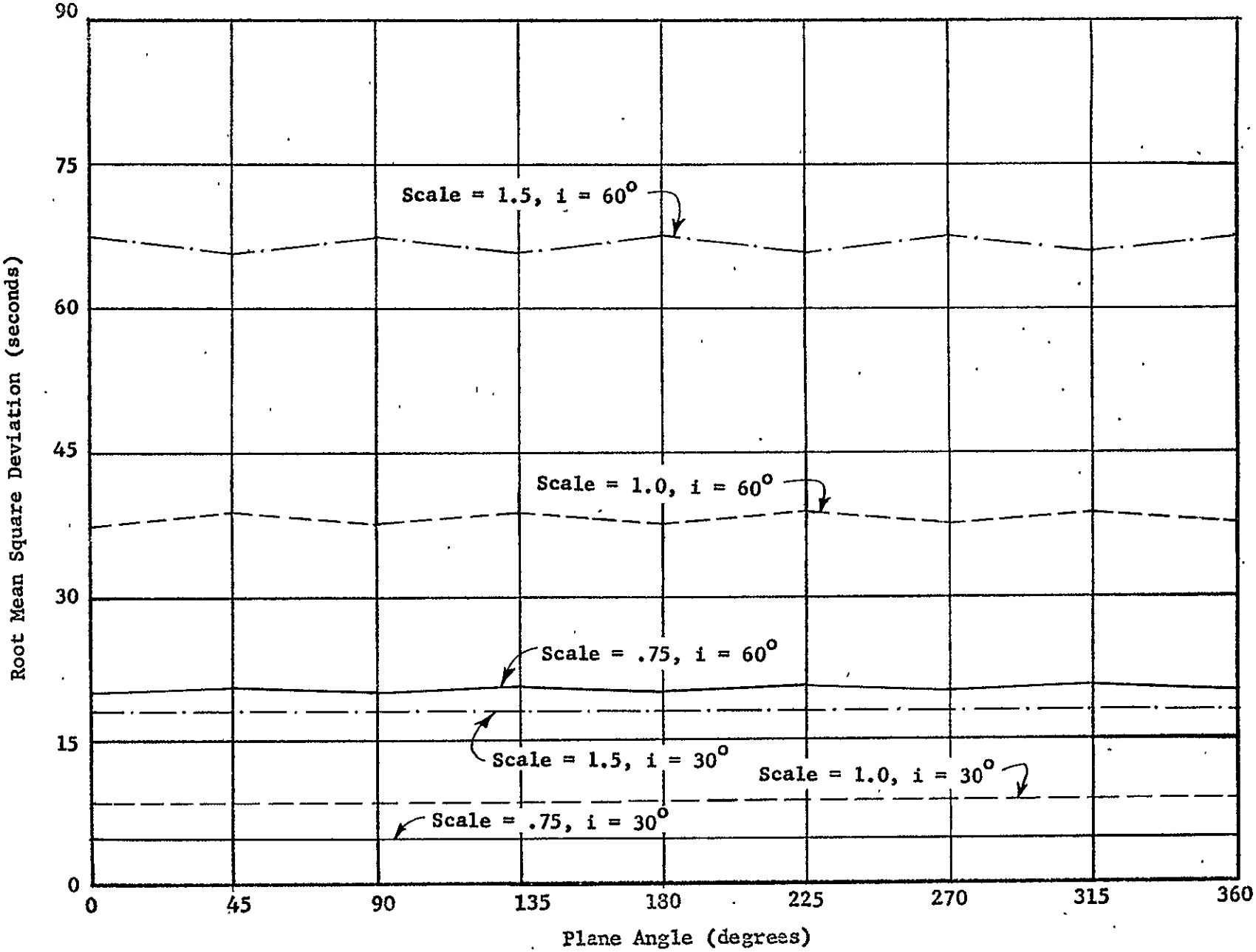

Figure 30. RMS of LOS Deviations - Variation of Dimensional Scale (Circle a)

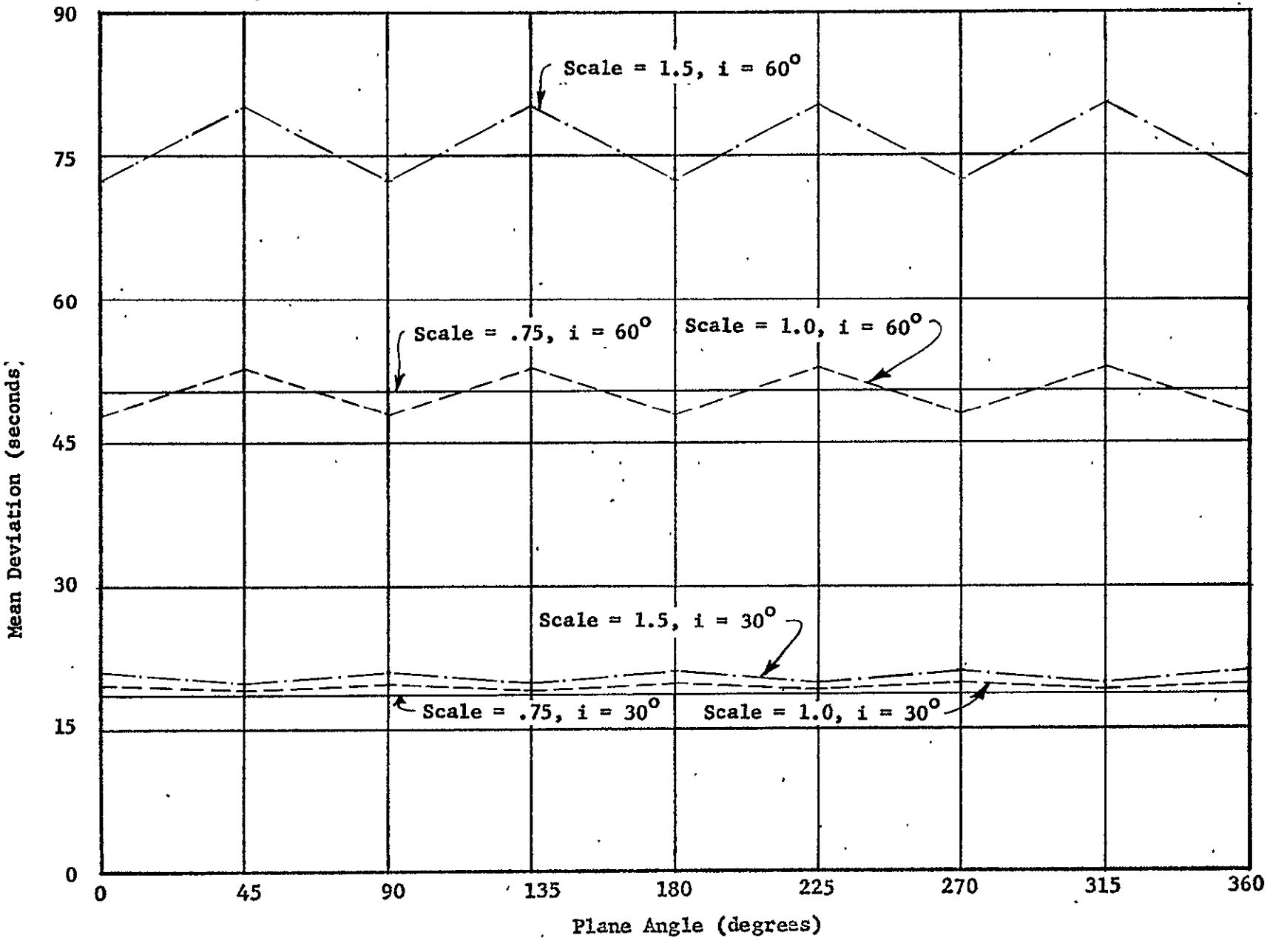

Figure 31. Mean of LOS Deviations - Variation of Dimensional Scale (Square d)

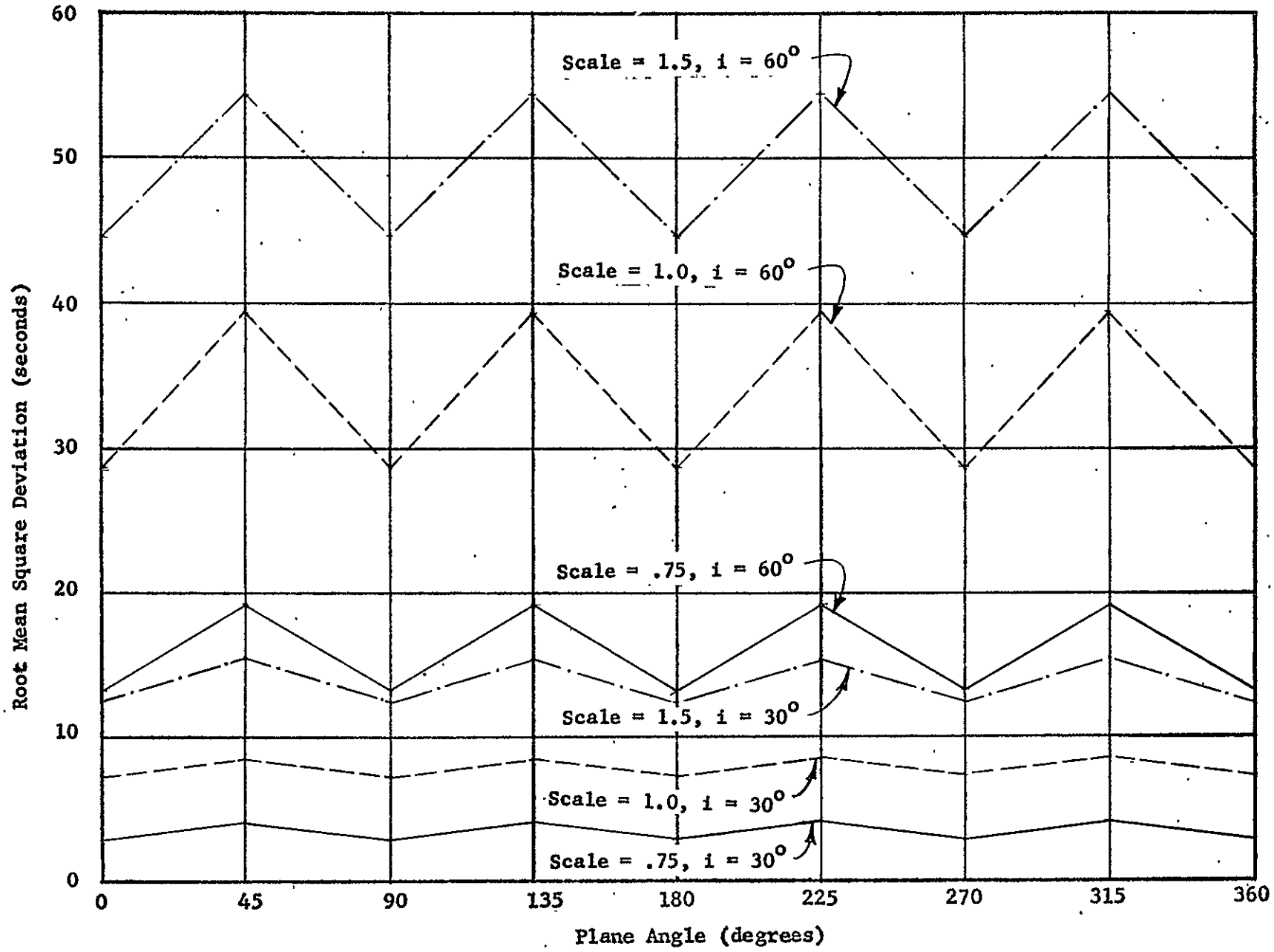

Figure 32. RMS of LOS Deviations - Variation of Dimensional Scale (Square d)

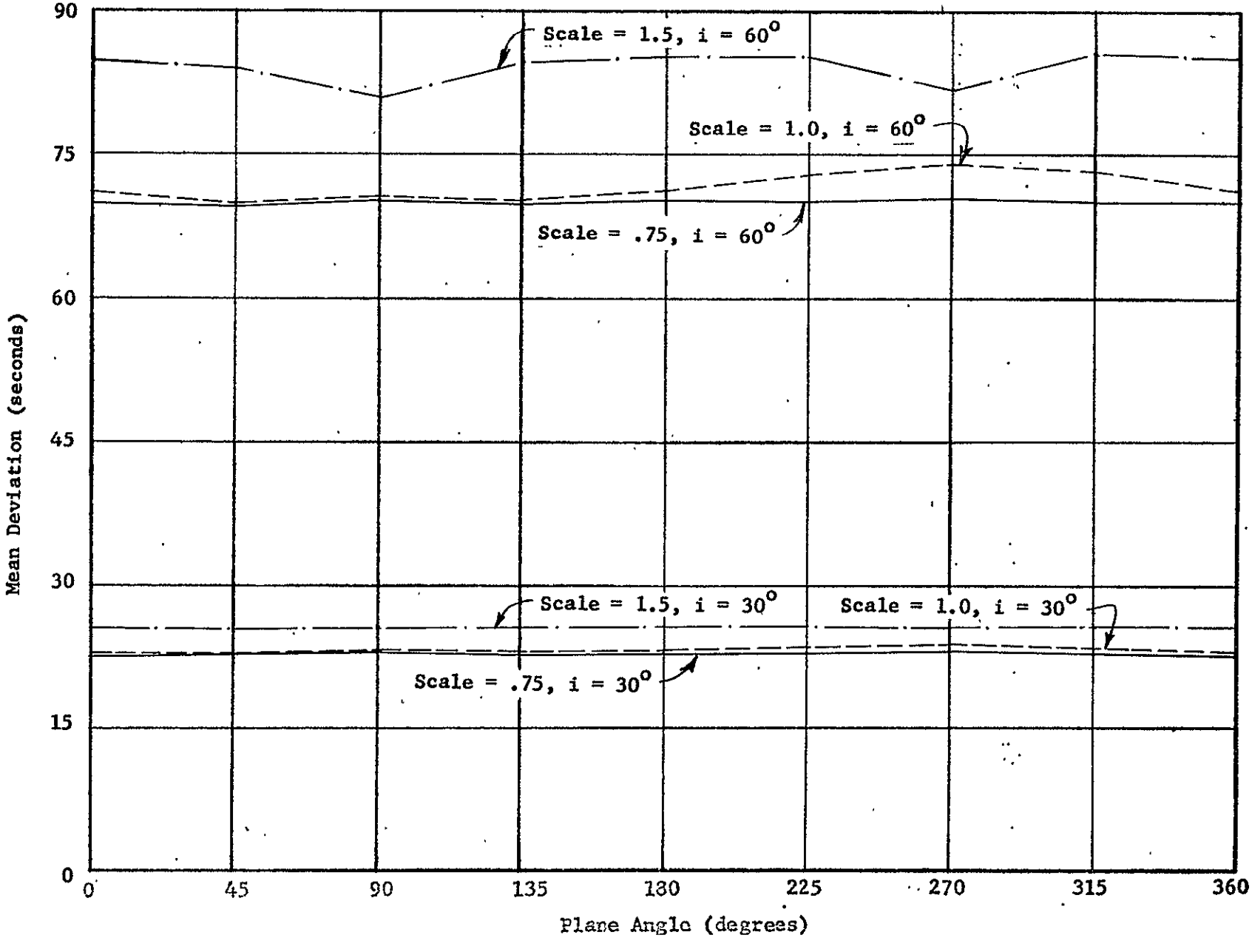

Figure 33. Mean of LOS Deviations - Variation of Dimensional Scale (Trapezoid g)

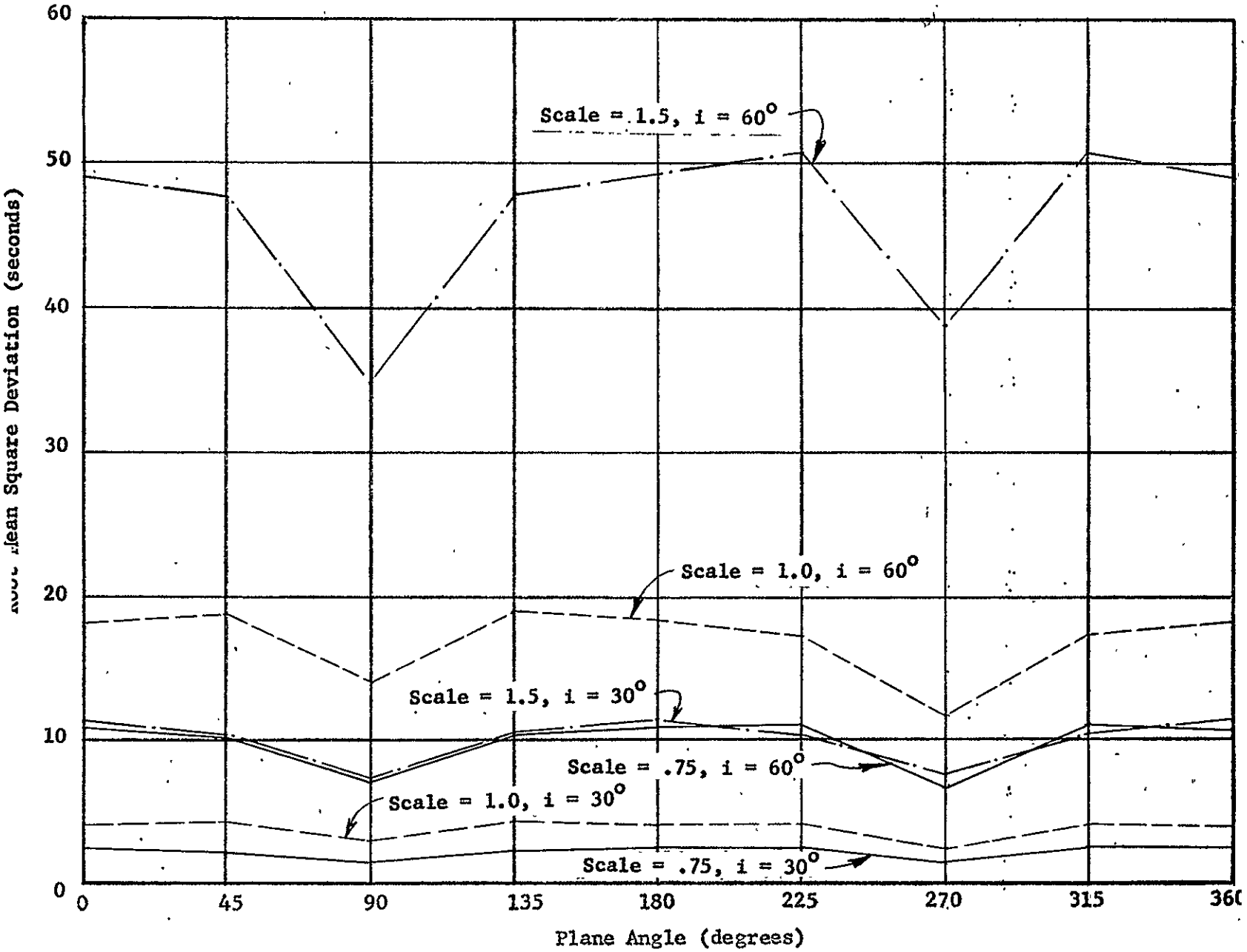

Figure 34. RMS of LOS Deviations - Variation of Dimensional Scale (Trapezoid g)

Table 5

Rankings for Variation of Dimensional Scale

Planform	Dimensional Scale	Mean Value	RMS Value	Mean Value Variation	Overall Ranking
Circle a	0.75	4	8	6	18
Circle a	1.0	1	12	2	15
Circle a	1.5	9	18	10	37
Square d	0.75	2	6	4	12
Square d	1.0	3	10	16	29
Square d	1.5	7	16	18	41
Trapezoid g	0.75	5	2	8	15
Trapezoid g	1.0	6	4	14	24
Trapezoid g	1.5	8	14	12	34

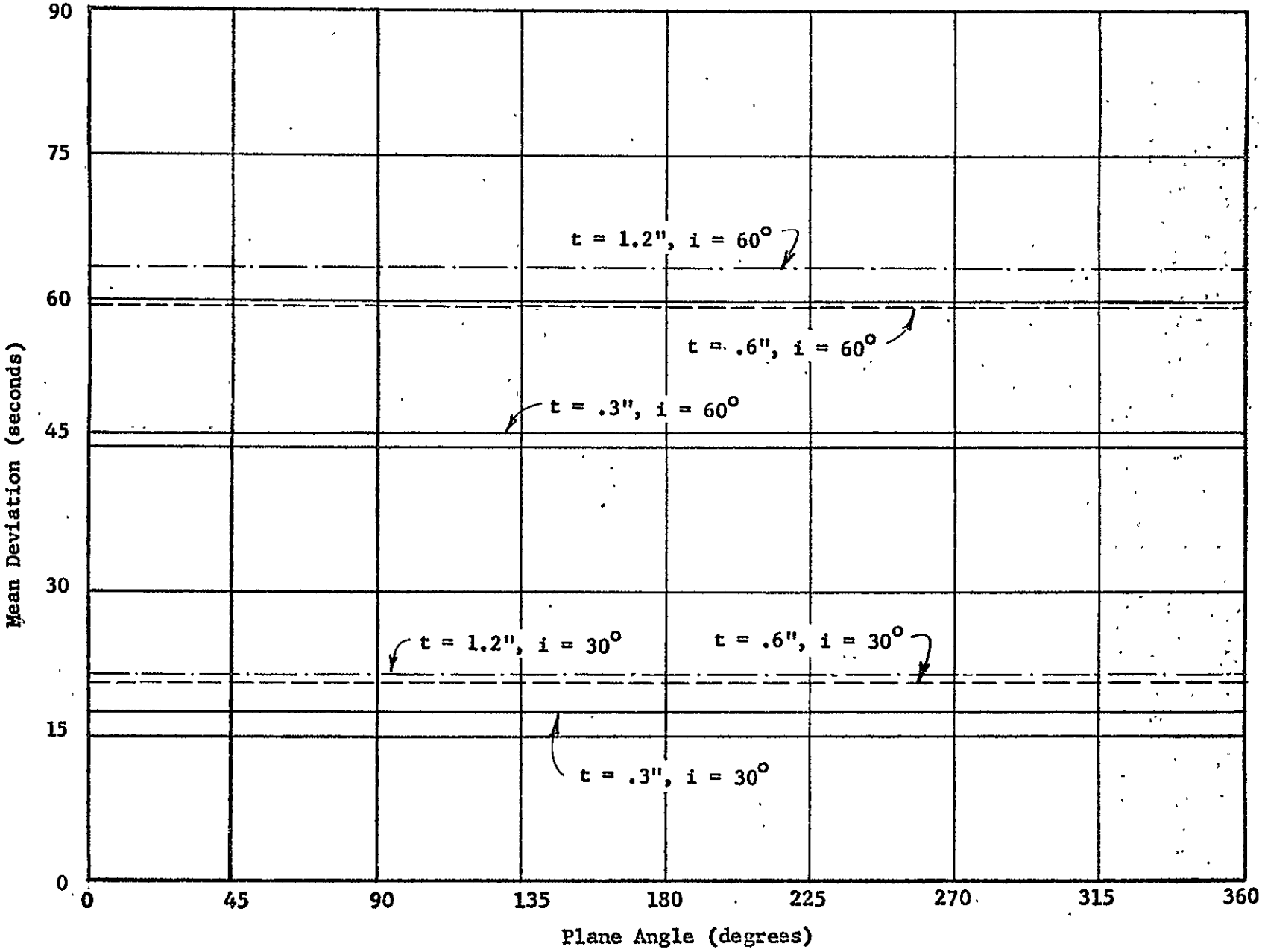

Figure 35. Mean of LOS Deviations - Variation of Pane Thickness (Circle a)

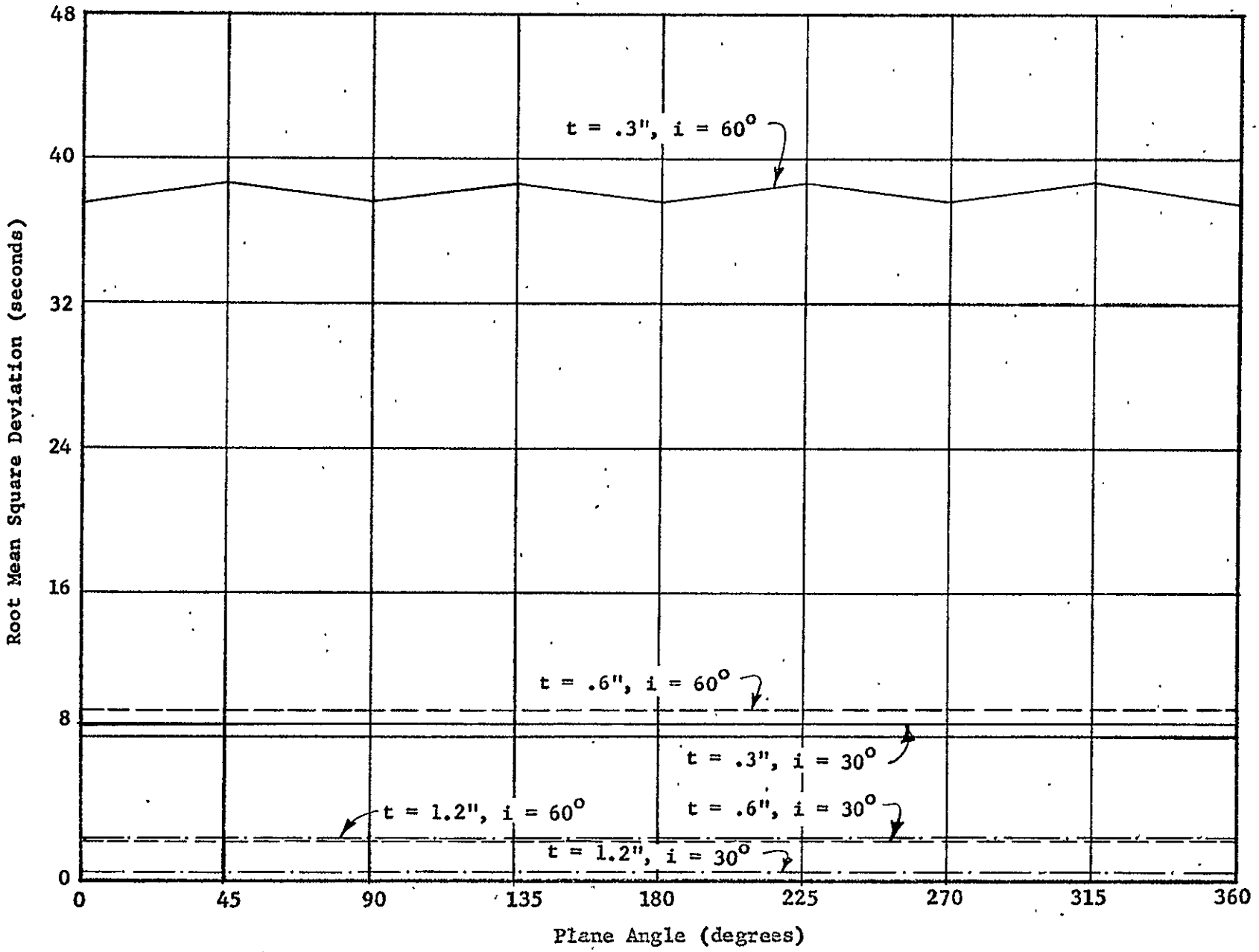

Figure 36. RMS of LOS Deviations - Variation of Pane Thickness (Circle a)

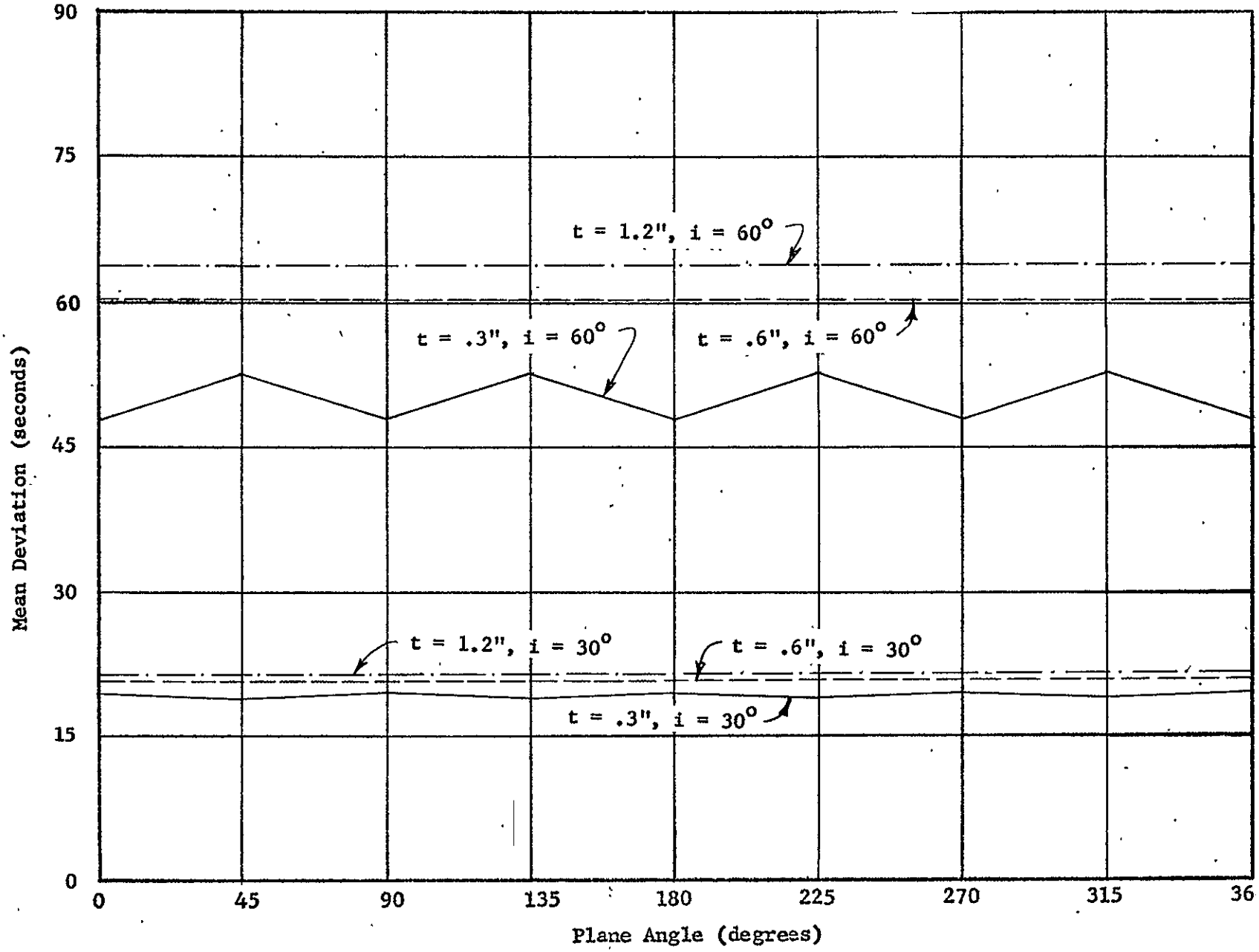

Figure 37. Mean of LOS Deviations - Variation of Pane Thickness (Square d)

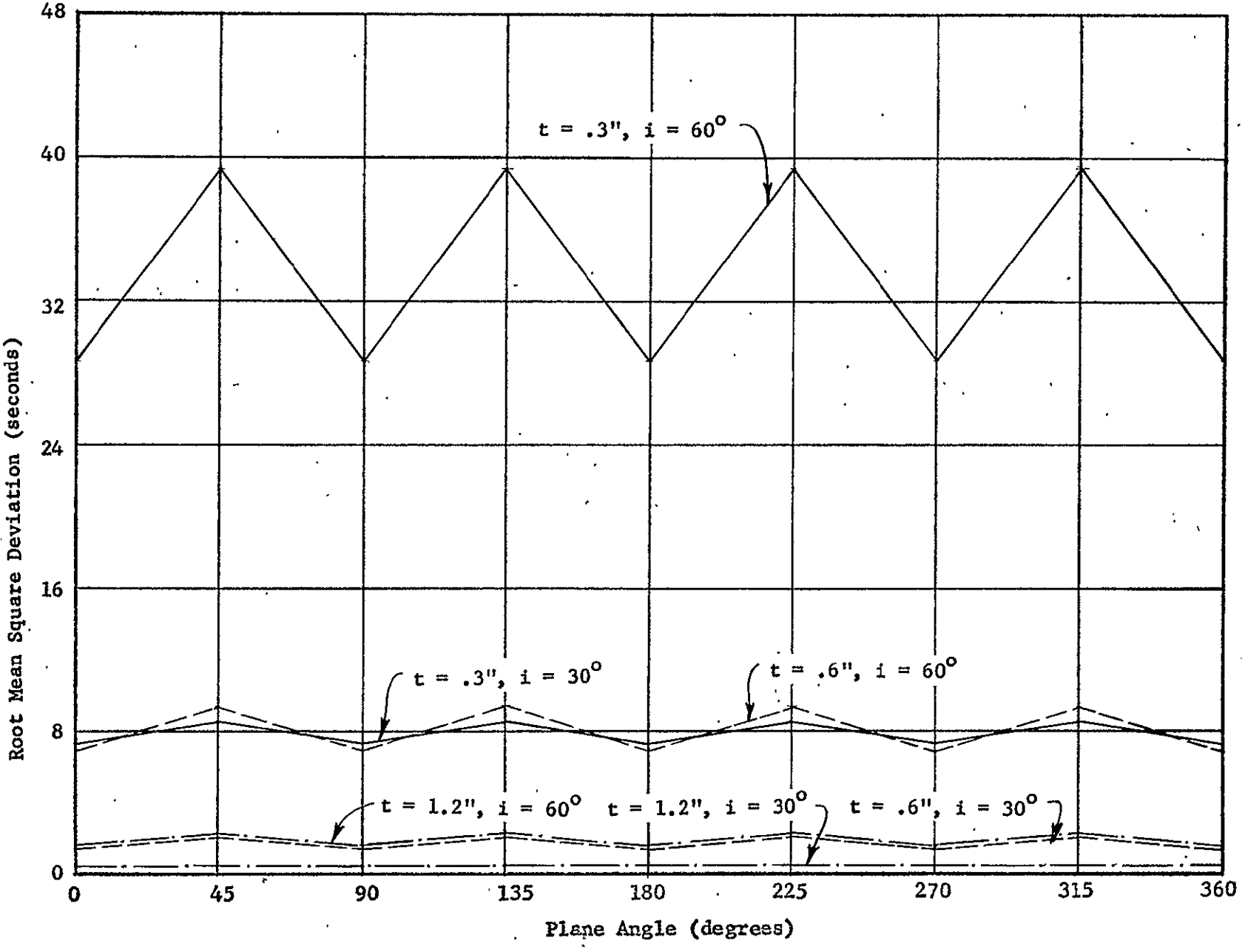

Figure 38. RMS of LOS Deviations - Variation of Pane Thickness (Square d)

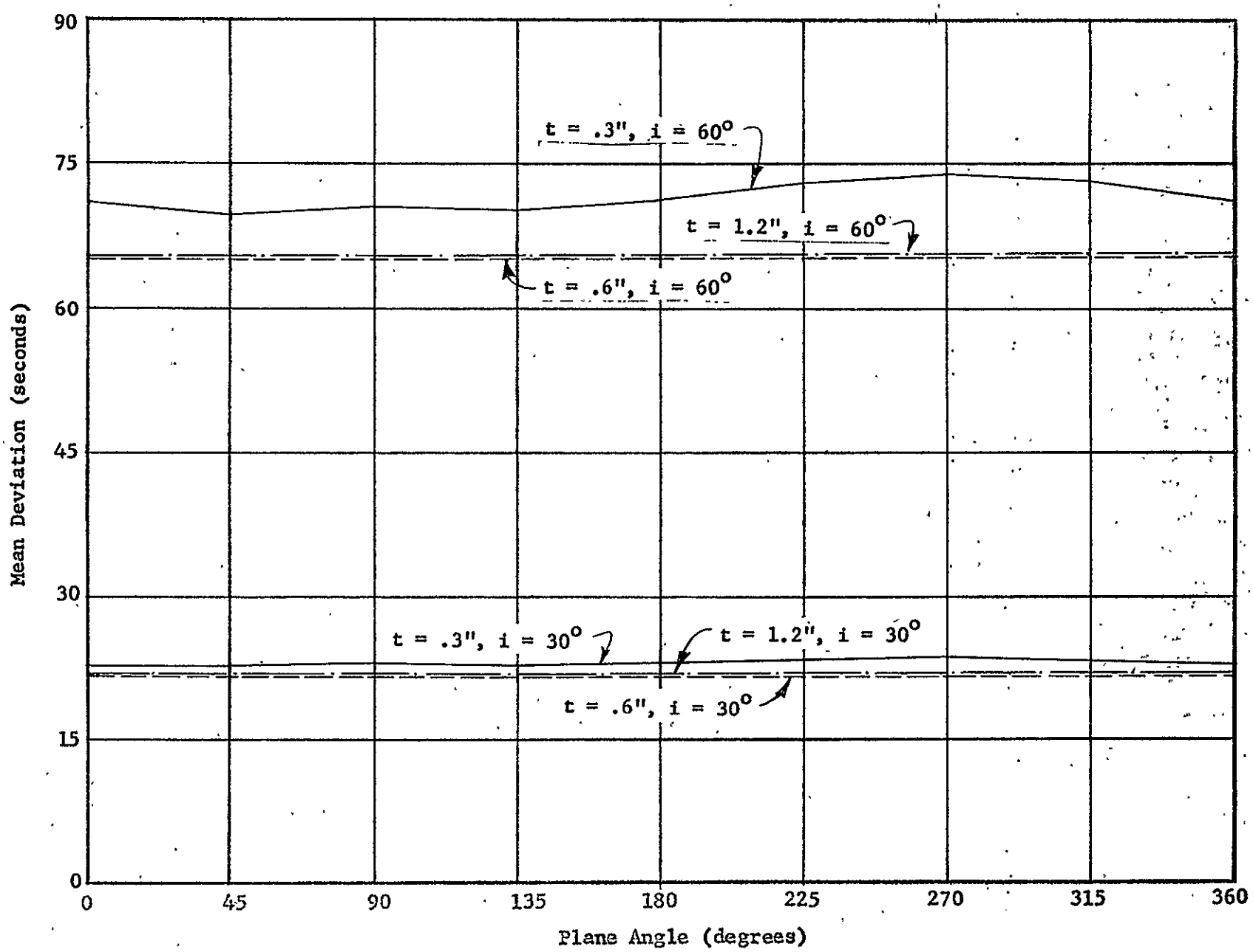

Figure 39. Mean of LOS Deviations - Variation of Pane Thickness (Trapezoid g)

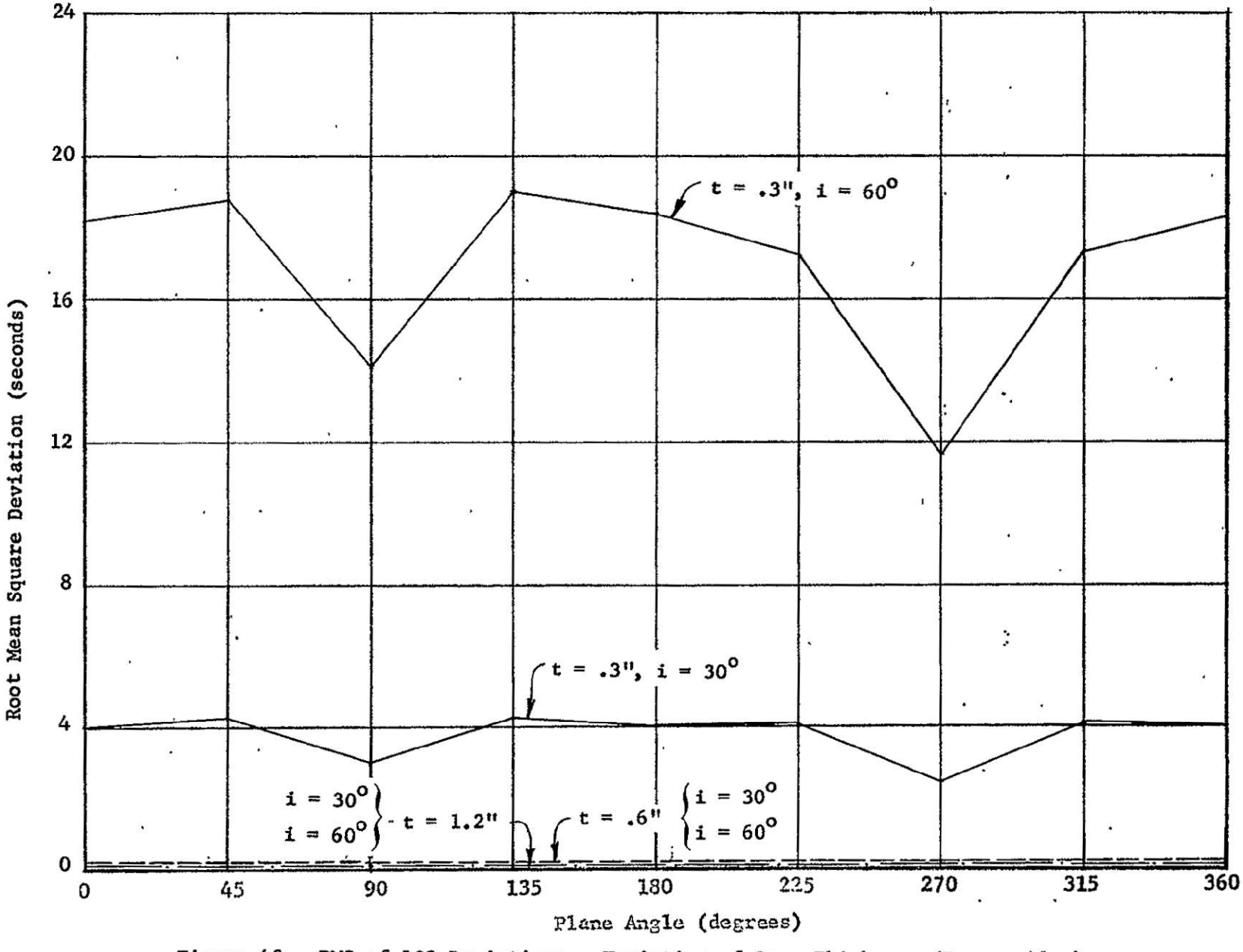

Figure 40. RMS of LOS Deviations - Variation of Pane Thickness (Trapezoid g)

Table 6

Rankings for Variation of Pane Thickness

Planform	Pane Spacing	Mean Value	RMS Value	Mean Value Variation	Overall Ranking
Circle a	0.3"	1	16	2	19
Circle a	0.6"	3	10	2	15
Circle a	1.2"	5	4	2	11
Square d	0.3"	2	14	6	22
Square d	0.6"	4	8	2	14
Square d	1.2"	6	2	2	10
Trapezoid g	0.3"	9	12	4	25
Trapezoid g	0.6"	7	6	2	15
Trapezoid g	1.2"	8	4	2	14

has one of the higher mean deviation values but the lowest rms deviation values and variations in the mean values.

Effects of varying the edge support conditions are studied by considering the data presented in Figs. 41 through 46. In addition to the nominal parameter values, the analyses performed to obtain the data of these figures used simply supported edge conditions. The data for circle a are presented in Figs. 41 and 42, for square d in Figs. 43 and 44, and for trapezoid g in Figs. 45 and 46.

Table 7 presents the rankings for the six configurations investigated in this study. The overall rankings indicate that trapezoid g with clamped edge conditions has the best characteristics. While the mean deviation values for this configuration are not very low it has the lowest rms deviation values and one of the lowest variations in the mean values.

The effect of variations in the incidence angle is studied using the data presented in Figs. 47 through 52. The analyses from which these data were obtained were performed using the nominal parameter values. Figures 47 and 48 present the data for circle a, Figs. 49 and 50 the data for square d, and Figs. 51 and 52 the data for trapezoid g.

The data of these figures indicate that the LOS deviations increase with an increase in the angle of incidence. This is true for all three statistical measures of the LOS deviations. From this, it is concluded that observations should be made at as low an incidence angle as practicable.

Several general conclusions may be drawn based on the above studies of single-pane configurations:

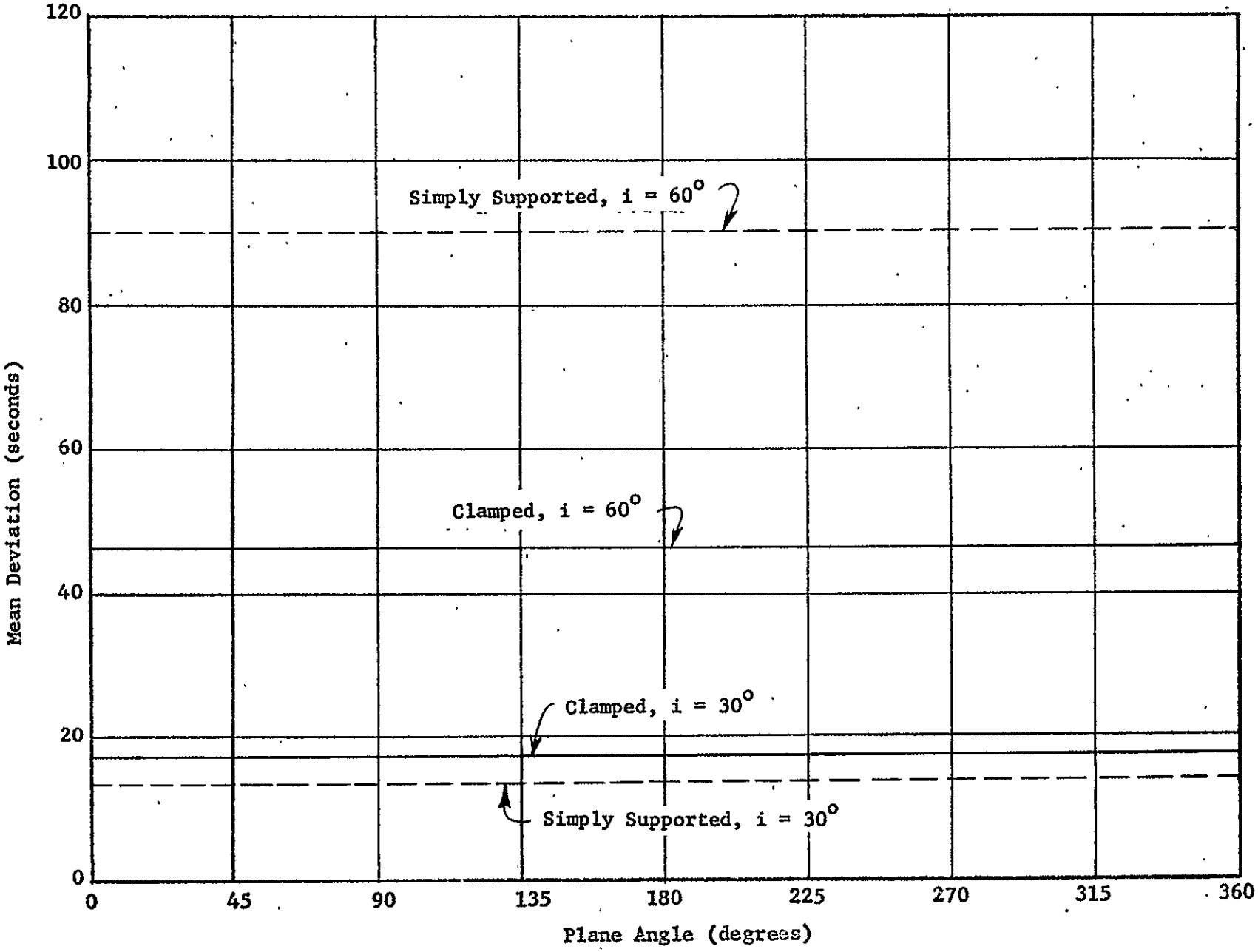

Figure 41. Mean of LOS Deviations - Variation of Edge Condition (Circle a)

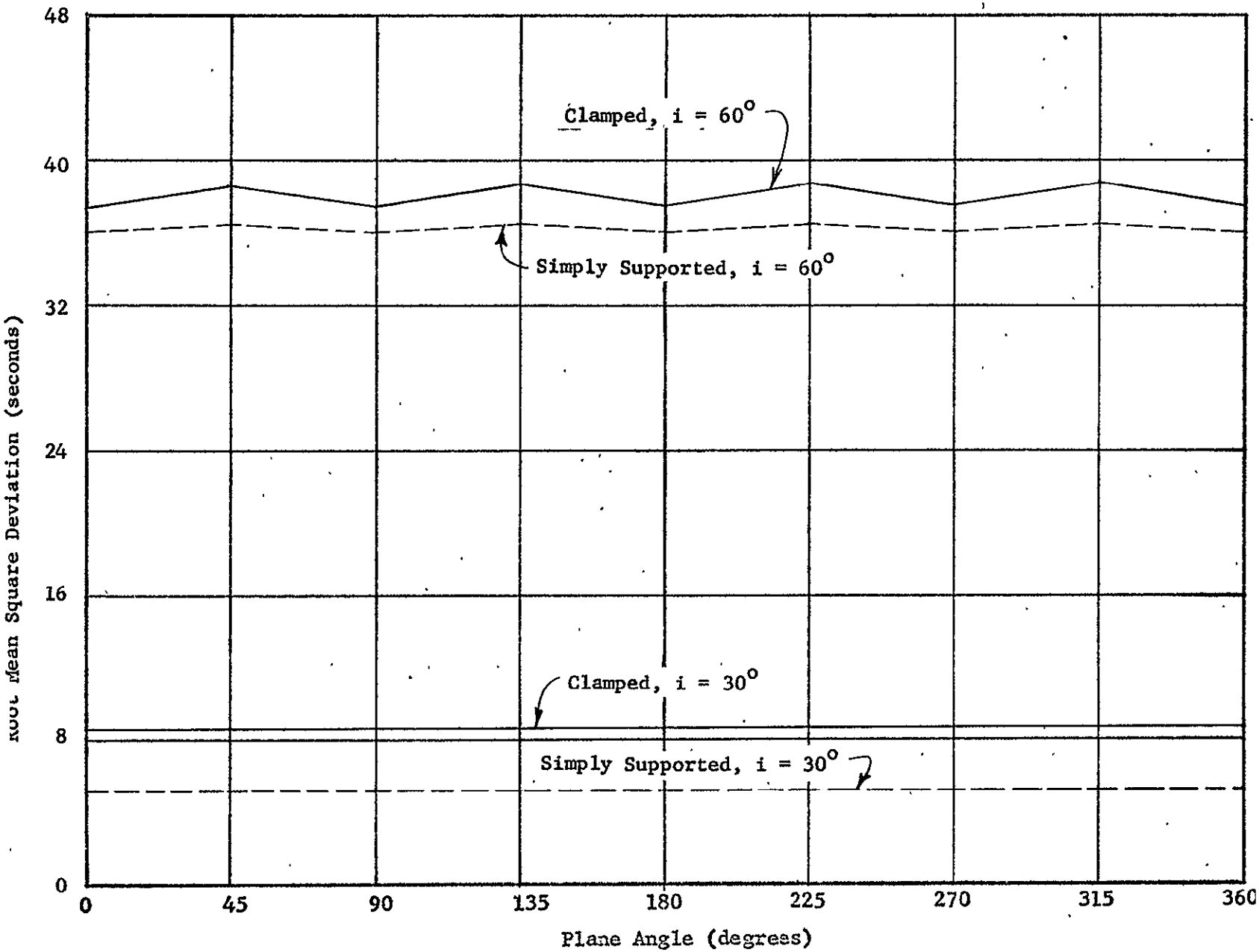

Figure 42. RMS of LOS Deviations - Variation of Edge Condition (Circle a)

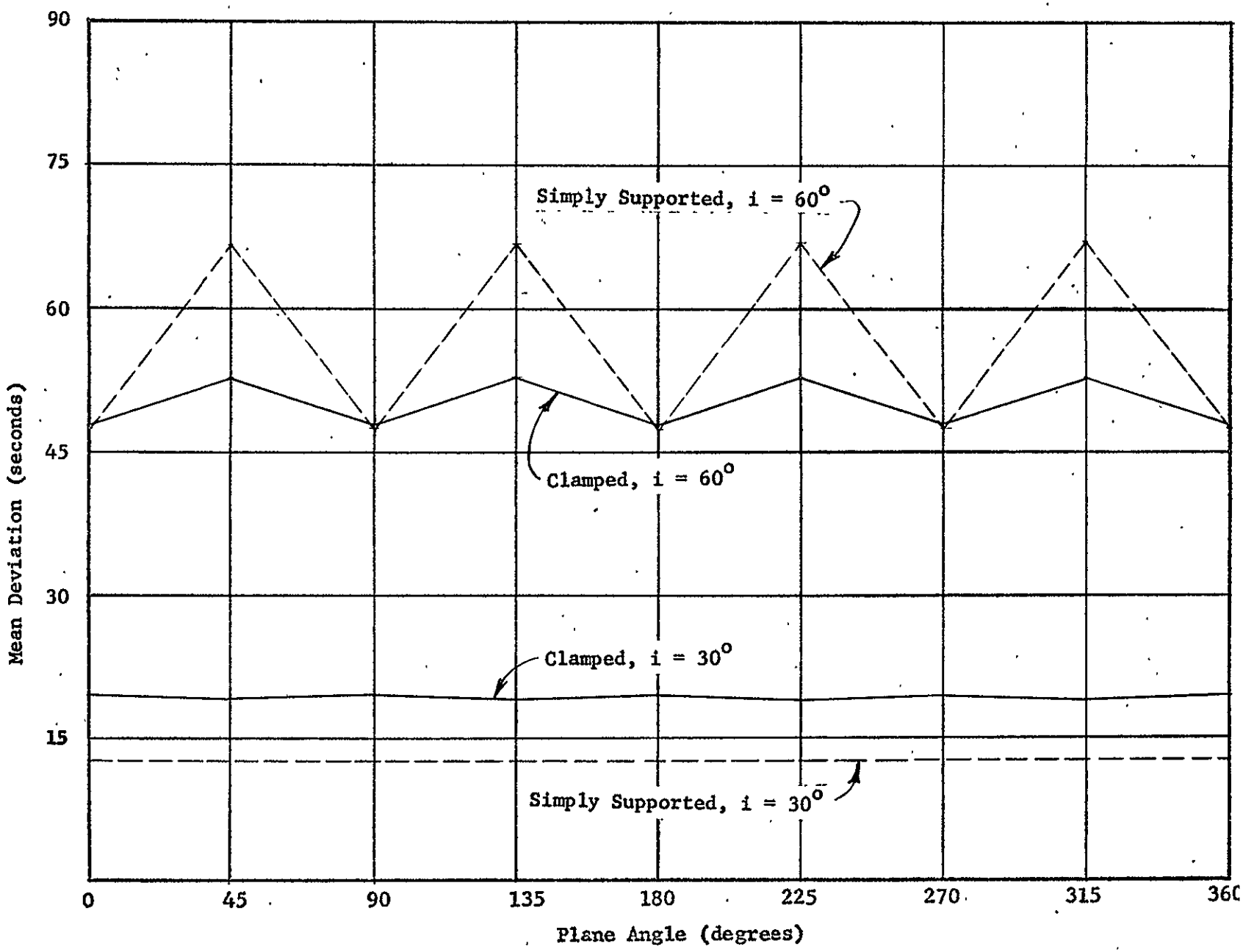

Figure 43. Mean of LOS Deviations - Variation of Edge Condition (Square d)

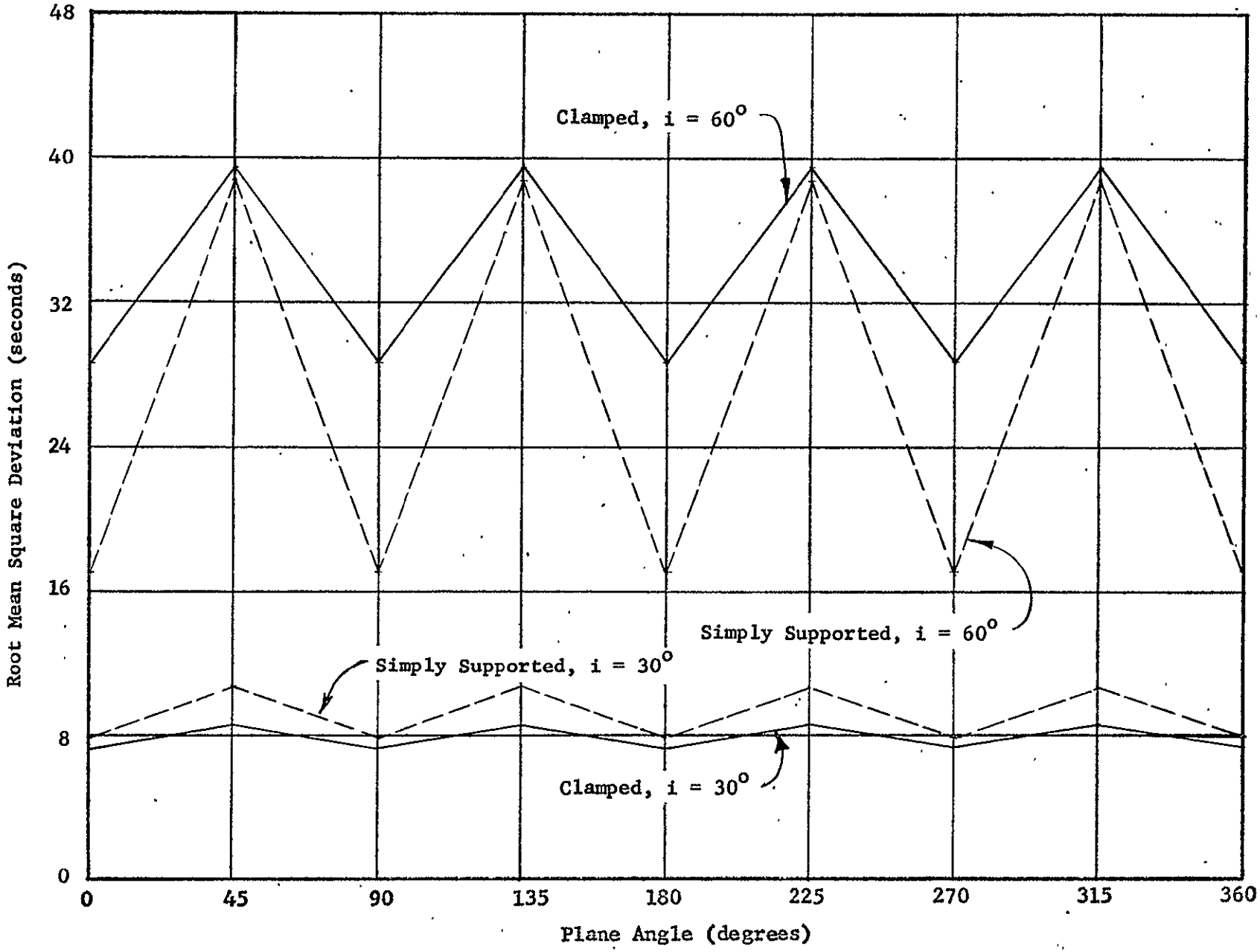

Figure 44. RMS of LOS Deviations - Variation of Edge Condition (Square d)

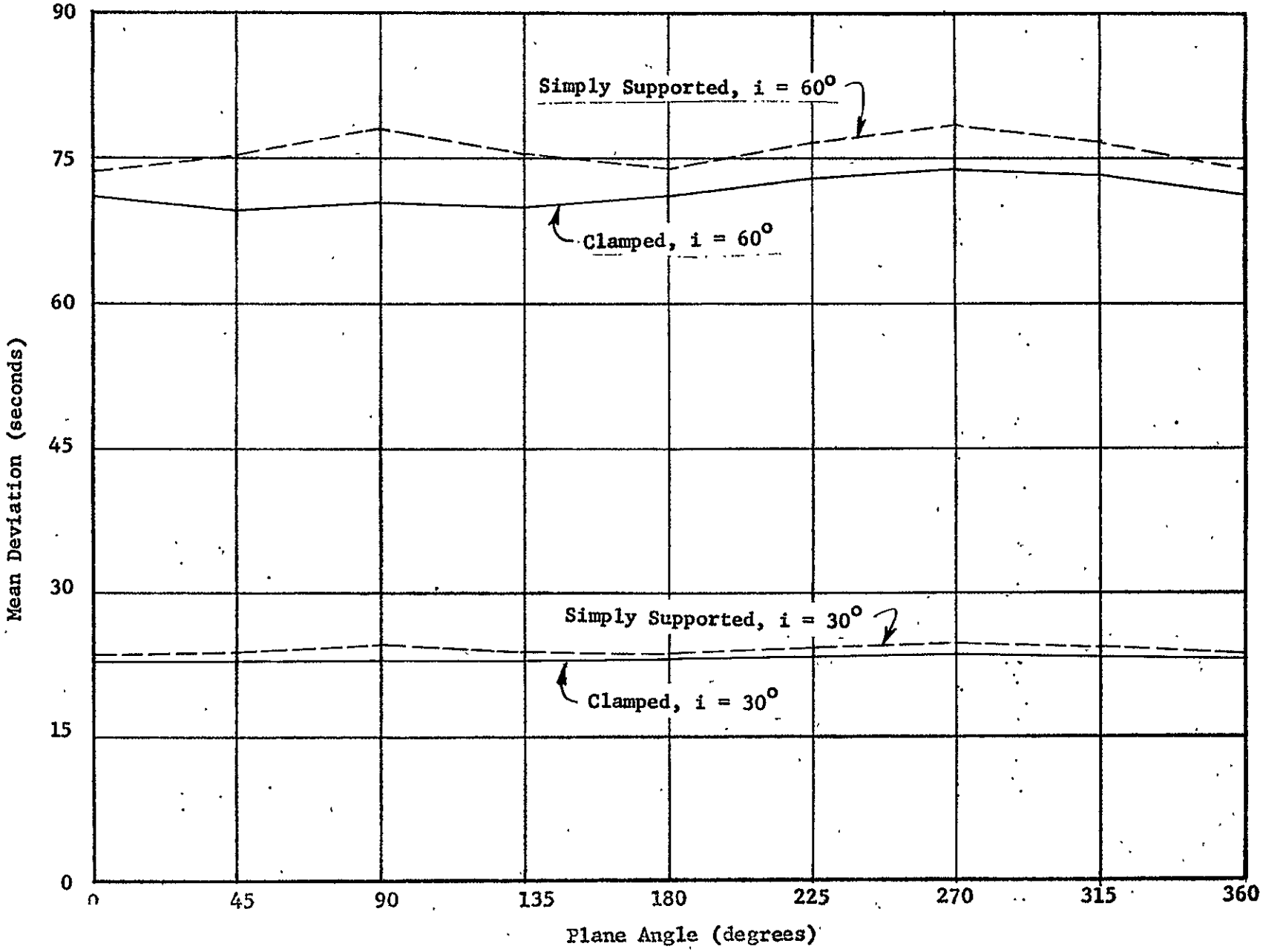

Figure 45. Mean of LOS Deviations - Variation of Edge Condition (Trapezoid g)

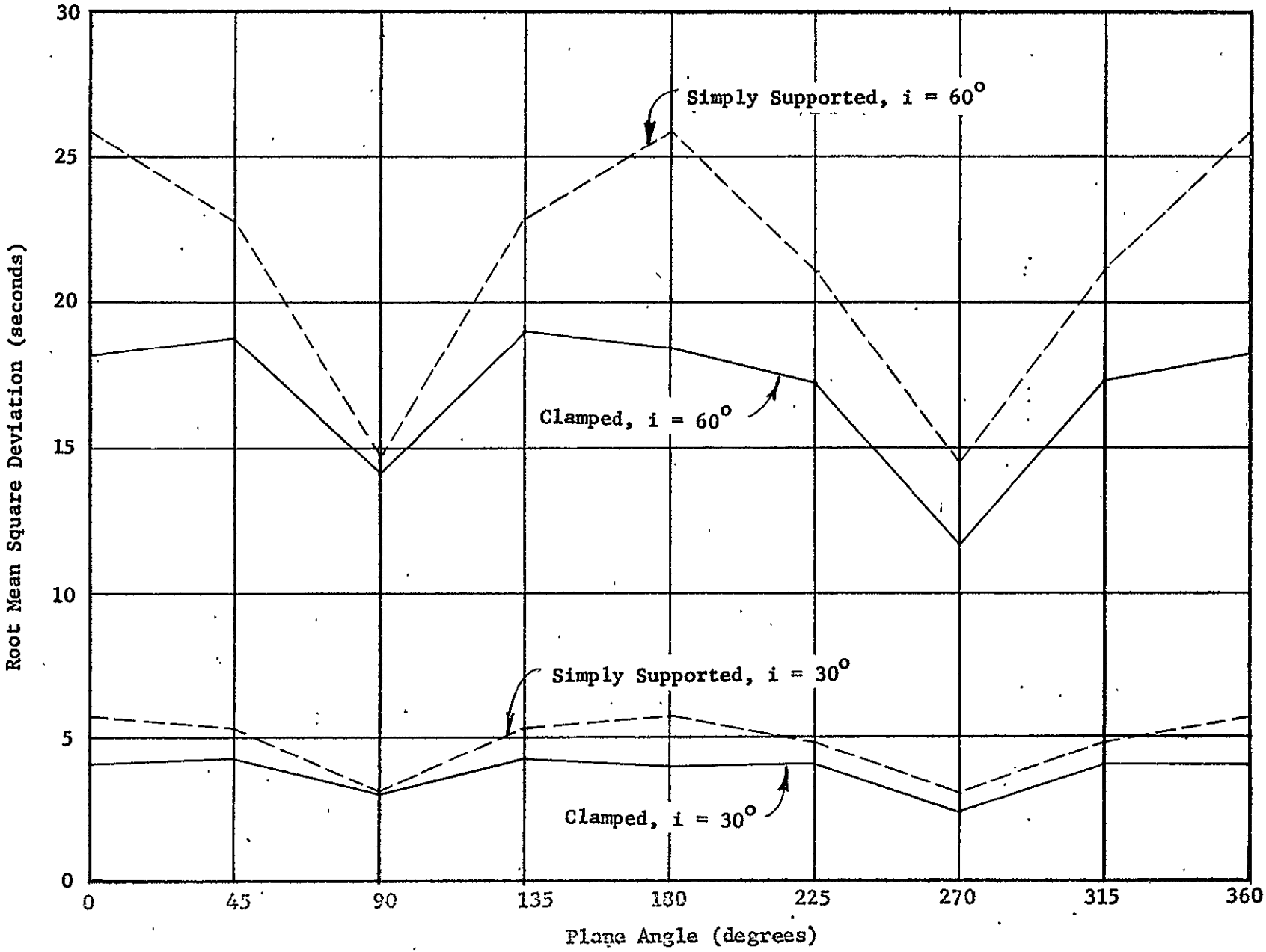

Figure 46. RMS of LOS Deviations - Variation of Edge Condition (Trapezoid g)

Table 7

Rankings for Variation of Edge Support Condition

Planform	Edge Condition	Mean Value	RMS Value	Mean Value Variation	Overall Ranking
Circle a	Clamped	1	12	2	15
Circle a	Simply Supported	6	8	2	16
Square d	Clamped	3	10	6	19
Square d	Simply Supported	2	6	8	16
Trapezoid g	Clamped	4	2	4	10
Trapezoid g	Simply Supported	5	4	6	15

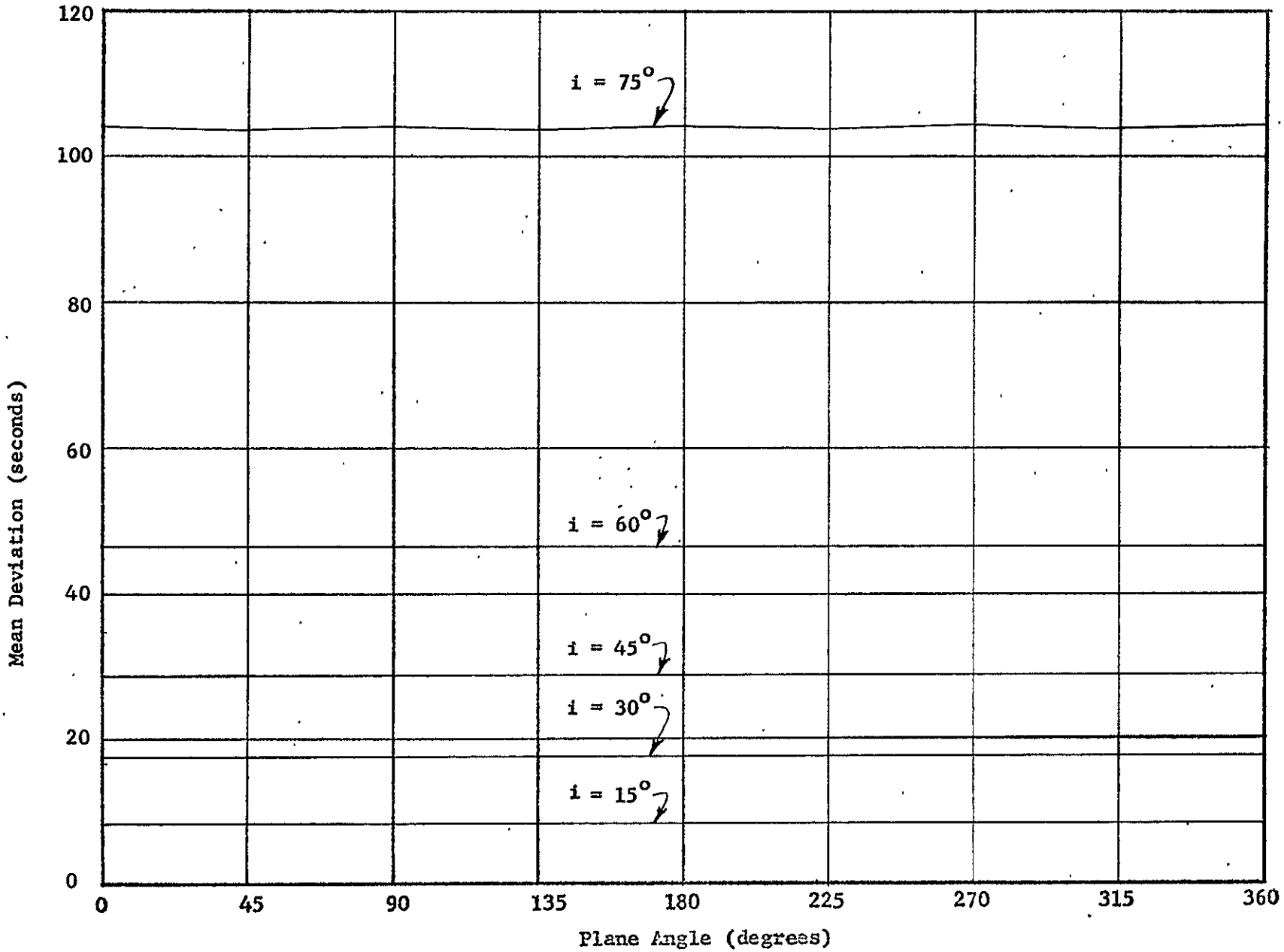

Figure 47. Mean of LOS Deviations - Variation of Incidence Angle (Circle a)

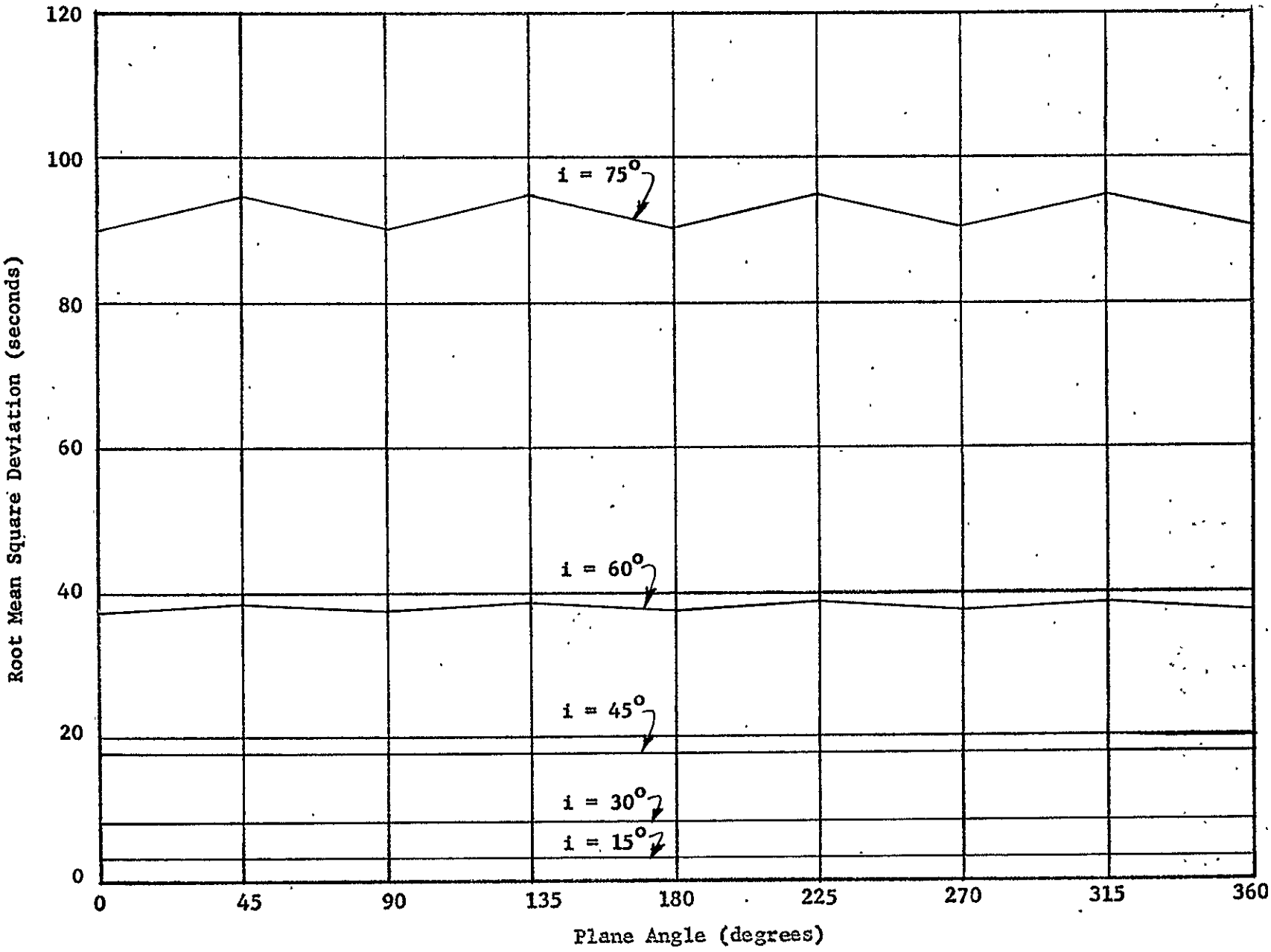

Figure 48. RMS of LOS Deviations - Variation of Incidence Angle (Circle a)

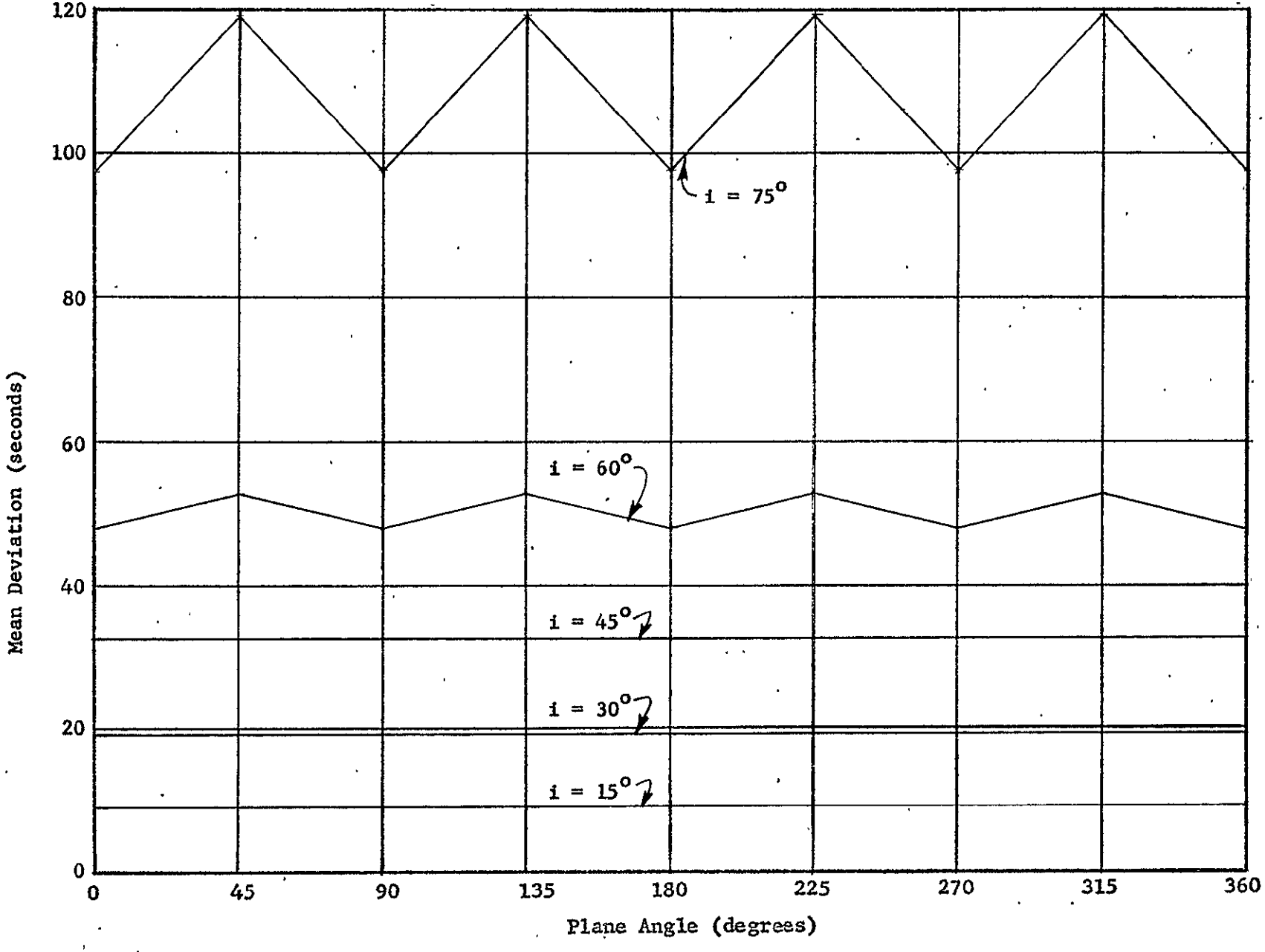

Figure 49. Mean of LOS Deviations - Variation of Incidence Angle (Square d)

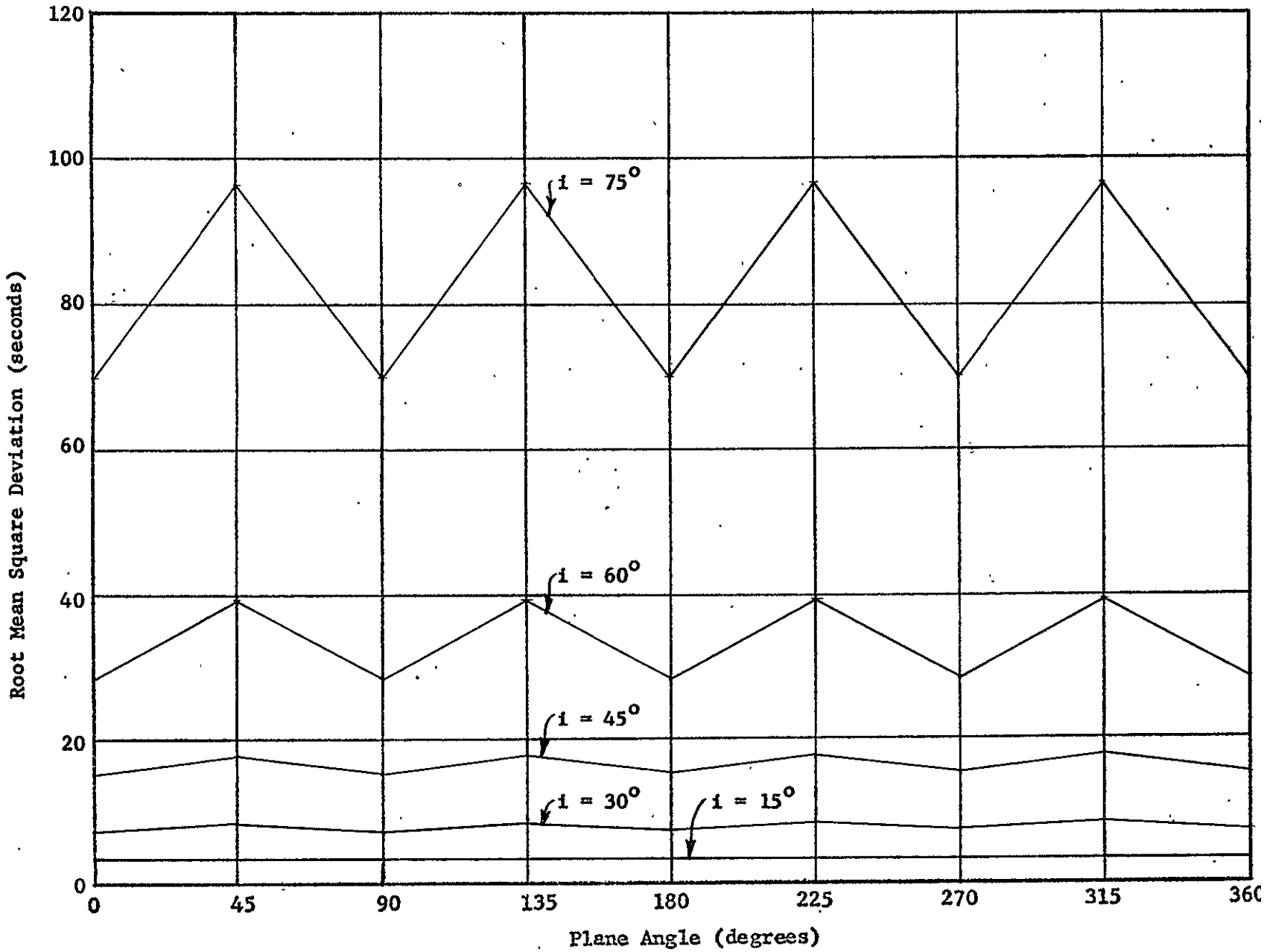

Figure 50. RMS of LOS Deviations - Variation of Incidence Angle (Square d)

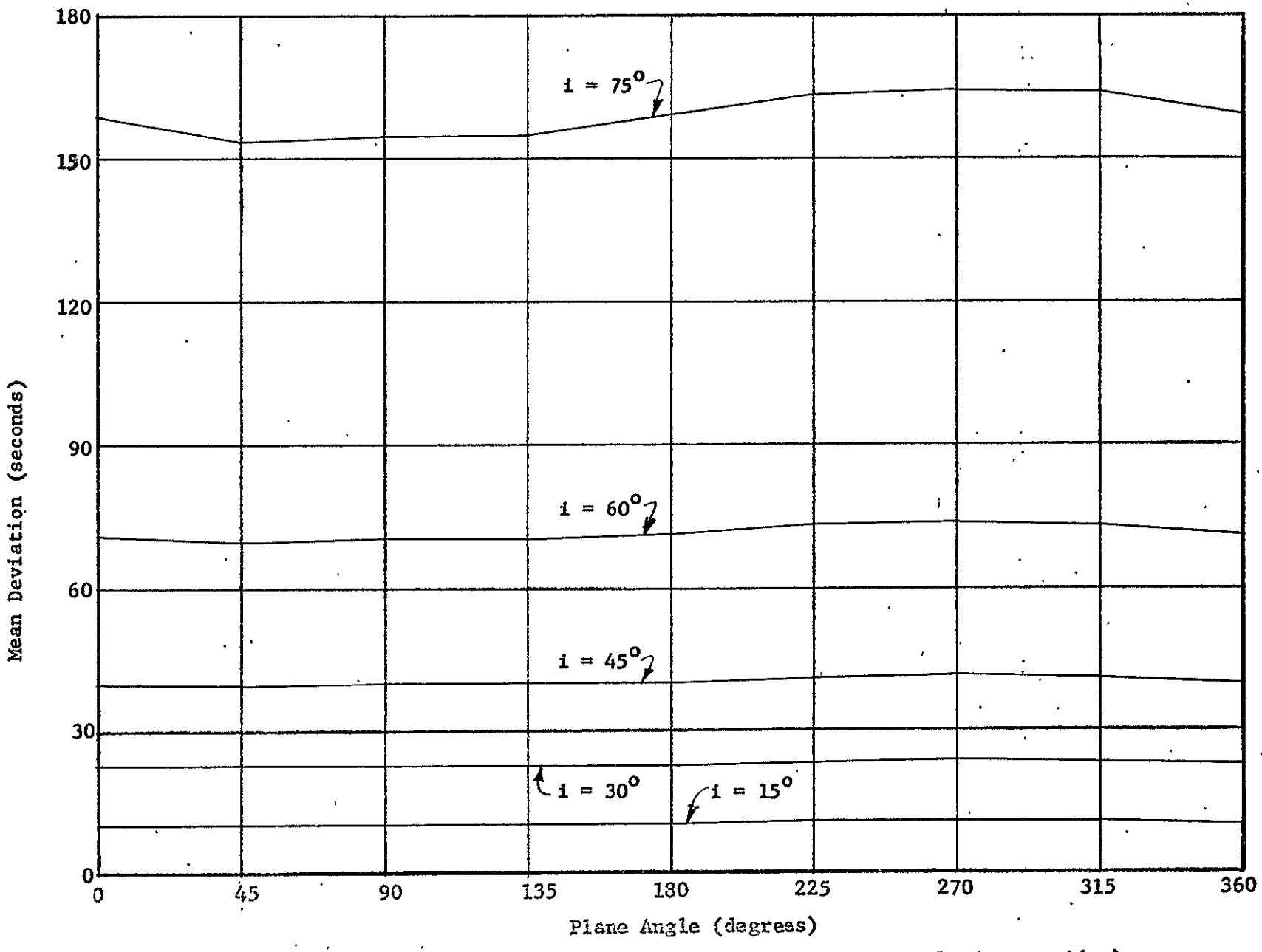

Figure 51. Mean of LOS Deviations - Variation of Incidence Angle (Trapezoid g)

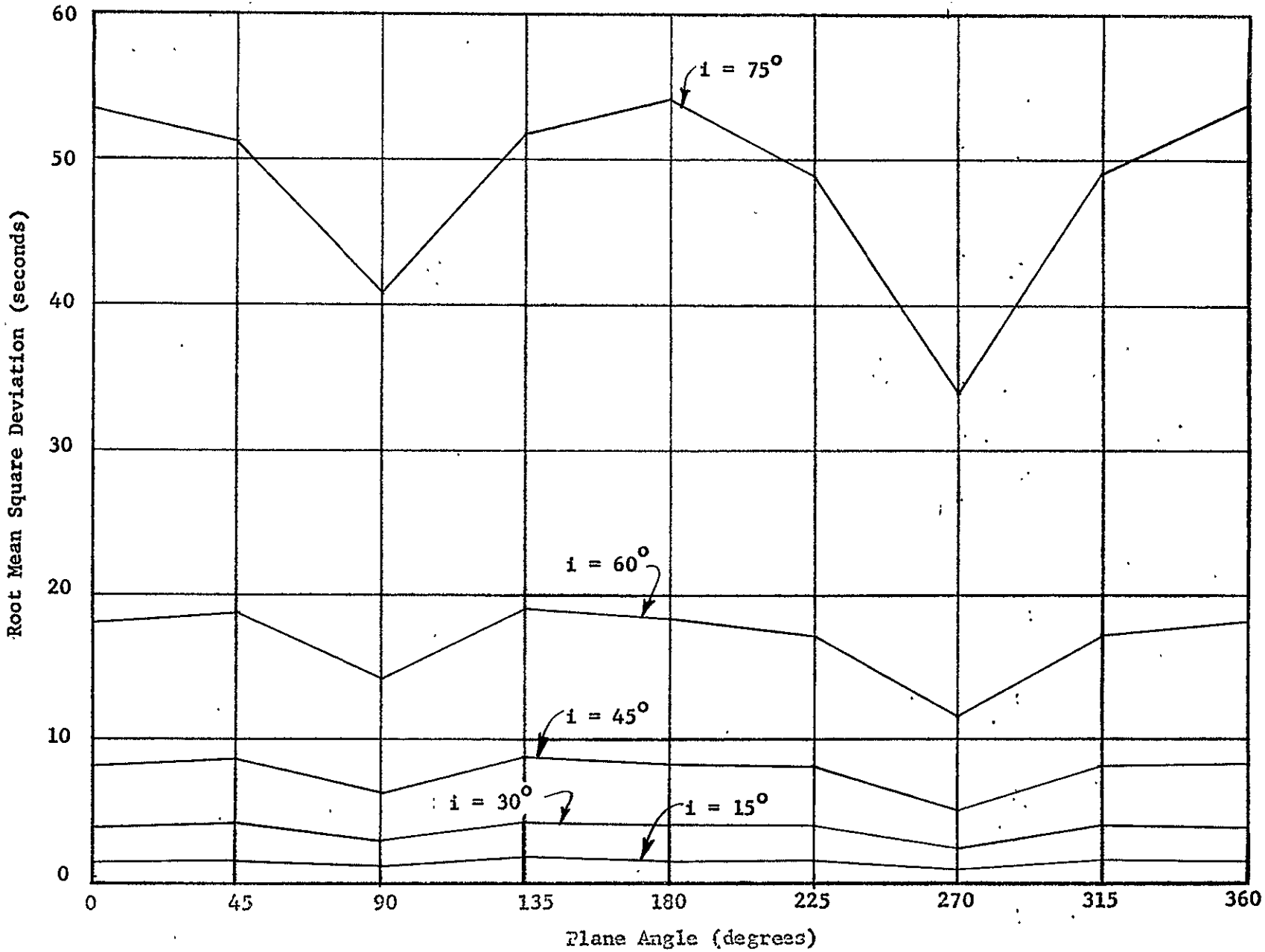

Figure 52. RMS of LOS Deviations - Variation of Incidence Angle (Trapezoid g)

1. The best window rankings occur for low incidence angles, small pressure differentials, and clamped edge conditions.

2. The studies of variations in the dimensional scale and pane thickness indicate the smallest and thickest windows have the best ranking.

3. Small pressure differentials, clamped edge conditions, small dimensional scales, and large pane thicknesses all tend to decrease the deflections of the window. This in turn causes less variation in the slopes and results in less deviation of lines-of-sight through the window.

4. The best planform shape is trapezoid h. In fact, the trapezoidal shape is better in general than either the elliptical (circular) or rectangular (square) shapes.

Double-Pane Configurations.- The design data studied in this subsection results from analyses performed on circle a, square d, rectangles e and f, and trapezoid g using certain nominal parameter values. These values consist of an interior pressure (P_1) of 5.2 psia, an interstitial pressure (P_2) of 10.0 psia, an exterior pressure (P_3) of zero psia, a dimensional scale of 1.0, pane thicknesses of 0.3 inch, a pane separation distance of 0.5 inch, and clamped edge conditions. The data for the double-pane configurations are presented in a form similar to that used for the single-pane configurations.

The effect of varying the shape of the panes in a double-pane configuration is studied using the data presented in Figs. 53 and 54.

These figures show the mean and rms deviations for circle a, square d, and trapezoid g as functions of the plane angle.

Table 8 gives the performance rankings for the three shapes considered in this study. This information indicates that circle a has the best characteristics in a double-pane configuration. It has the lowest mean deviation values, the second lowest rms deviation values, and the least variation in the mean deviation values.

The effect of variations in the pressure environment is determined by a study of Figs. 55 through 60. The analyses to obtain the data presented in these figures were performed for the nominal parameter values and additional interstitial pressures (P_2) of 7.5 and 15.0 psia. Figures 55 and 56 present the data for circle a, Figs. 57 and 58 the data for square d, and Figs. 59 and 56 the data for trapezoid g.

Rankings for the nine configurations of pressure environments investigated in this study are given in Table 9. The data in this table indicate that for circle a and square d the smallest interstitial pressure results in the best optical performance. Variations of the pressure environment for trapezoid g has no effect on the characteristics of the window.

Variations in the pane spacing value (i.e., the distance between the two panes of glass) are studied using the data shown in Figs. 61 through 66. In addition to the nominal parameter values, the analyses performed to obtain the data for these figures used pane spacing values of 0.25, 1.0, and 2.0 inches. Figures 61 and 62 present the data for circle a, Figs. 63 and 64 the data for square d, and Gis. 65 and 66 the data for trapezoid g.

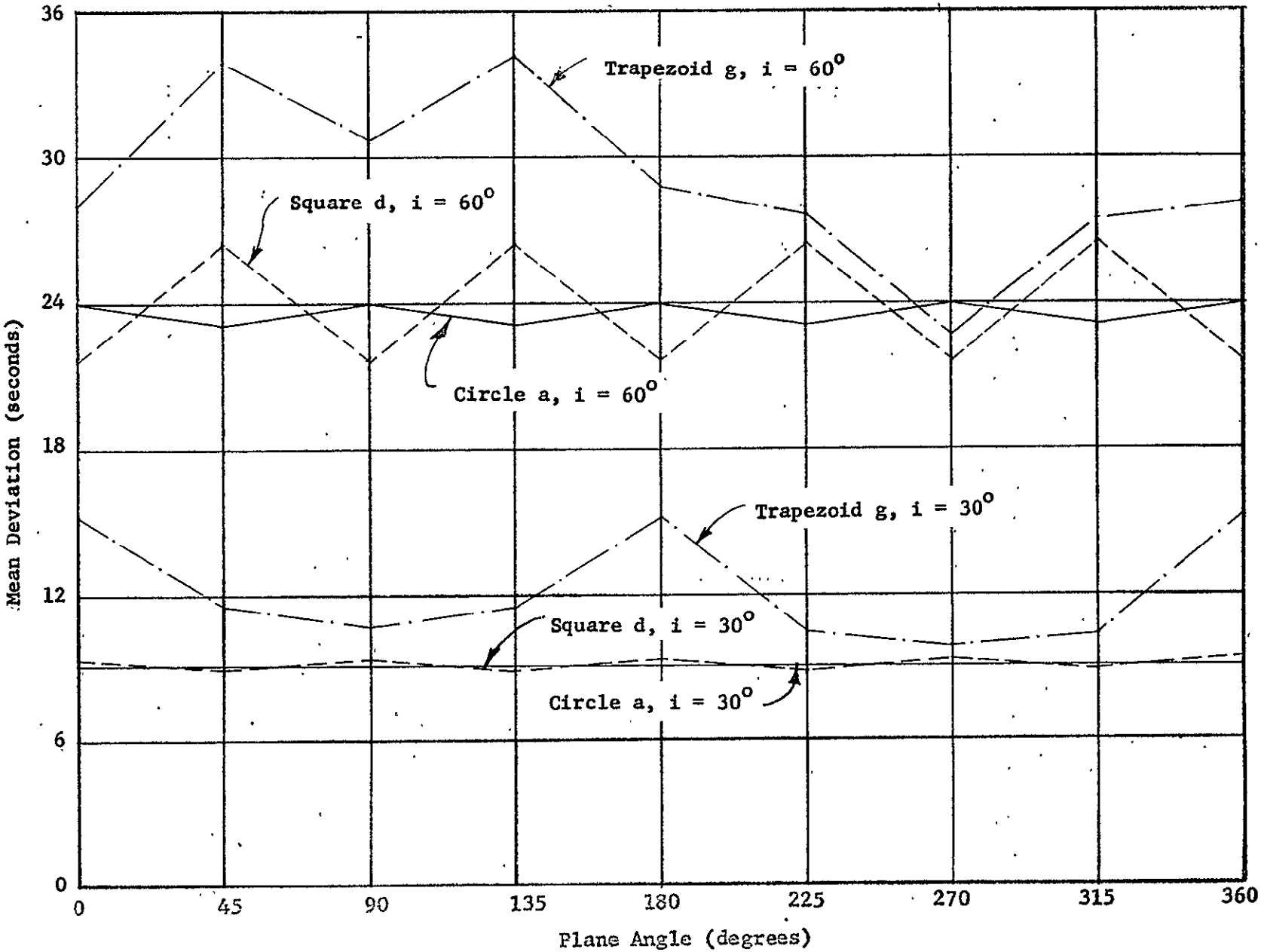

Figure 53. Mean of LOS Deviations - Variation of Pane Shape

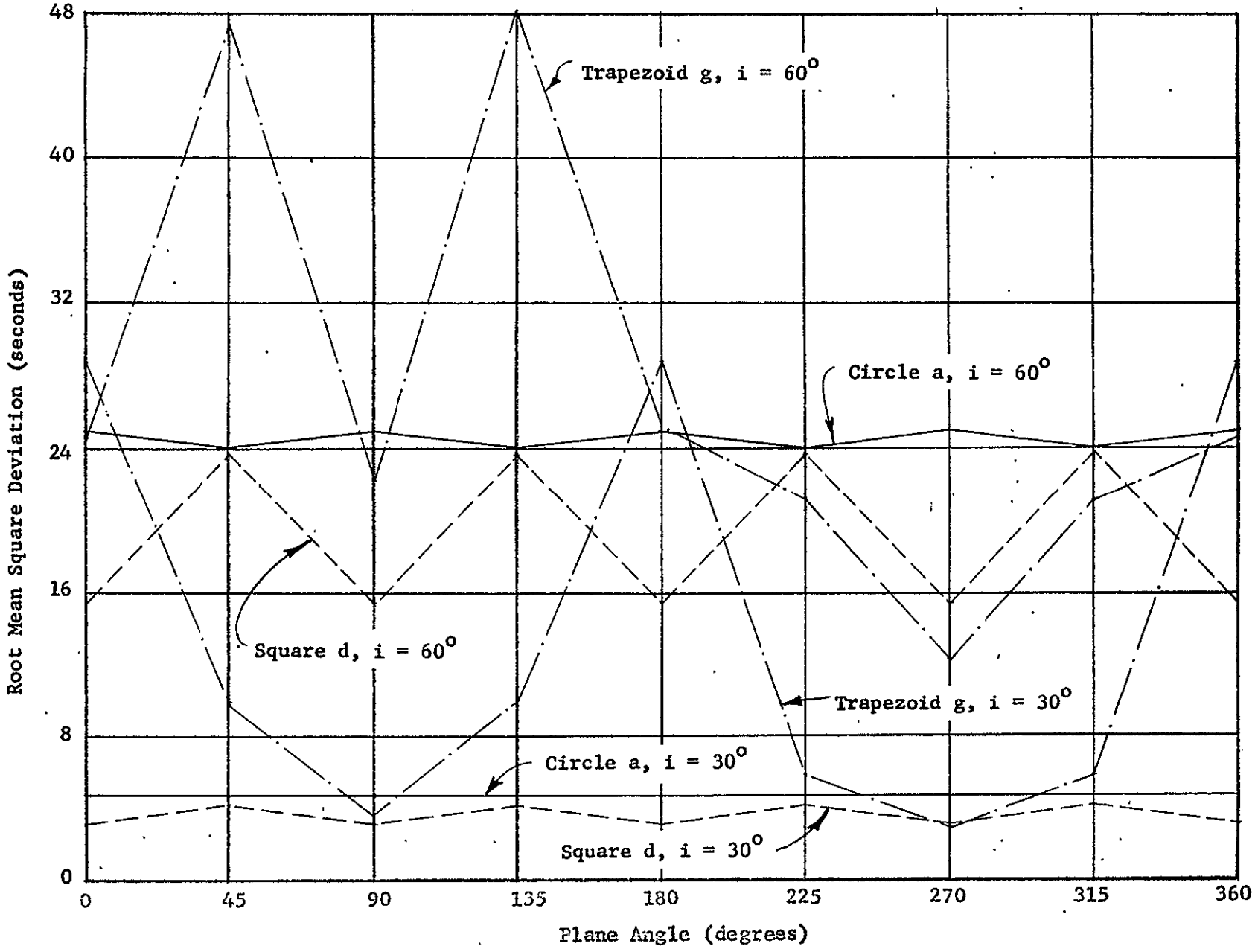

Figure 54. RMS of LOS Deviations - Variation of Pane Shape

Table 8

Rankings for Variation of Pane Shapes

Shape	Mean Value	RMS Value	Mean Value Variation	Overall Ranking
Circle a	1	4	2	7
Square d	2	2	4	8
Trapezoid g	3	6	6	15

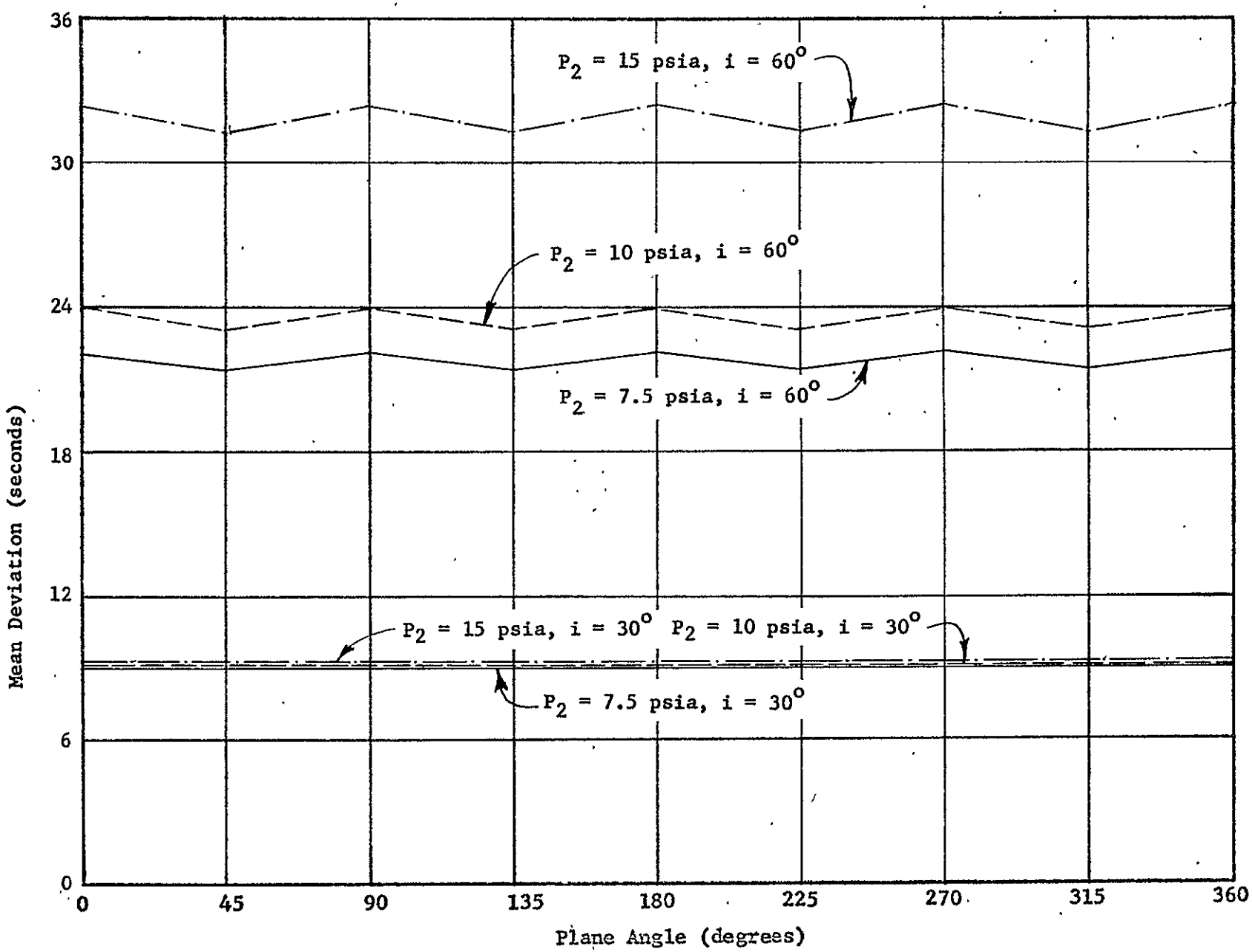

Figure 55. Mean of LOS Deviations - Variation of Pressure Environment (Circle a)

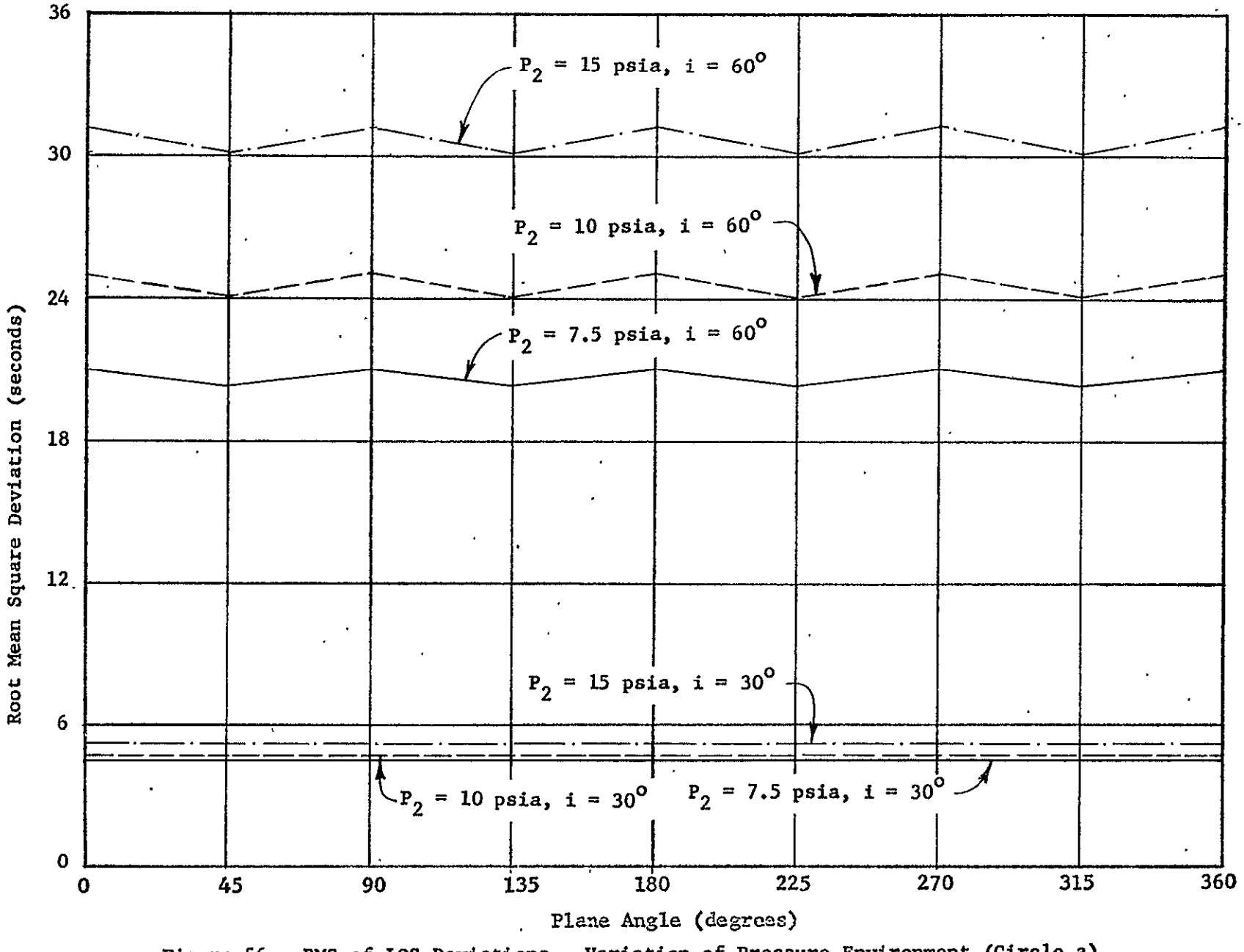

Figure 56. RMS of LOS Deviations - Variation of Pressure Environment (Circle a)

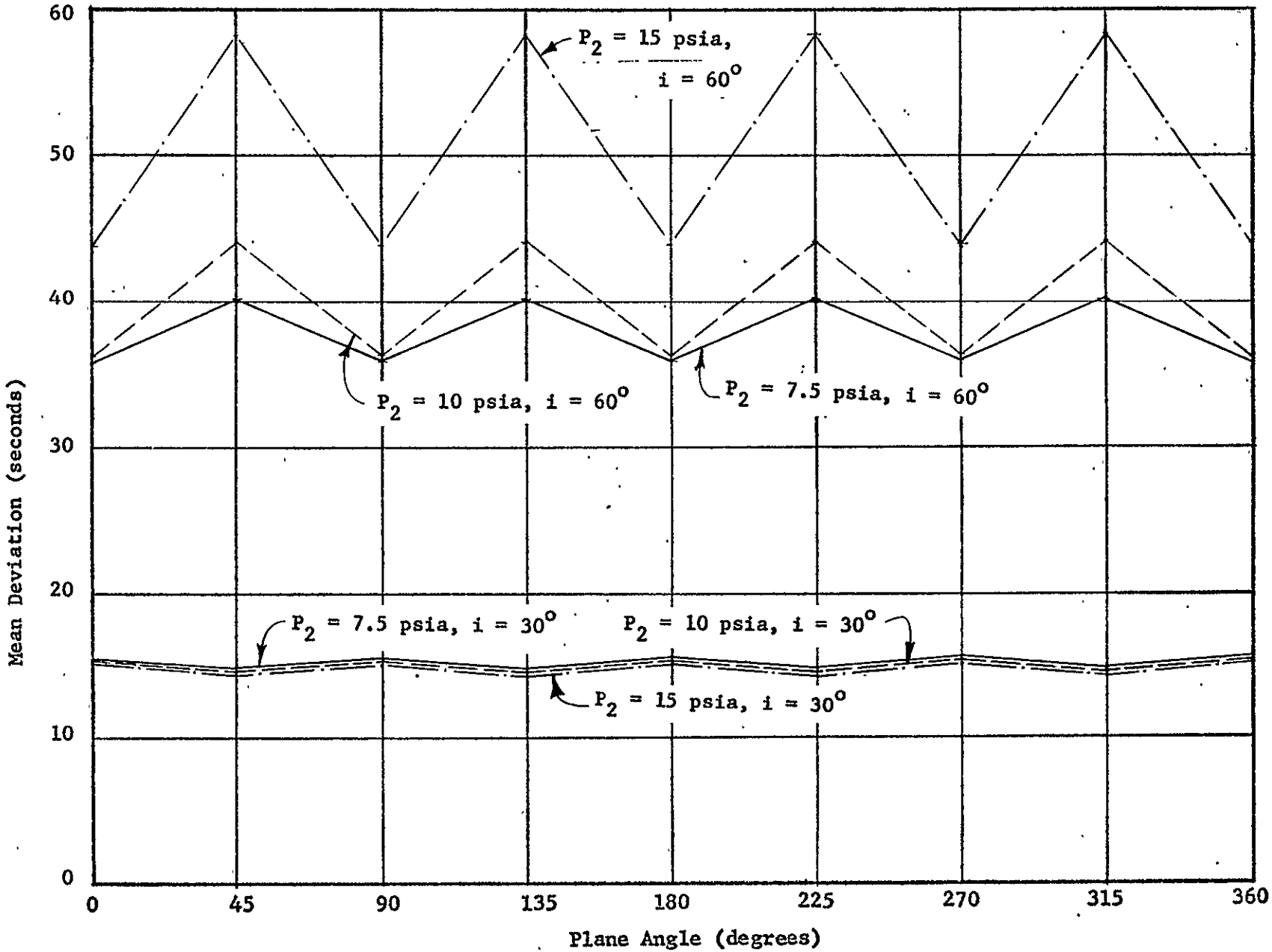

Figure 57. Mean of LOS Deviations - Variation of Pressure Environment (Square d)

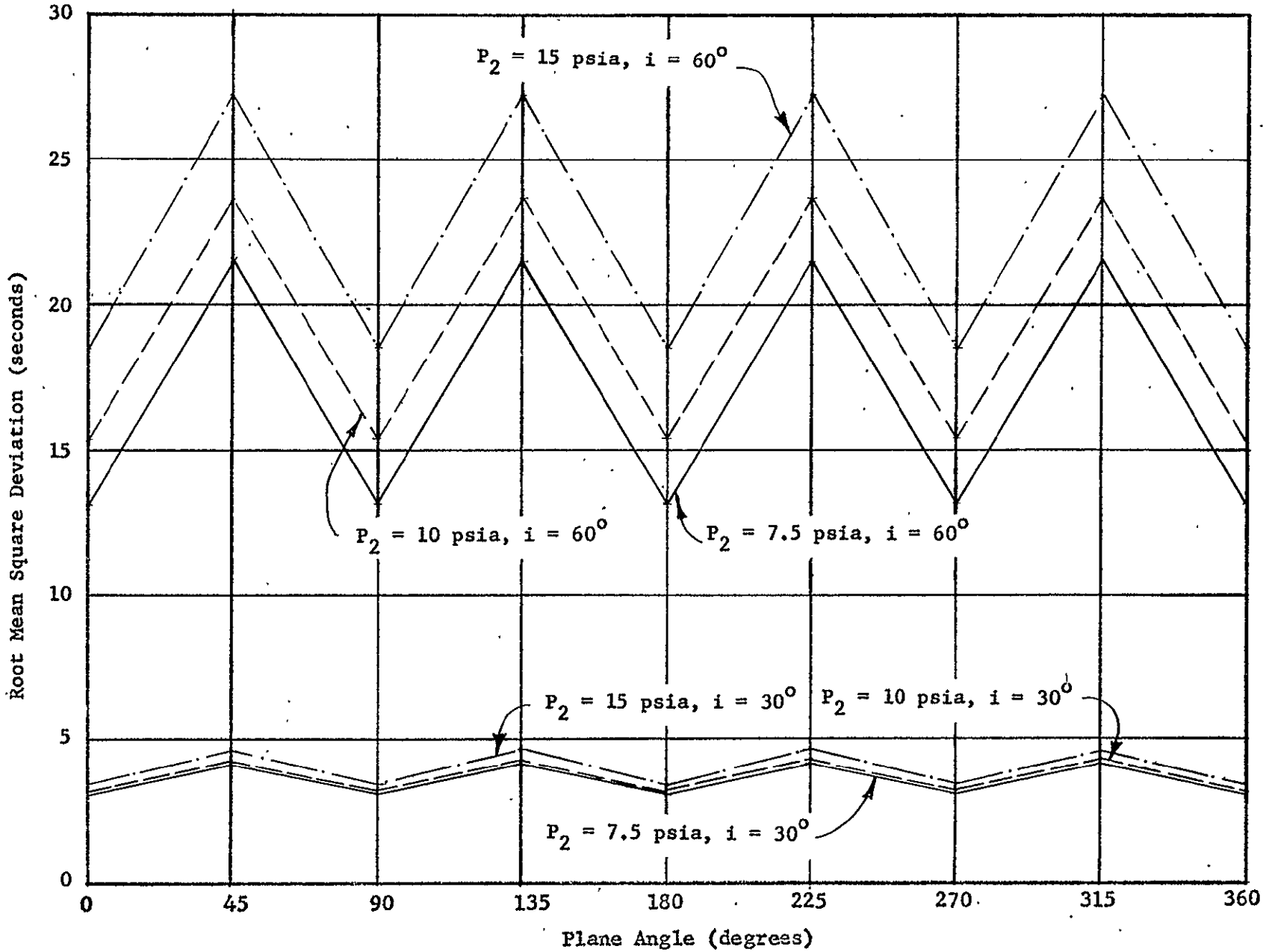

Figure 58. RMS of LOS Deviations - Variation of Pressure Environment (Square d)

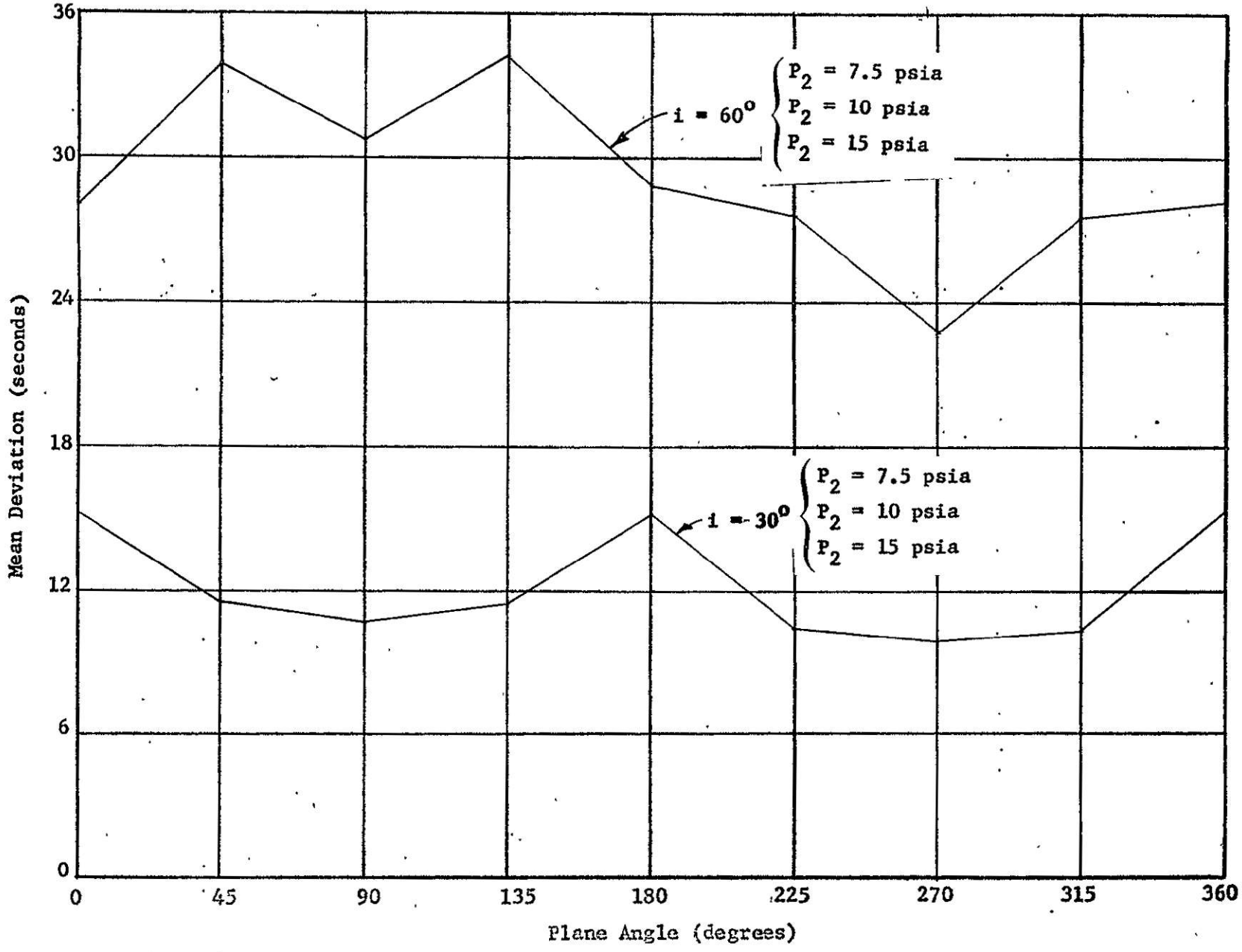

Figure 59. Mean of LOS Deviations - Variation of Pressure Environment (Trapezoid g)

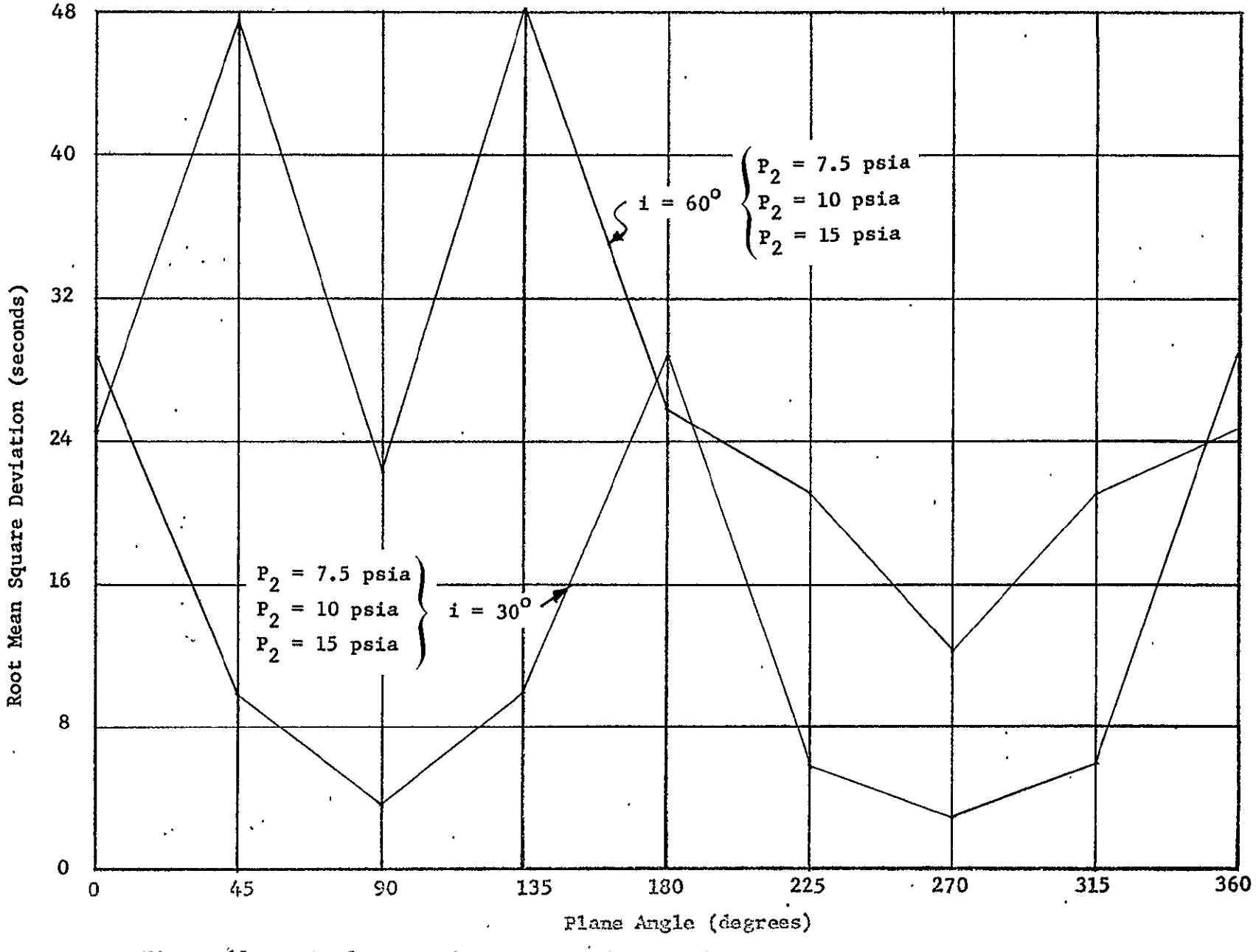

Figure 60. RMS of LOS Deviations - Variation of Pressure Environment (Trapezoid g)

Table 9

Rankings for Variation of Pressure Environment

Planform	P_2 (psia)	Mean Value	RMS Value	Mean Value Variation	Overall Ranking
Circle a	7.5	1	6	2	9
Circle a	10.0	3	10	4	17
Circle a	15.0	6	12	6	24
Square d	7.5	2	2	8	12
Square d	10.0	4	4	10	18
Square d	15.0	5	6	12	23
Trapezoid g	7.5	6	14	14	34
Trapezoid g	10.0	6	14	14	34
Trapezoid g	15.0	6	14	14	34

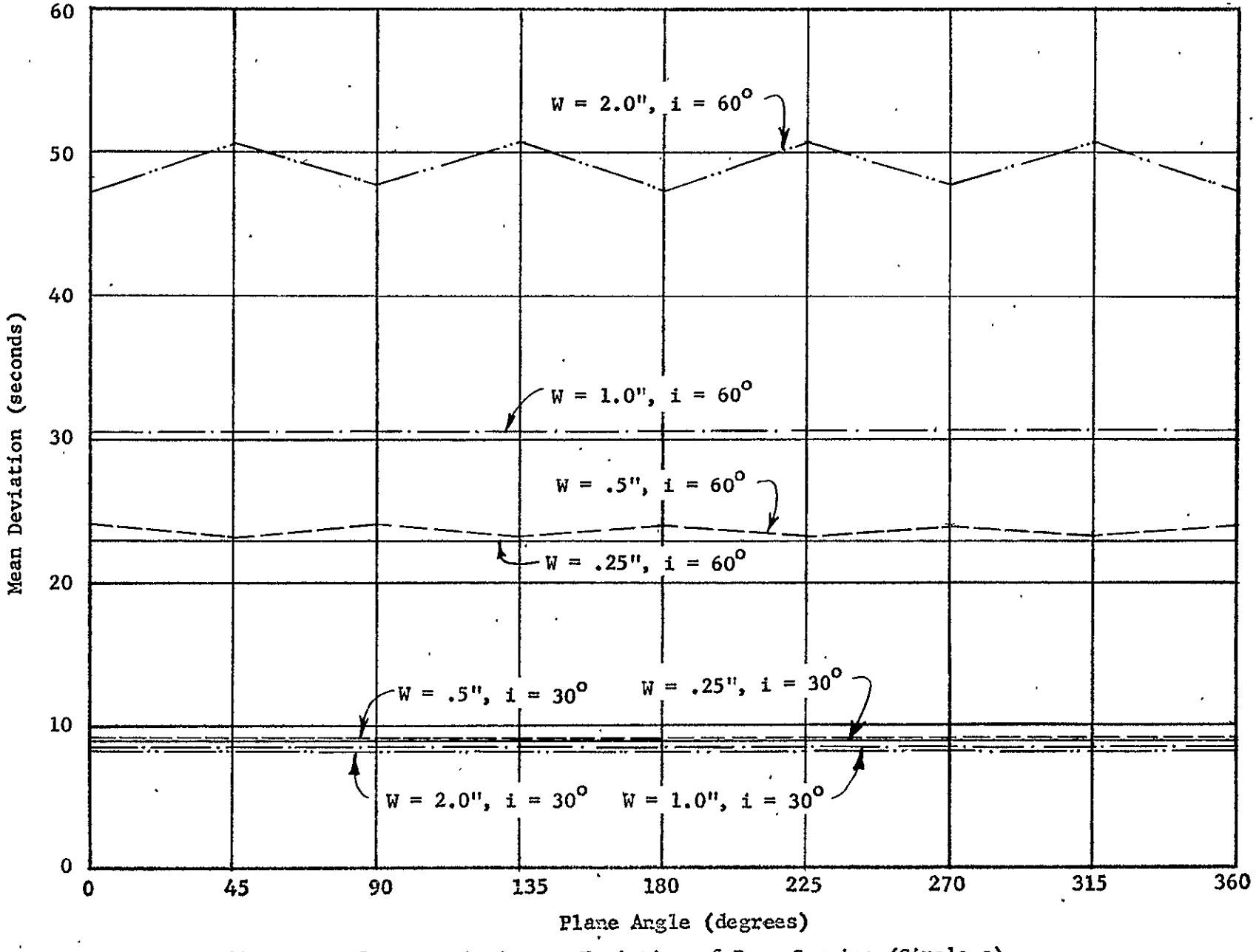

Figure 61. Mean of LOS Deviations - Variation of Pane Spacing (Circle a)

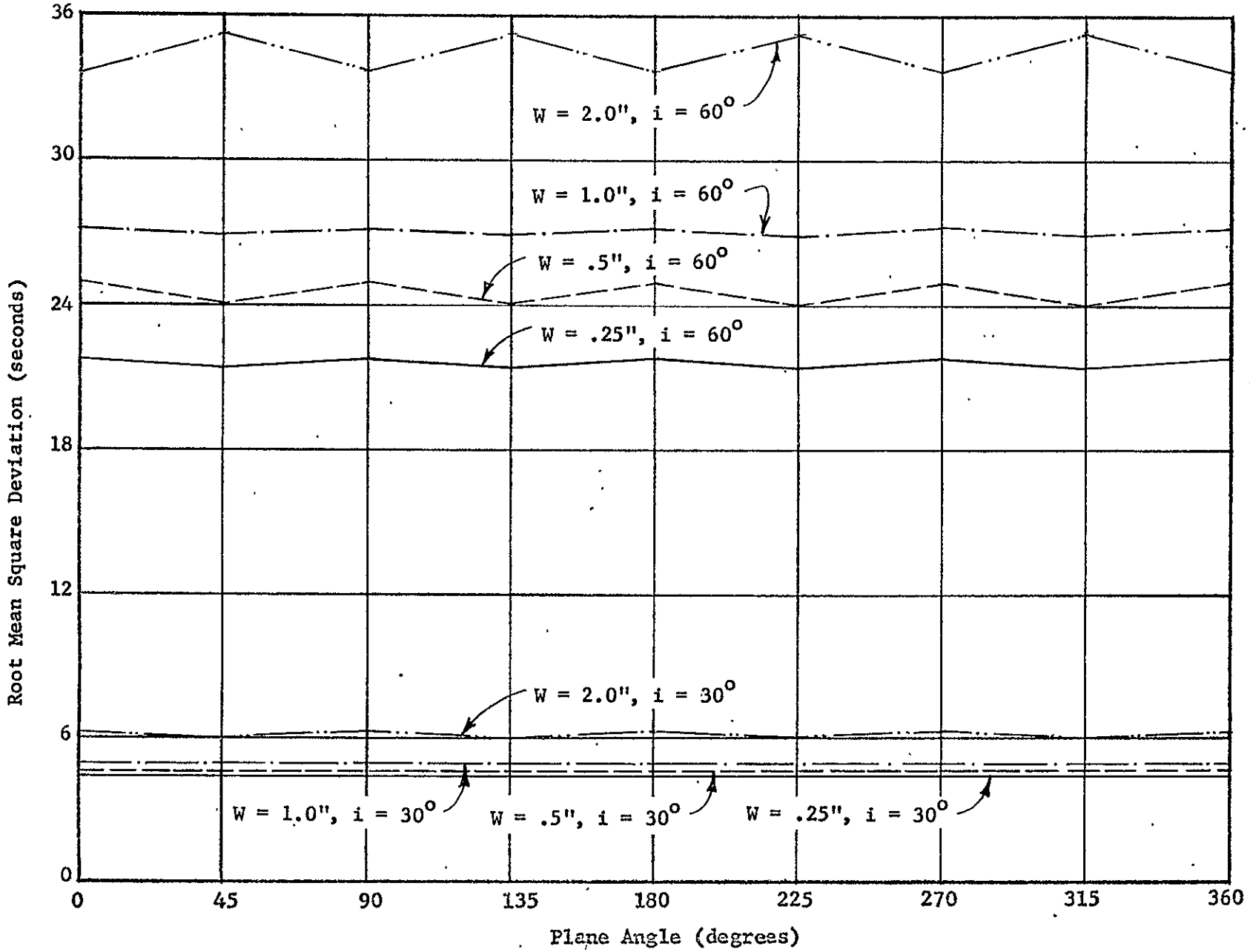

Figure 62. RMS of LOS Deviations - Variation of Pane Spacing (Circle a)

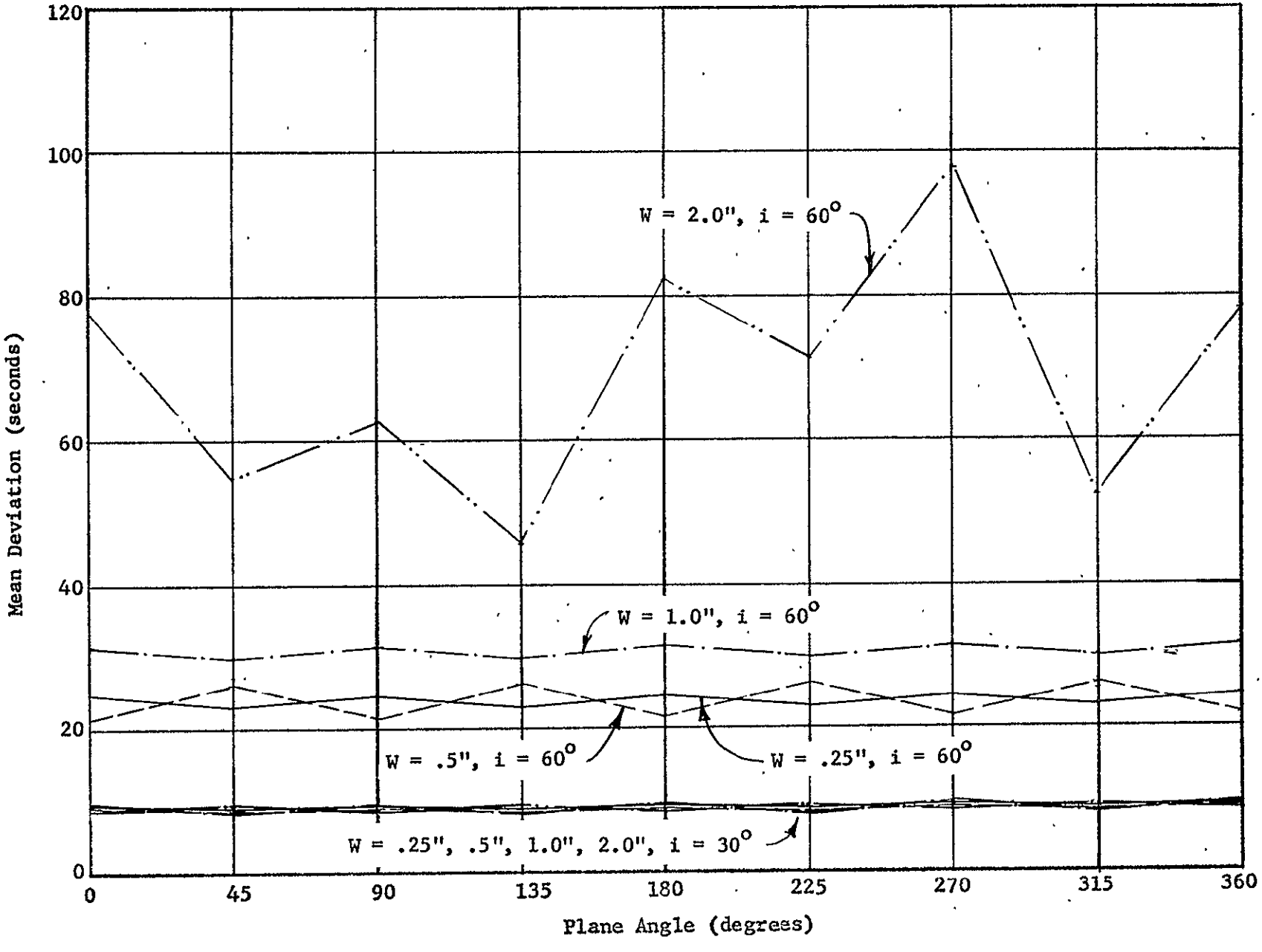

Figure 63. Mean of LOS Deviations - Variation of Pane Spacing (Square d)

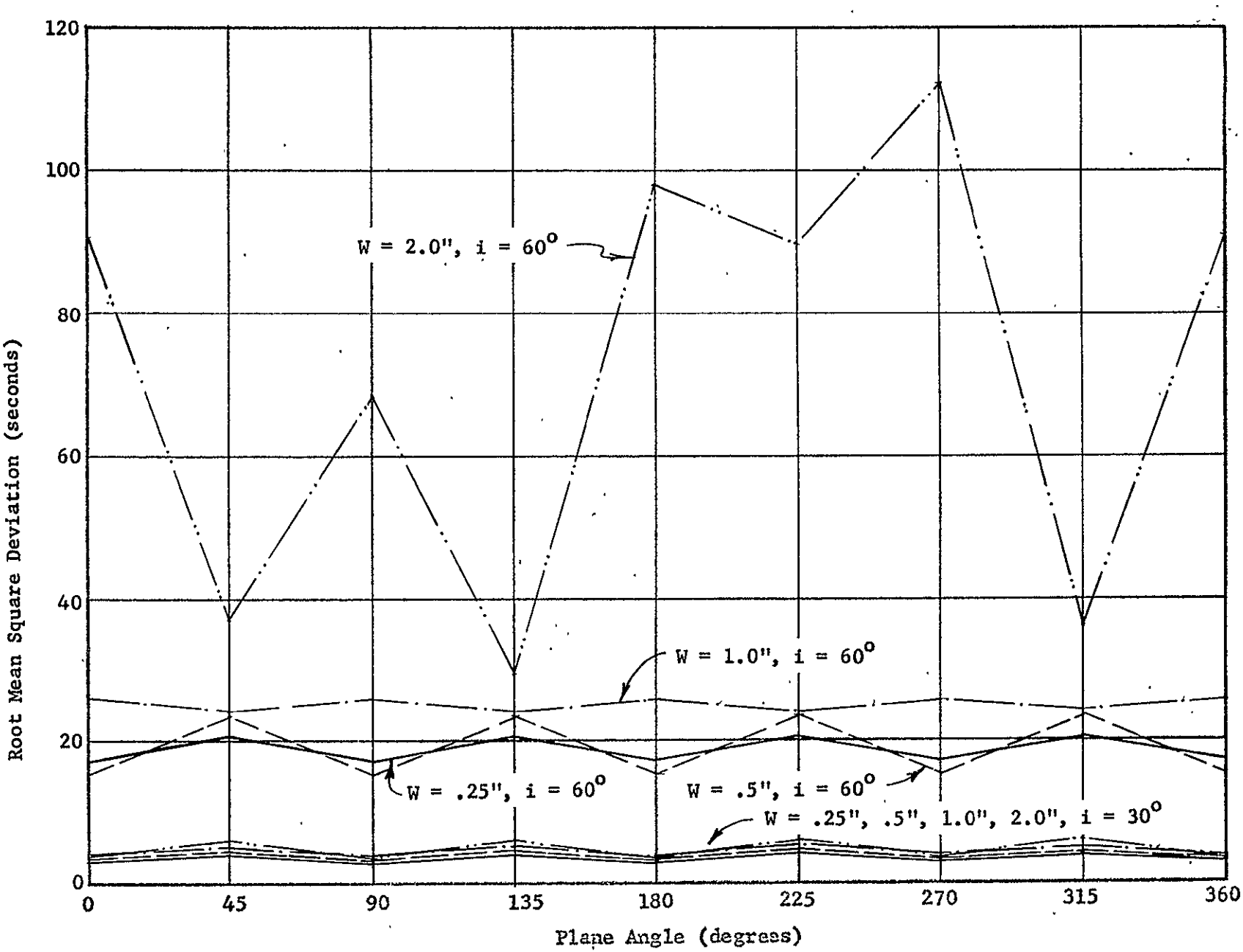

Figure 64. RMS of LOS Deviations - Variation of Pane Spacing (Square d)

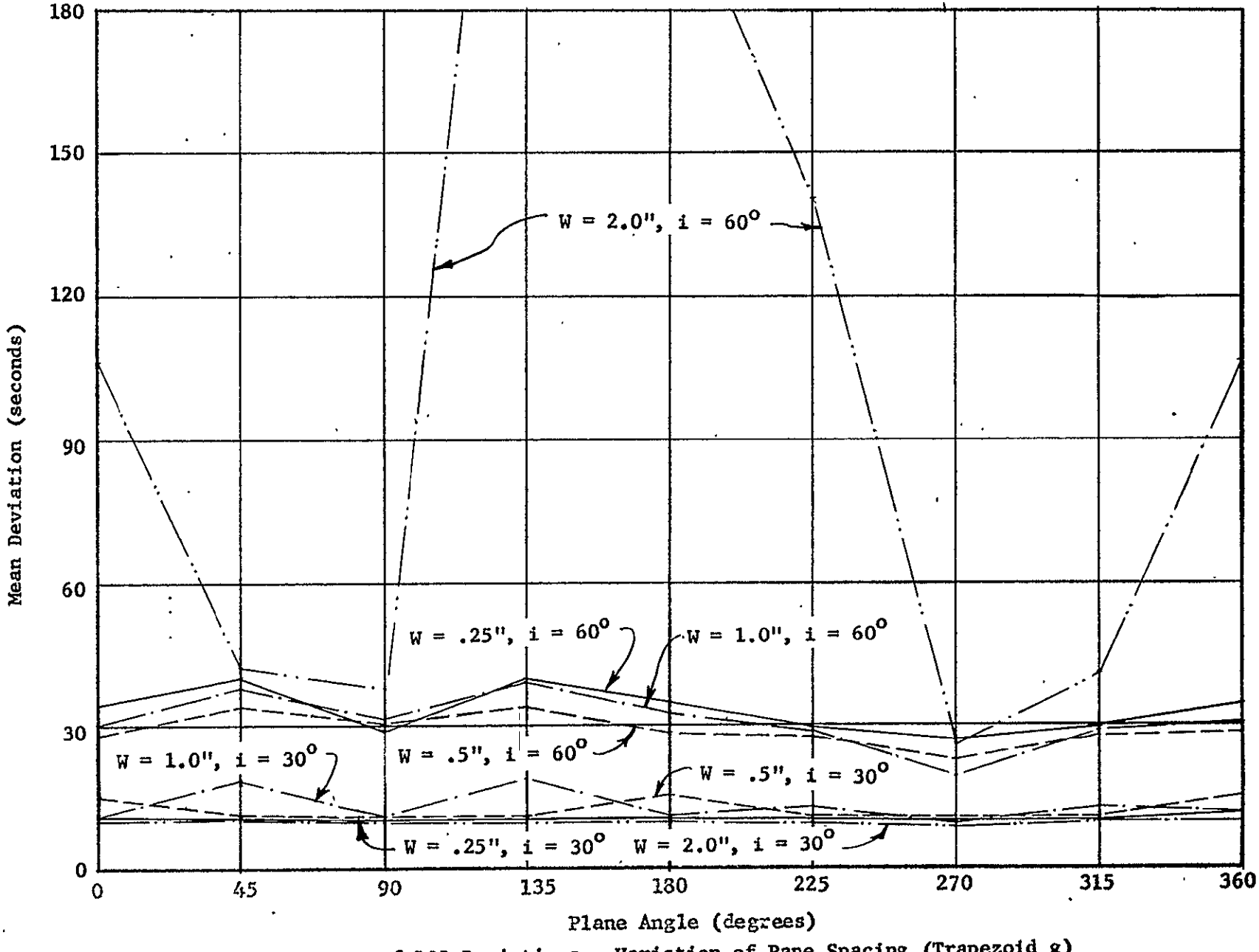

Figure 65. Mean of LOS Deviations - Variation of Pane Spacing (Trapezoid g)

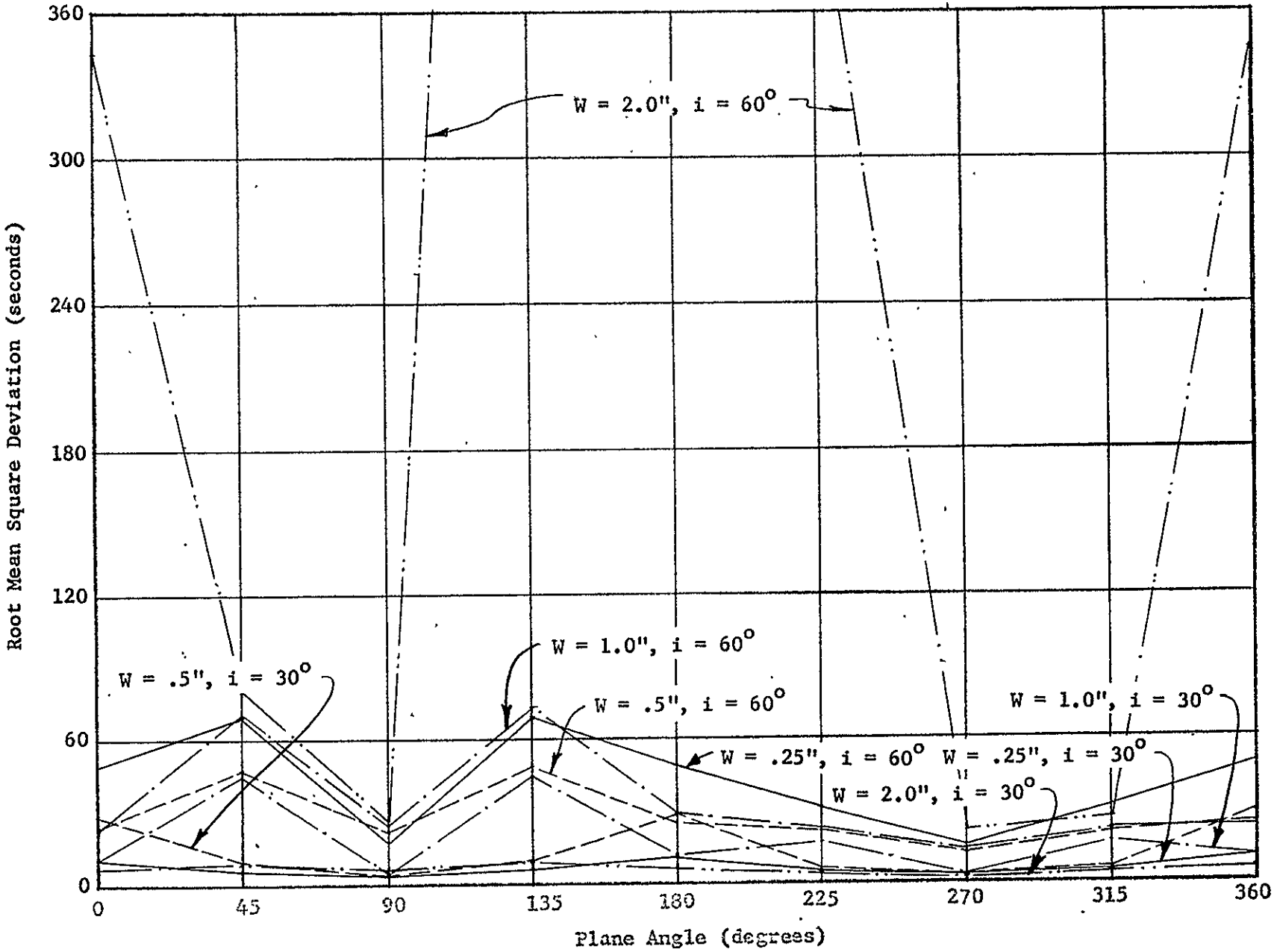

Figure 66. RMS of LOS Deviations - Variation of Pane Spacing (Trapezoid g)

Rankings for the twelve configurations of pane spacings investigated are given in Table 10. The rankings indicate that circle a with a pane spacing of 0.25 inch has the best characteristics. This circle has the lowest mean deviation values, the third lowest rms deviation values, and the second lowest mean value variations. The table also indicates that the spacing of 0.25 inch gives the best characteristics for square d and that of 0.5 inch the best for trapezoid g.

Effects of varying the edge support conditions are studied by considering the data presented in Figs. 67 through 72. In addition to the nominal parameter values, the analyses performed to obtain the data of these figures used simply supported edge conditions. The data for circle a are presented in Figs. 67 and 68, for square d in Figs. 69 and 70, and for trapezoid g in Figs. 71 and 72.

Table 11 presents the rankings for the six configurations investigated in this study. The data in this table indicate that for circle a and square d the clamped edge conditions give better ranking than the simply supported edge conditions. For trapezoid g, simply supported edge conditions produce the better ranking.

The effect on window optical performance of variations in the incidence angle is studied using the data presented in Figs. 73 through 78. The analyses from which these data were obtained were performed using the nominal parameter values. Figures 73 and 74 present the data for circle a, Figs. 75 and 76 the data for square d, and Figs. 77 and 78 the data for trapezoid g.

Table 10

Rankings for Variation of Pane Spacing

Planform	Pane Spacing	Mean Value	RMS Value	Mean Value Variation	Overall Ranking
Circle a	0.25"	1	6	4	11
Circle a	0.5"	2	8	6	16
Circle a	1.0"	5	12	2	19
Circle a	2.0"	10	14	12	36
Square d	0.25"	3	2	8	13
Square d	0.5"	4	4	14	22
Square d	1.0"	6	10	10	26
Square d	2.0"	11	22	22	55
Trapezoid g	0.25"	9	18	18	43
Trapezoid g	0.5"	7	16	16	39
Trapezoid g	1.0"	8	20	20	48
Trapezoid g	2.0"	12	24	24	60

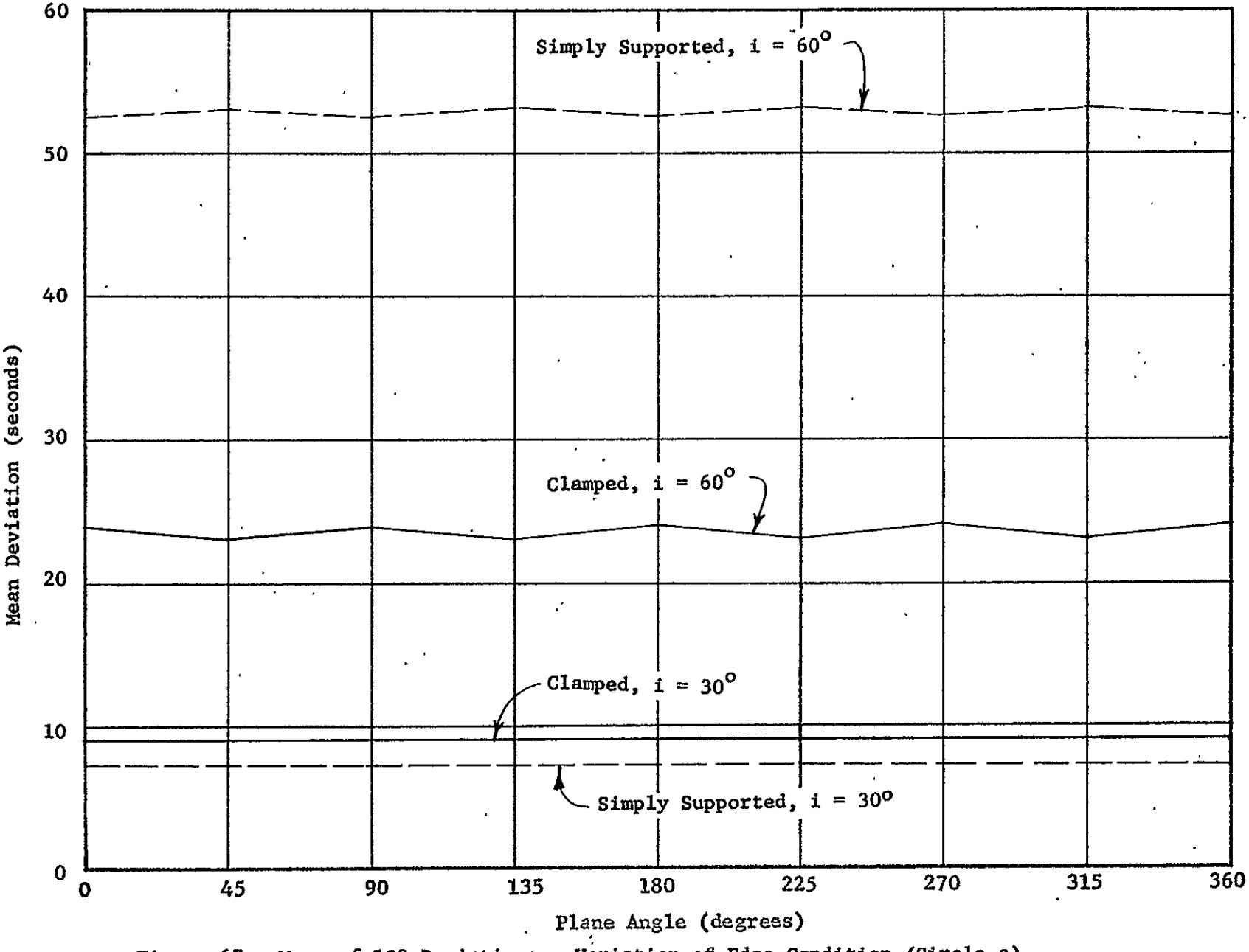

Figure 67. Mean of LOS Deviations - Variation of Edge Condition (Circle a)

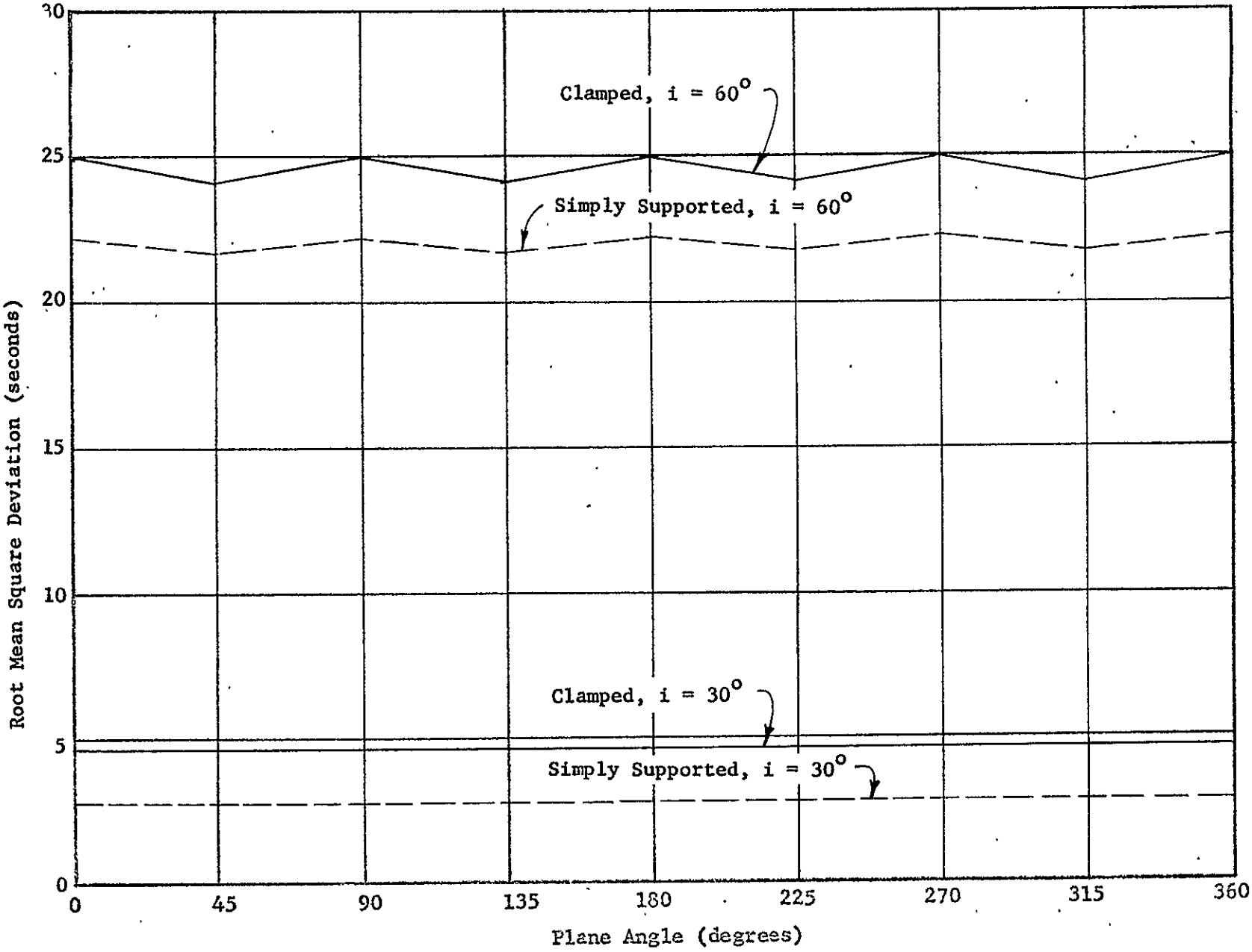

Figure 68. RMS of LOS Deviations - Variation of Edge Condition (Circle a)

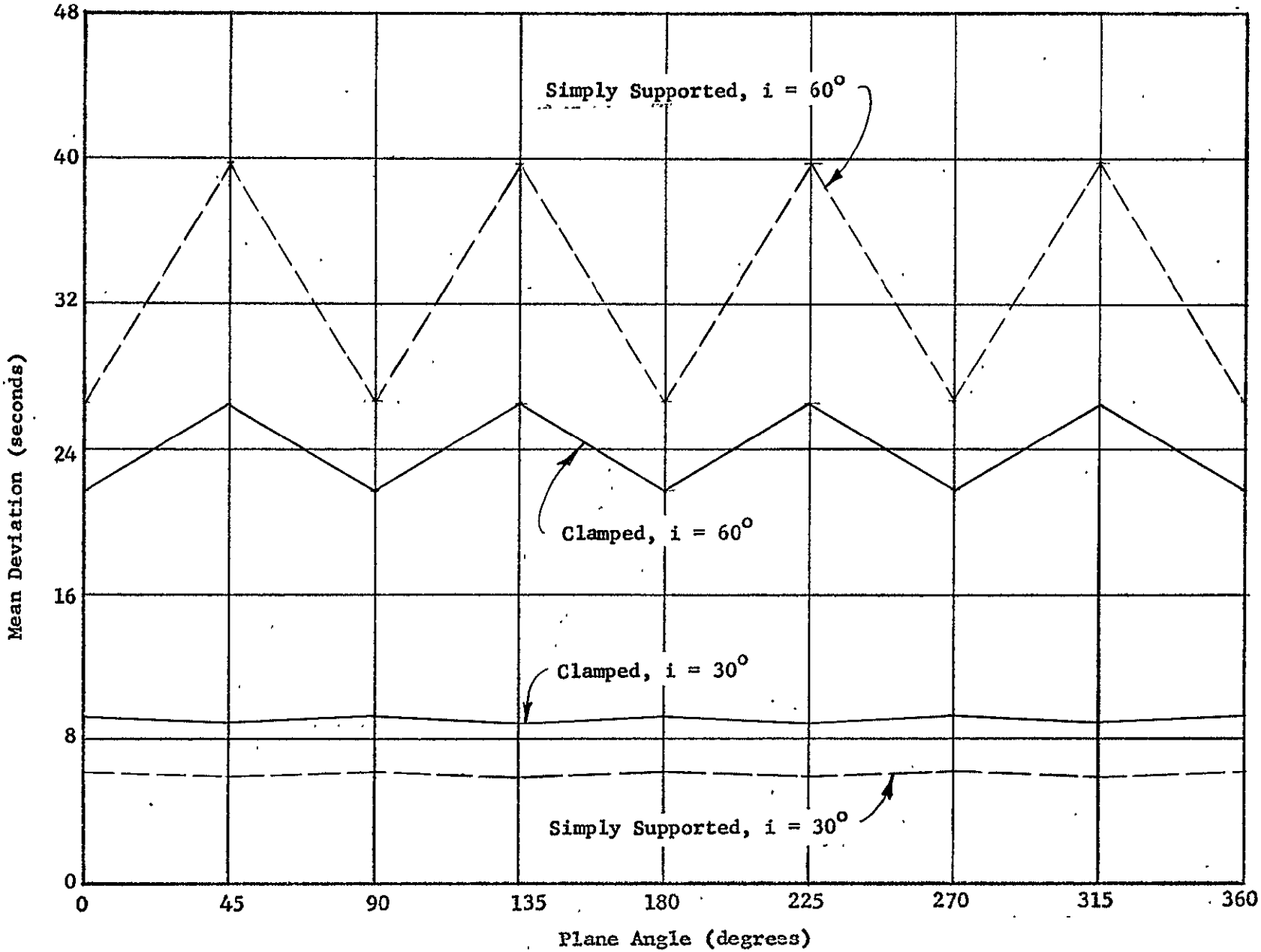

Figure 69. Mean of LOS Deviations - Variation of Edge Condition (Square d)

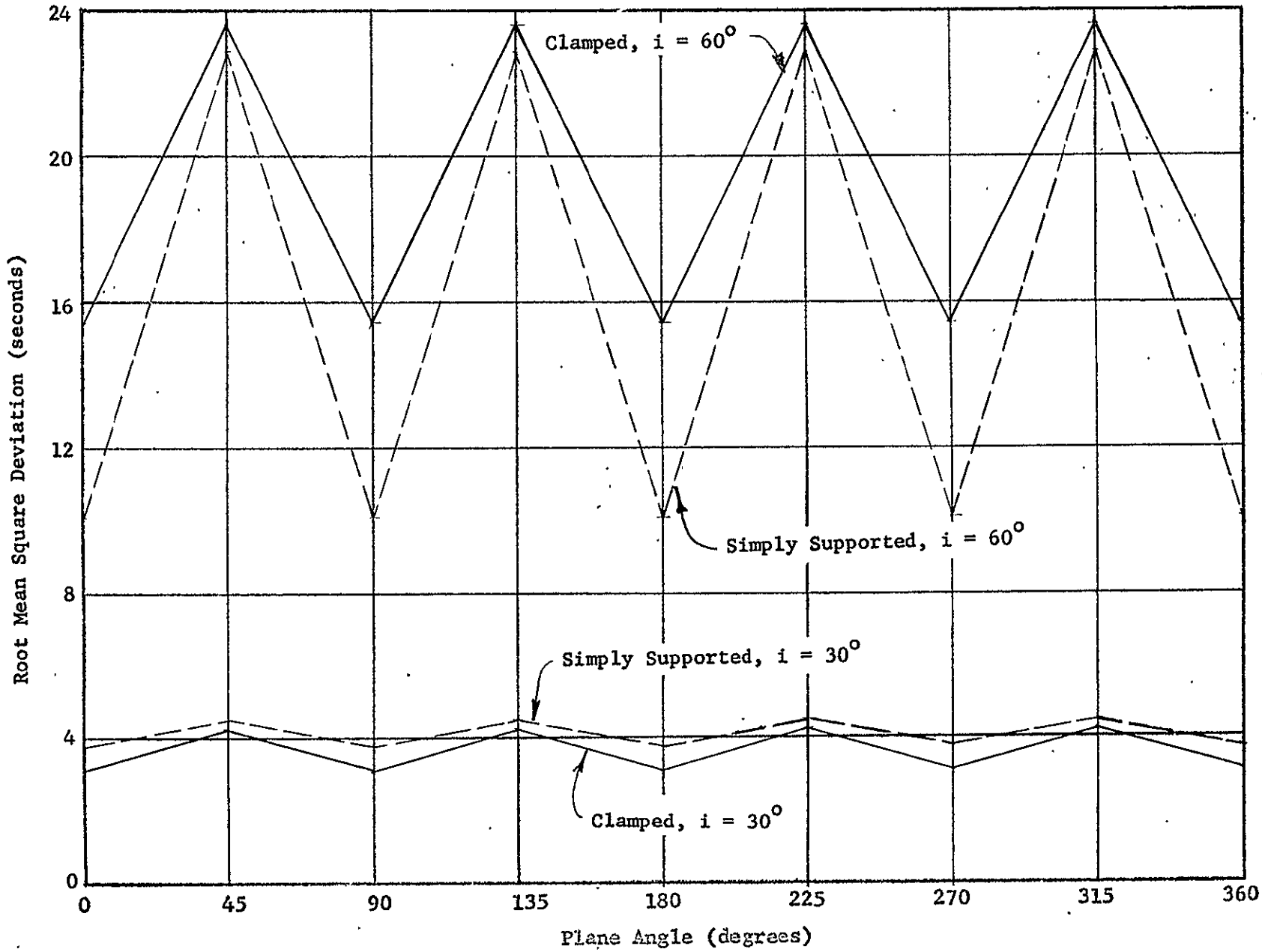

Figure 70. RMS of LOS Deviations - Variation of Edge Condition (Square d)

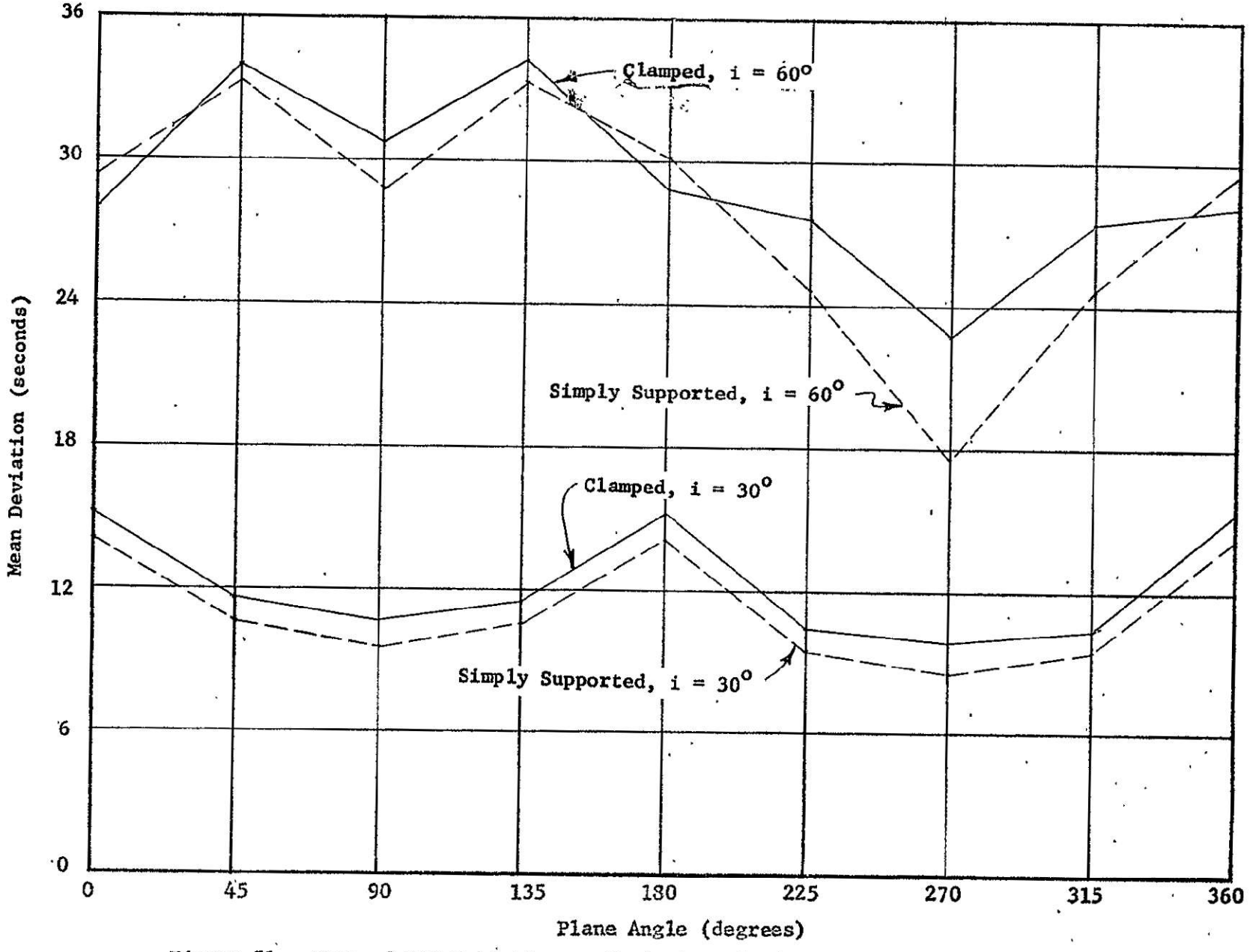

Figure 71. Mean of LOS Deviations - Variation of Edge Condition (Trapezoid g)

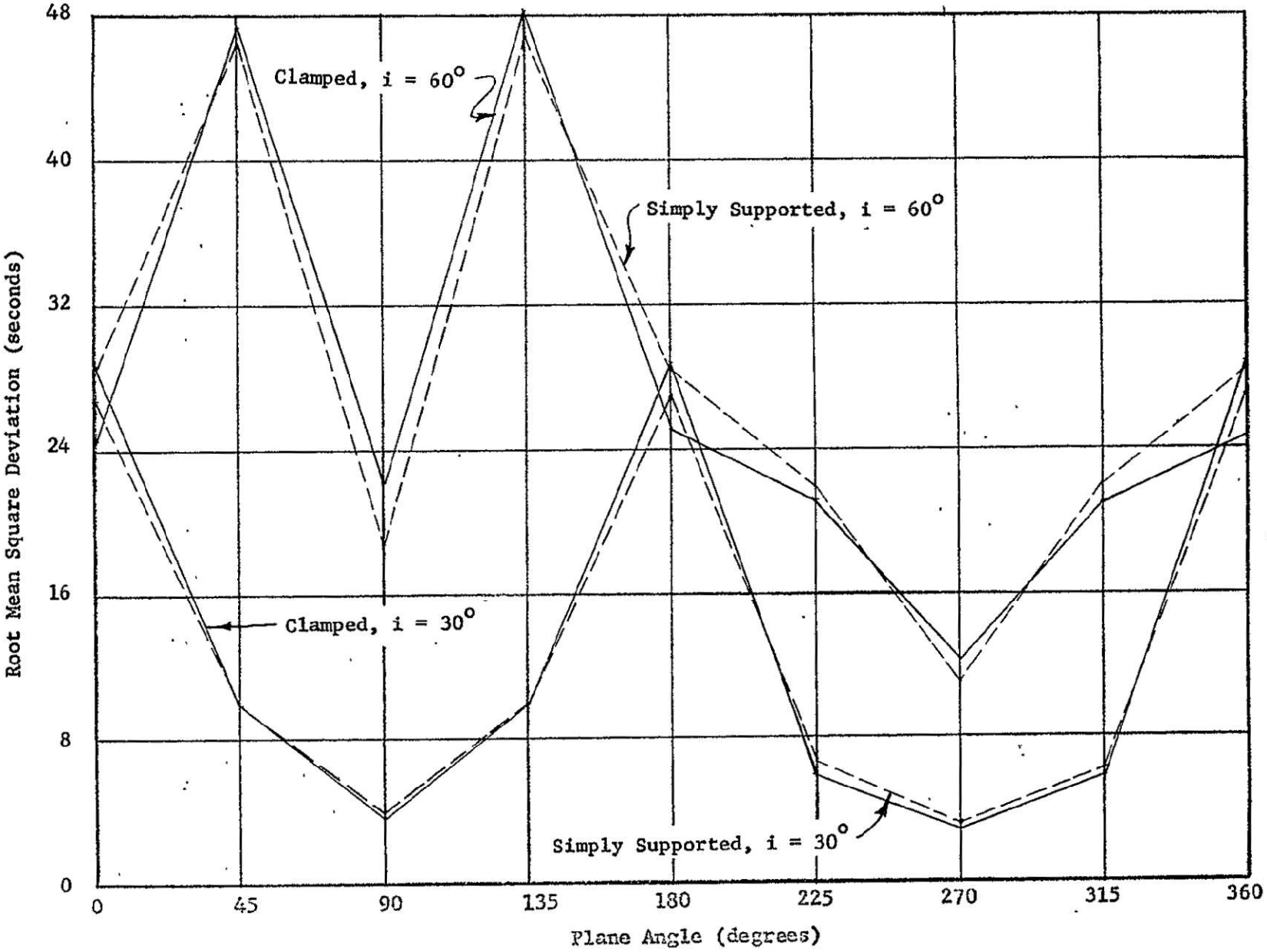

Figure 72. RMS of LOS Deviations - Variation of Edge Condition (Trapezoid g)

Table 11

Rankings for Variation of Edge Support Conditions

Planform	Edge Condition	Mean Value	RMS Value	Mean Value Variation	Overall Ranking
Circle a	Clamped	1	8	4	13
Circle a	Simply Supported	6	6	2	14
Square d	Clamped	2	4	6	12
Square d	Simply Supported	4	2	8	14
Trapezoid g	Clamped	5	12	10	27
Trapezoid g	Simply Supported	3	10	12	25

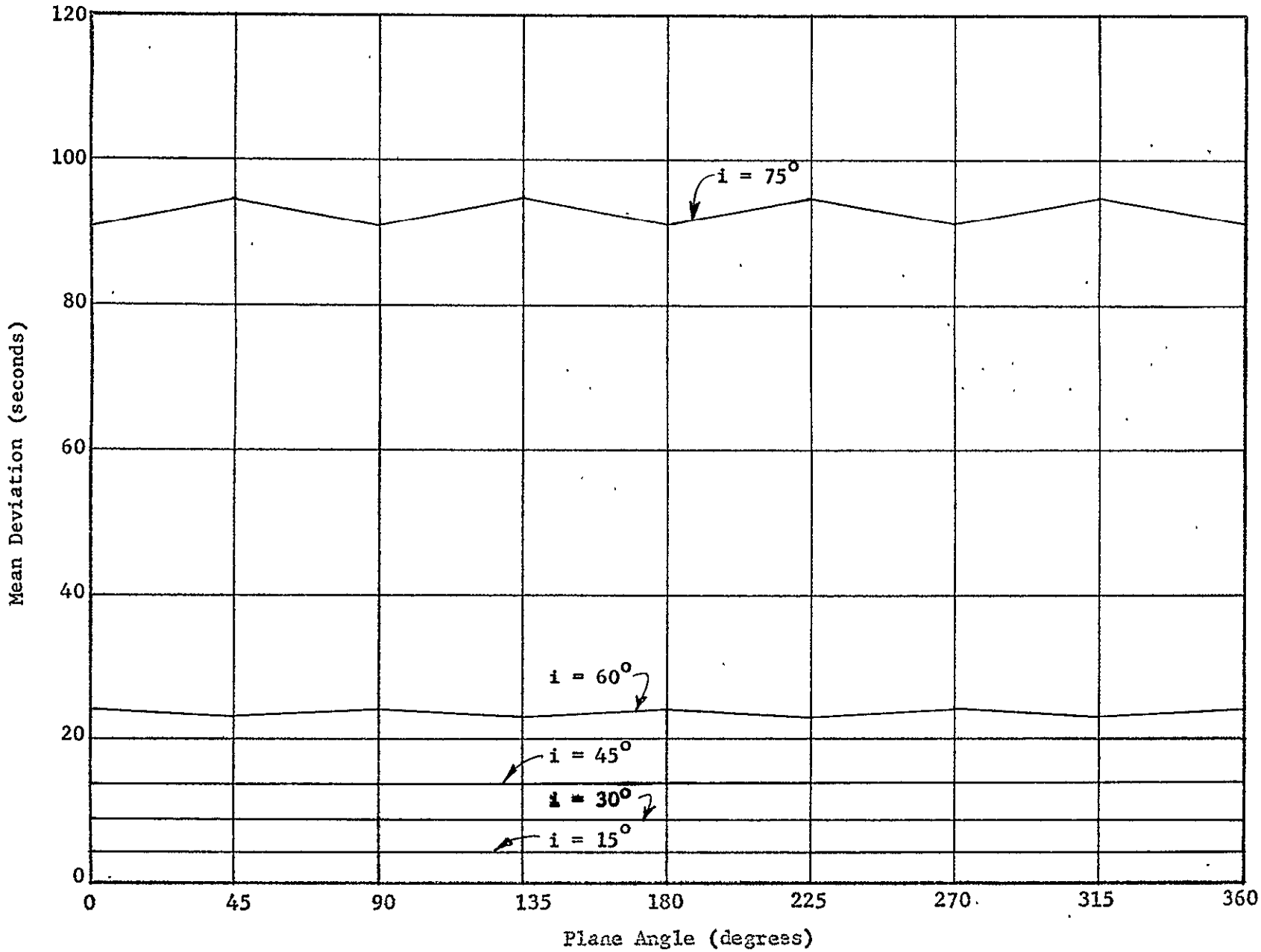

Figure 73. Mean of LOS Deviations - Variation of Incidence Angle (Circle a)

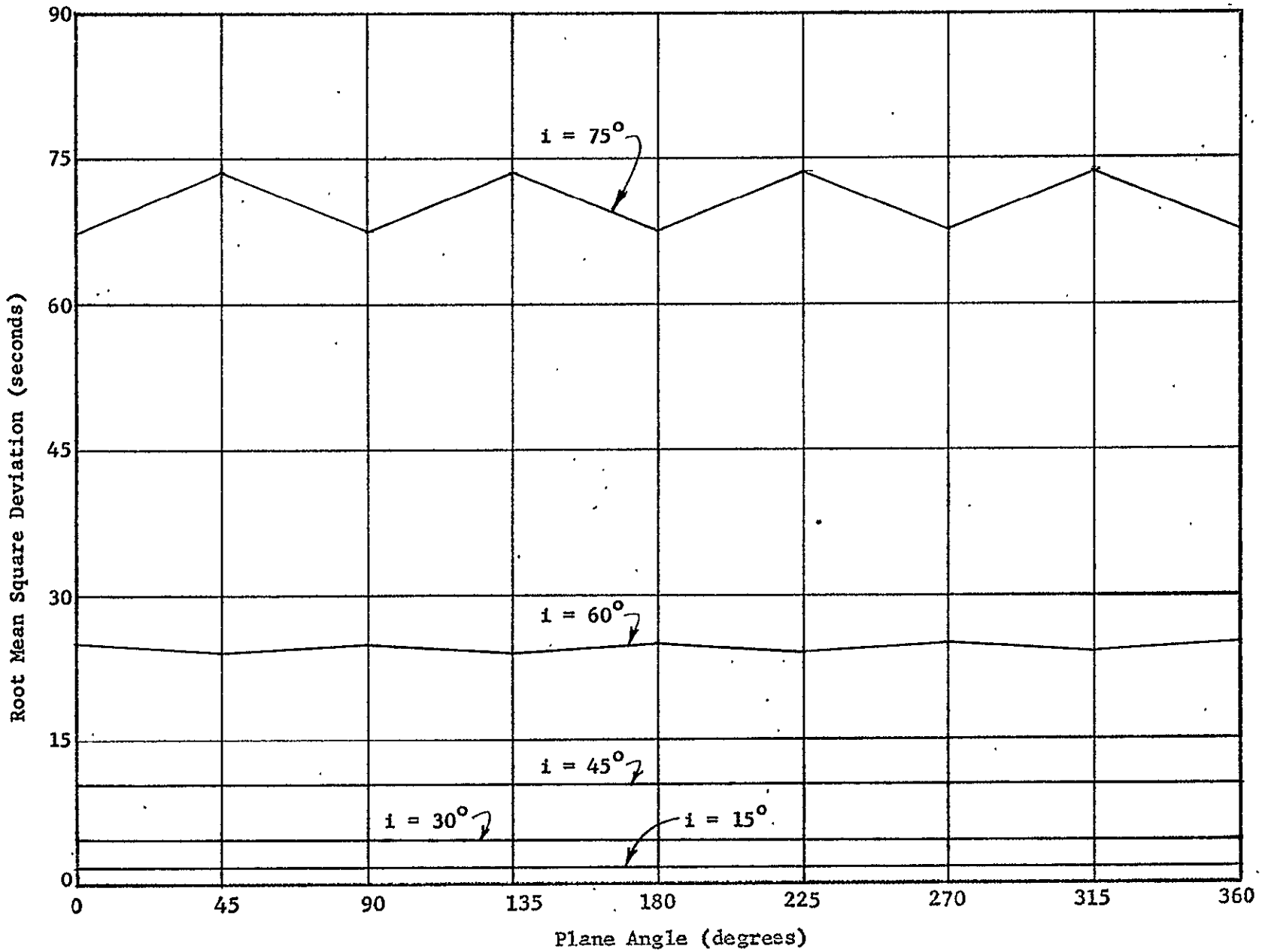

Figure 74. RMS of LOS Deviations - Variation of Incidence Angle (Circle a)

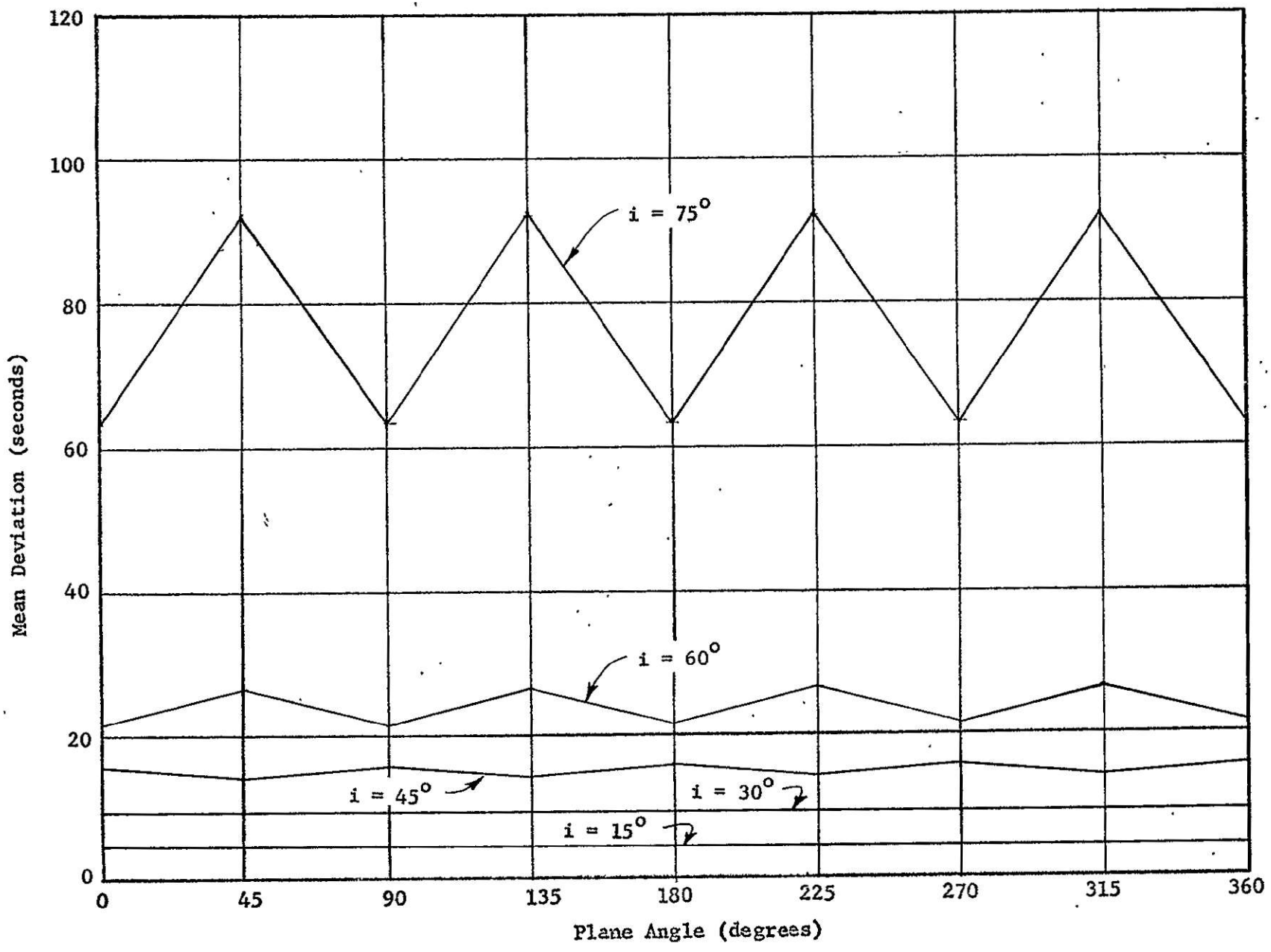

Figure 75. Mean of LOS Deviations - Variation of Incidence Angle (Square d)

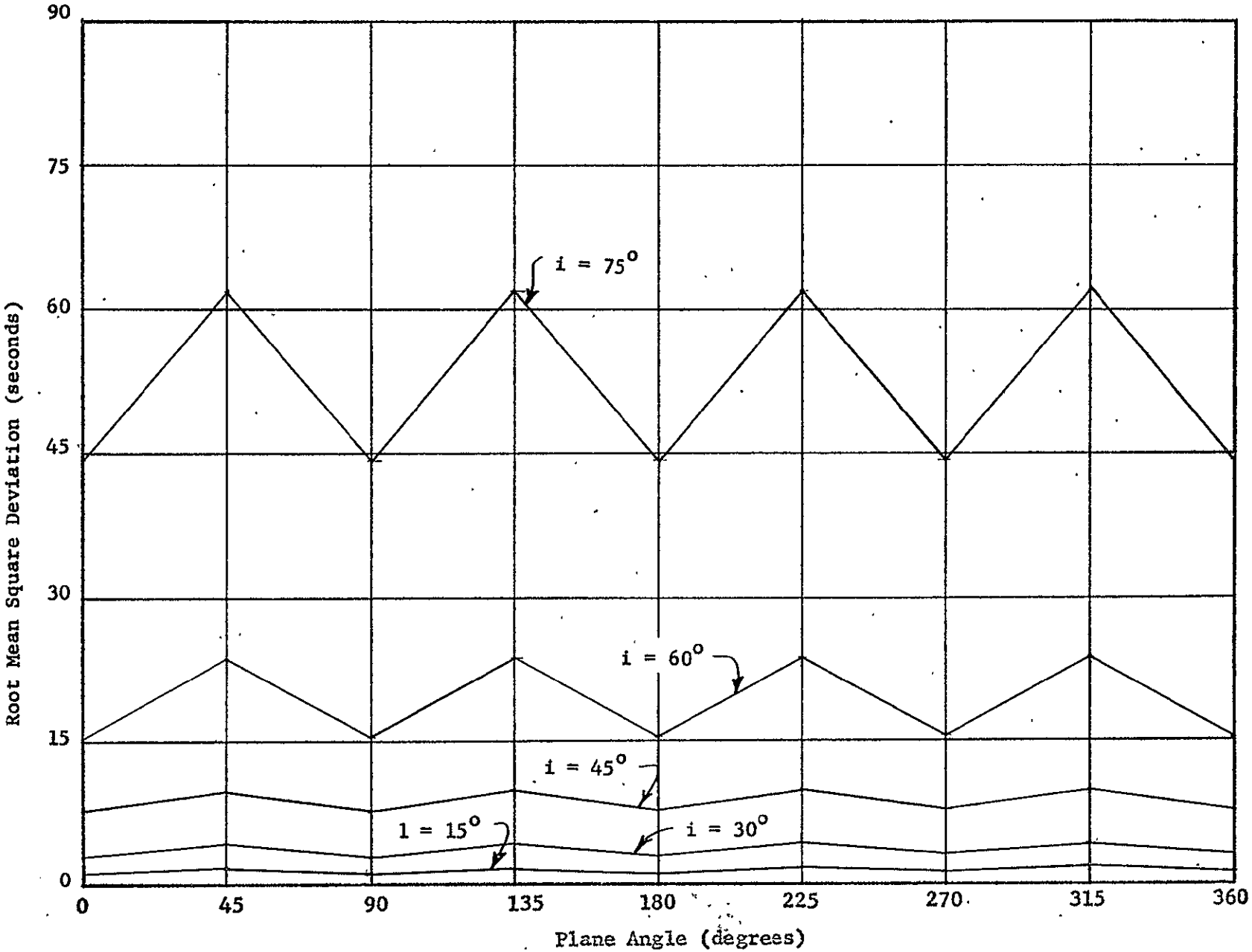

Figure 76. RMS of LOS Deviations - Variation of Incidence Angle (Square d)

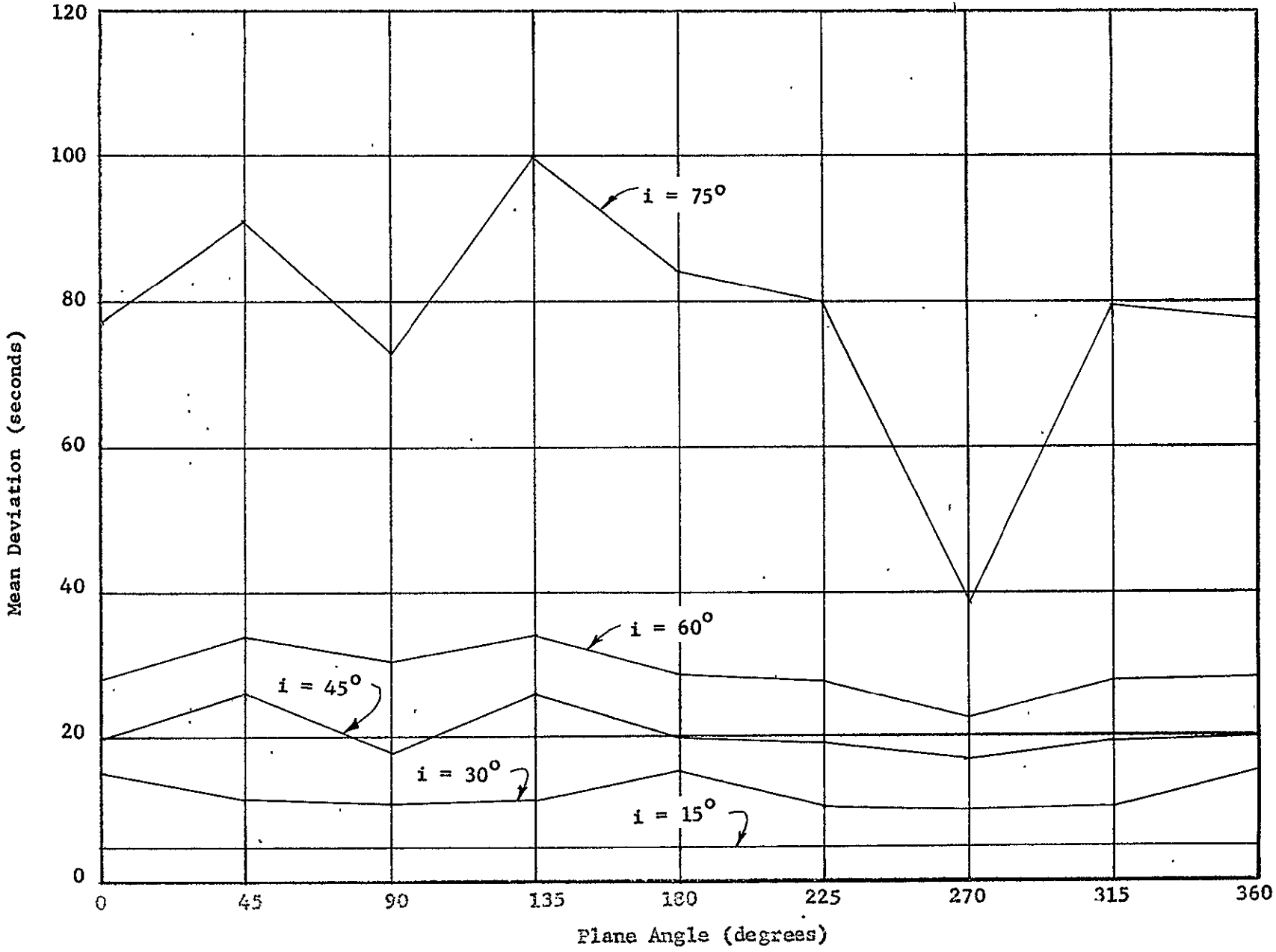

Figure 77. Mean of LOS Deviations - Variation of Incidence Angle (Trapezoid g)

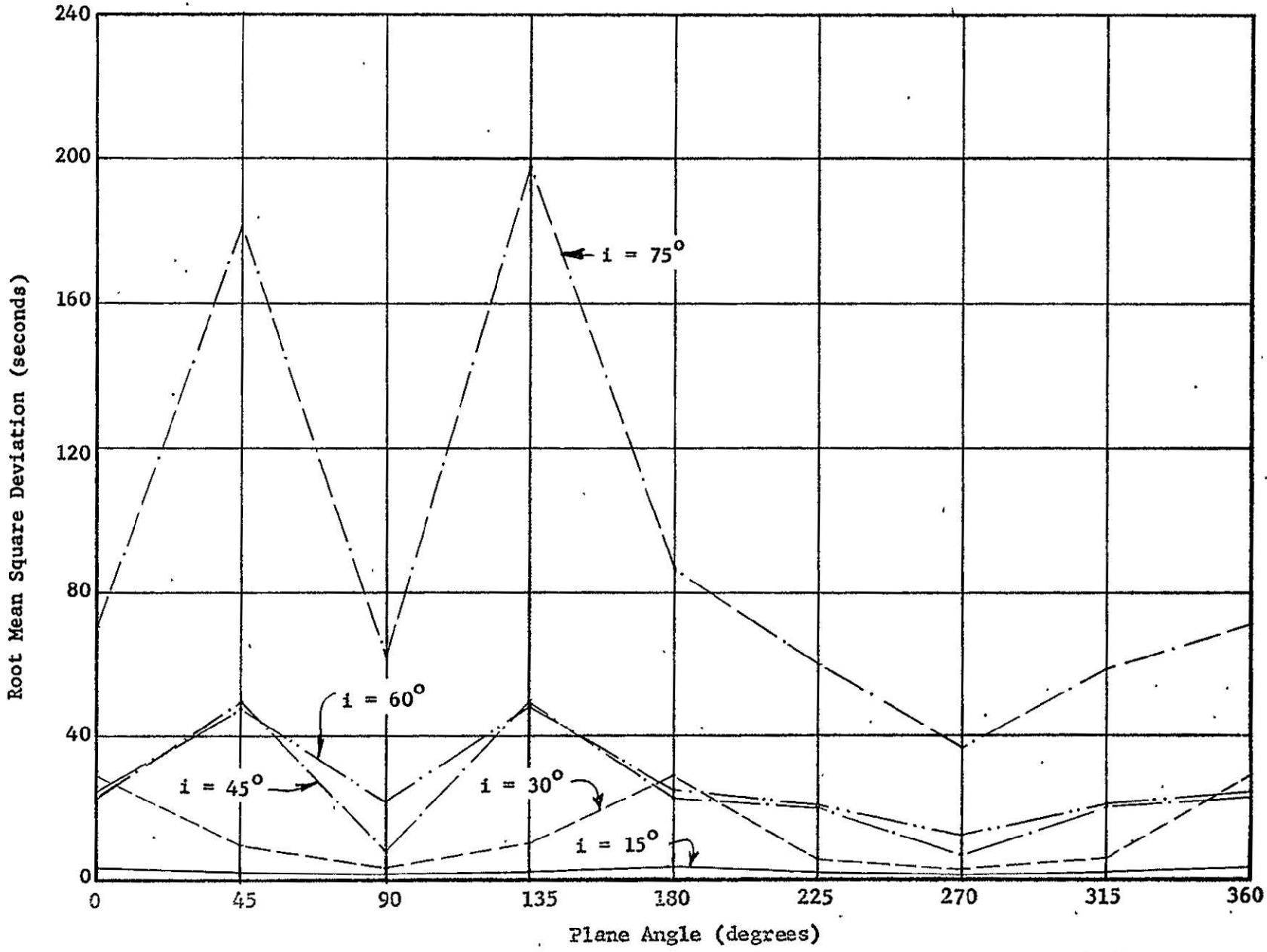

Figure 78. RMS of LOS Deviations - Variation of Incidence Angle (Trapezoid g)

The data of these figures indicate that the LOS deviations increase with an increase in the angle of incidence. This is true for all three statistical measures of the LOS deviations. From this it is again concluded that observations should be made at as low an incidence angle as practicable.

The effect on line-of-sight deviations of including large deflection effects in the prediction of deformations is studied by considering the data presented in Figs. 79 through 84. The analyses from which the data of these figures were obtained used the nominal parameter values with the exceptions that a dimensional scale of 1.5 rather than 1.0 and a pane separation distance of 1.0 rather than 0.5 inch were used.

Figures 79 and 80 indicate that the mean deviation values, the rms deviation values, and the variations of the mean values are smaller for square d when large deflection effects are included in the prediction of deformations. This is because large deflection effects reduce the total deflections, thus reducing the variations in the slope of the window surface. This in turn reduces the amount of line-of-sight deviation. The small differences in the magnitudes of the deflections calculated using small and large deflection theory result in larger differences in the amount of light ray deviations. The differences are further exaggerated by the fact that the light ray passes through two window panes each of which has small differences in deflection magnitudes.

Figures 81 and 82 show that the difference between the large and small deflection cases are even more pronounced for rectangles e and f. The curves of these figures are presented for an incidence angle of 60^{o}.

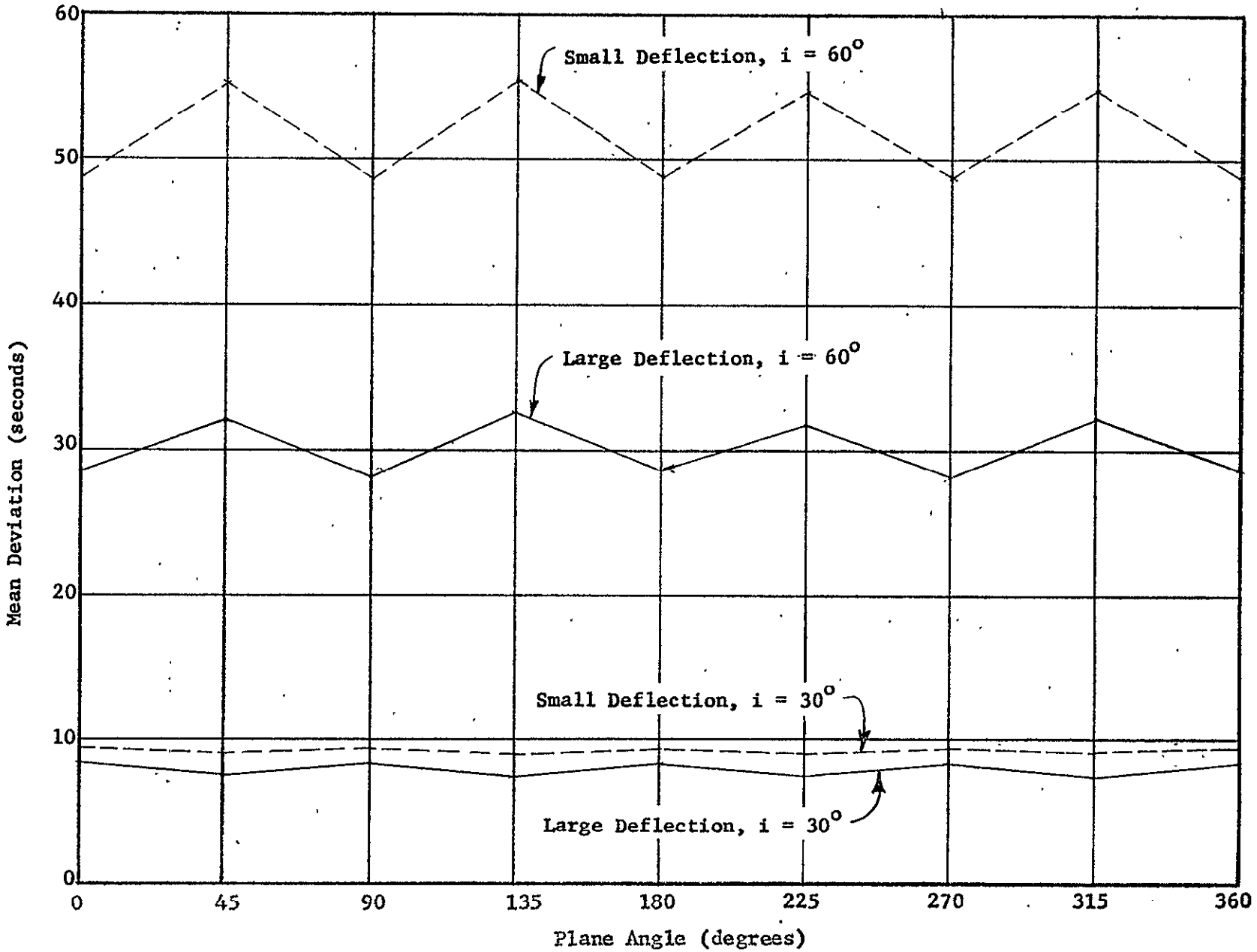

Figure 79. Mean of LOS Deviations - Variation of Deflection Prediction (Square d)

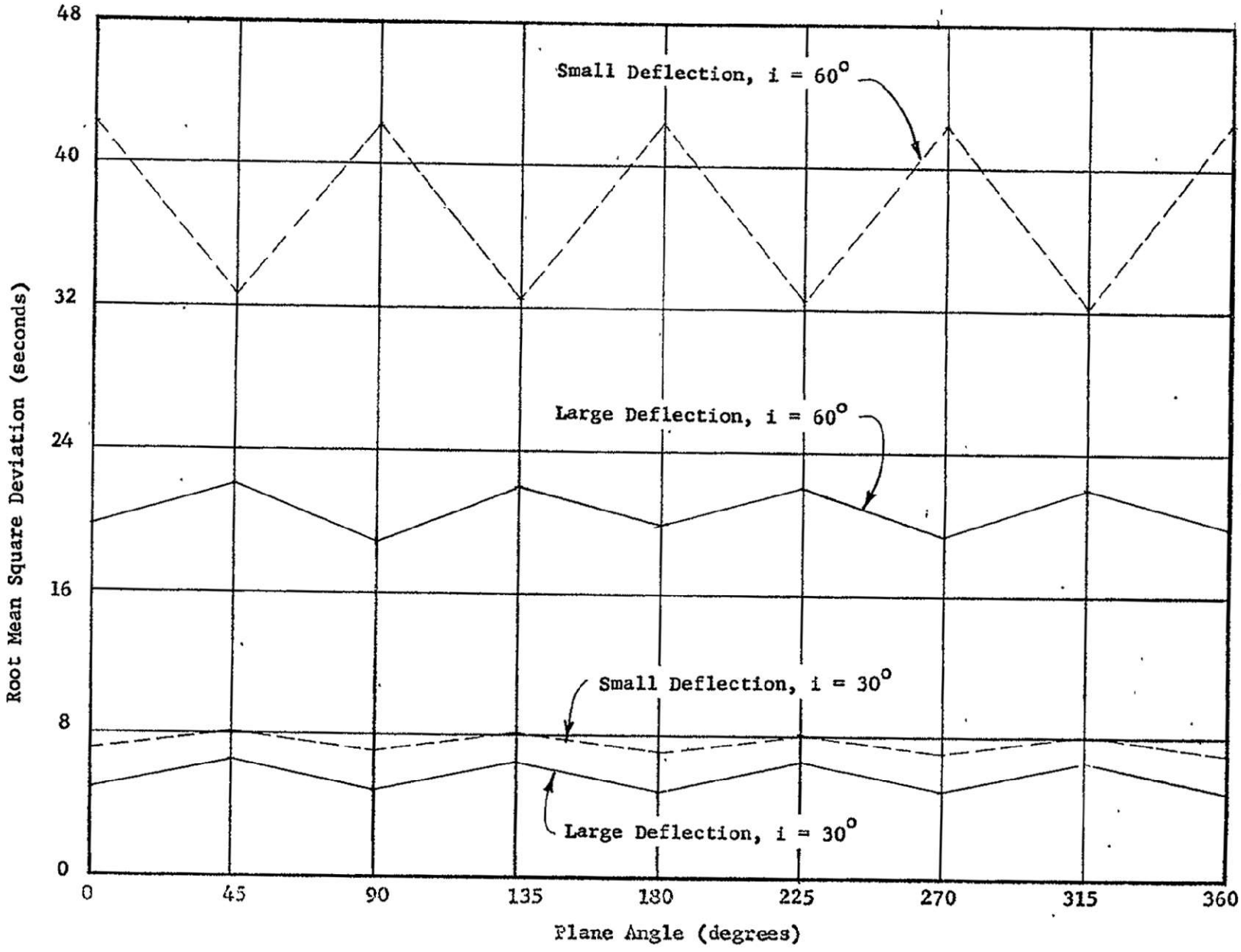

Figure 80. RMS of LOS Deviations - Variation of Deflection Prediction (Square d)

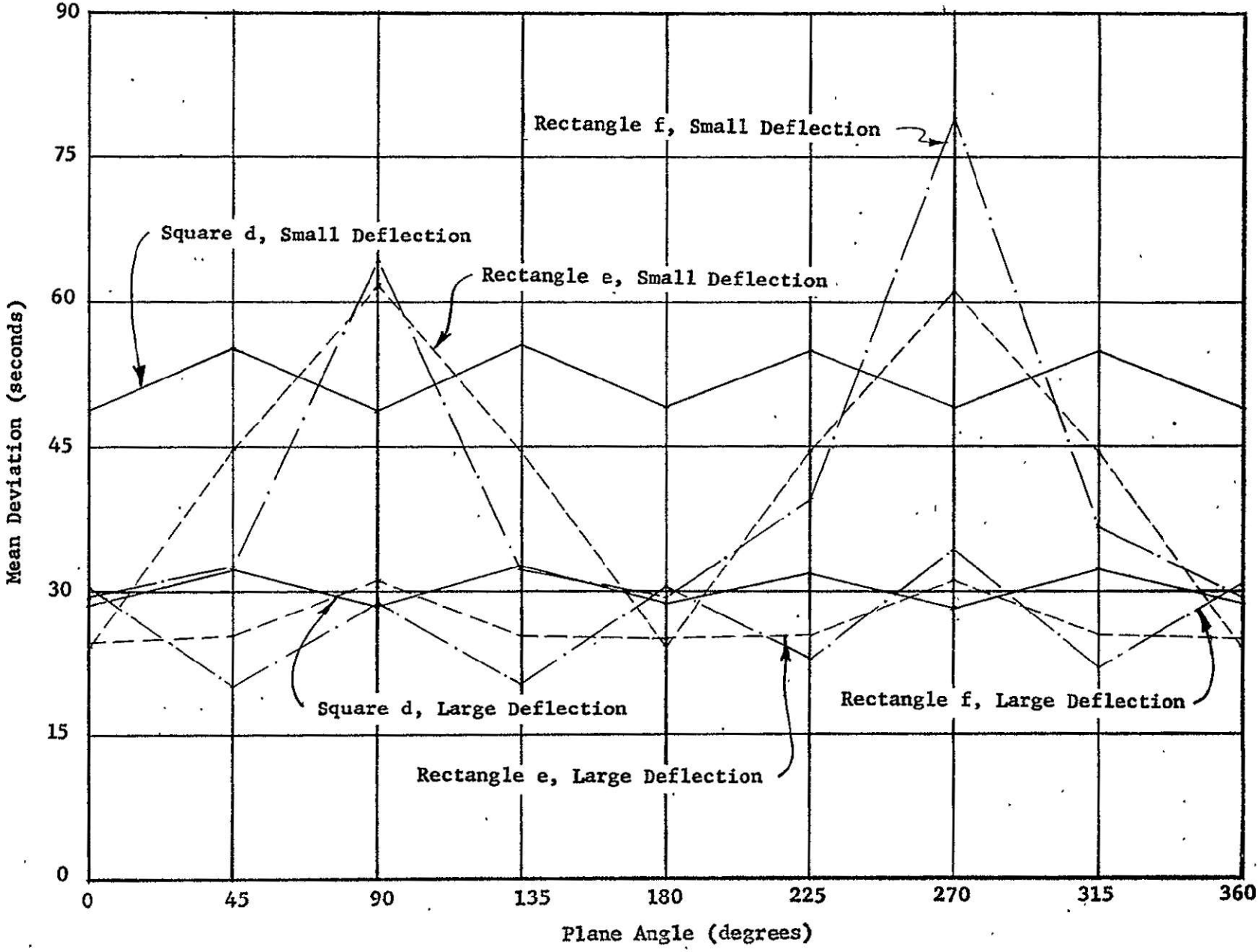

Figure 81. Mean of LOS Deviations - Variation of Deflection Prediction and Planform

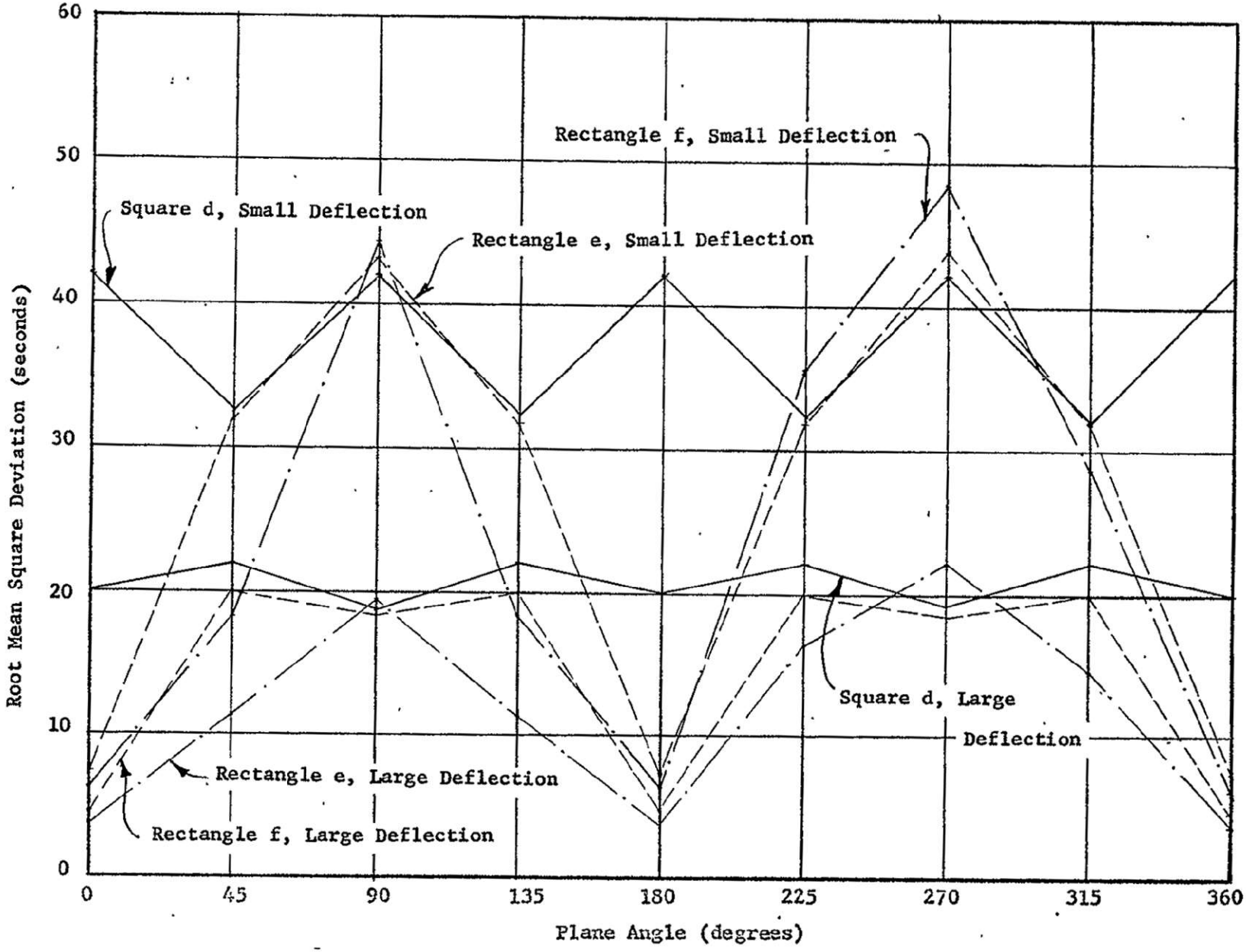

Figure 82. RMS of LOS Deviations - Variation of Deflection Prediction and Planform

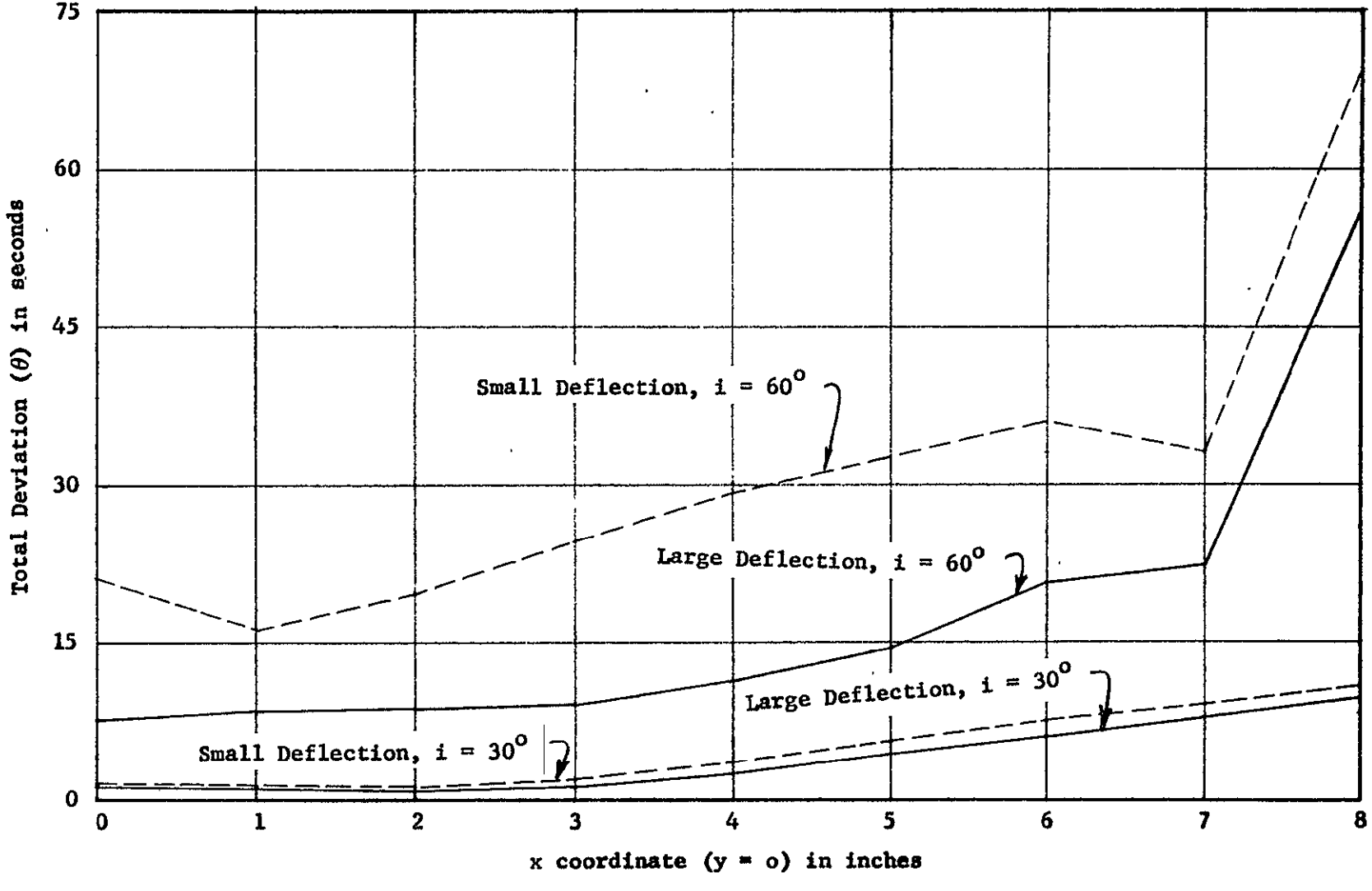

Figure 83. Total LOS Deviations Along x-axis (Large and Small Deflection)

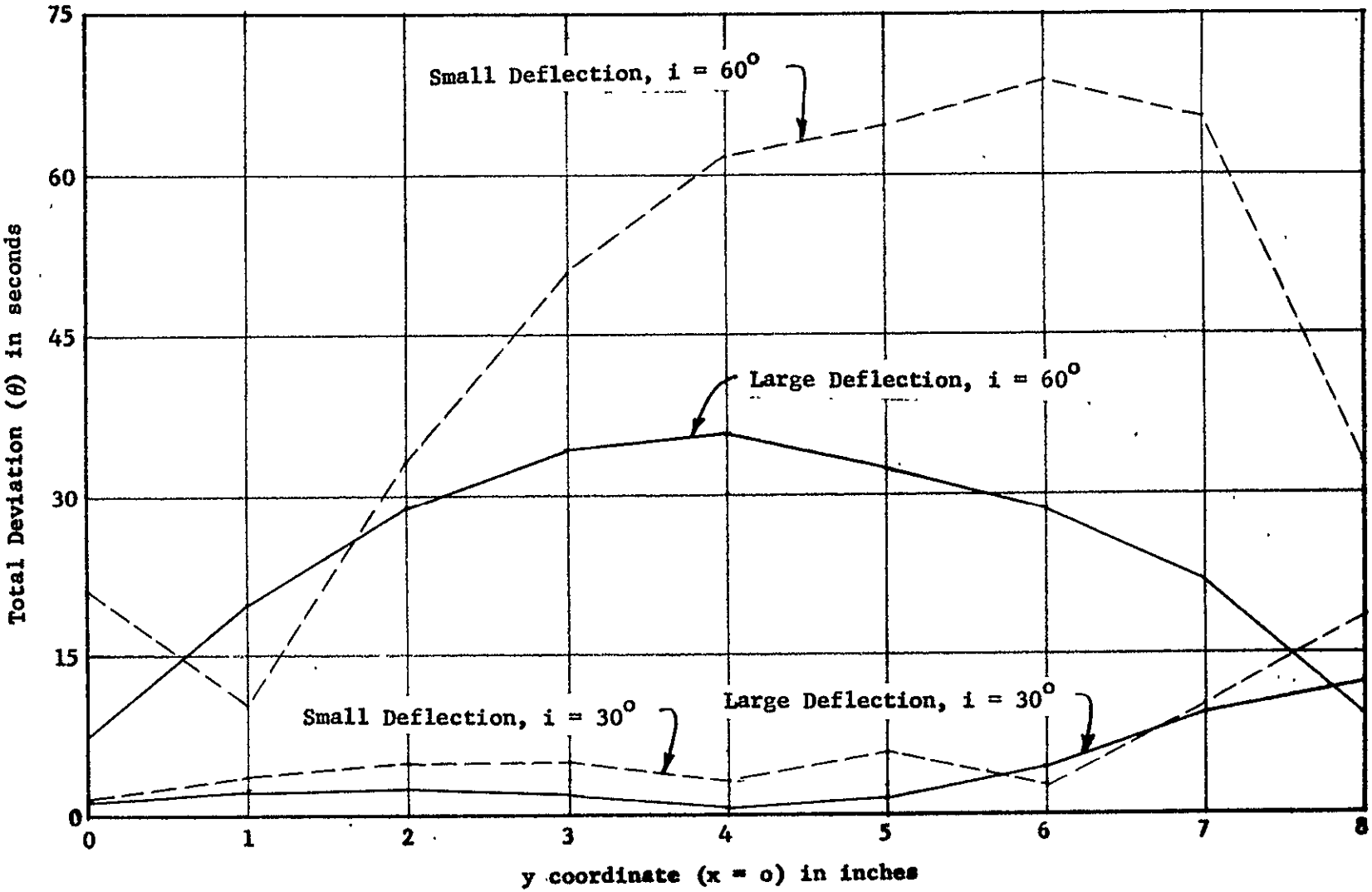

Figure 84. Total LOS Deviations Along y-axis (Large and Small Deflection)

Figures 83 and 84 indicate that the total line-of-sight deviations along either axes of square d are smaller when large deflection effects are included. The curves of these figures are presented for a plane angle of 270°.

The effect on line-of-sight deviations of including shear deformation effects in the prediction of deformations is studied by considering the data presented in Figs. 85 through 90. The analyses from which the data of these figures were obtained used the nominal parameter values with the exceptions that pane thicknesses of 1.2 inches rather than 0.3 inch and a pane separation distance of 1.0 inch rather than 0.5 inch were used.

Figures 85 and 86 indicate that while the mean deviation values, the rms deviation values, and the variations of the mean values are smaller for square d when shear deformation effects are included in the prediction of deformation, the difference is insignificant. Figures 87 and 88 which present curves for an incidence angle of 60° indicate the same holds true for rectangles e and f. Figures 89 and 90 indicate that the difference between including and excluding shear deformation effects has no significant effect on the total deviations along either axes of square d. The curves of these two figures are present for a plane angle of 270°.

Constant line-of-sight deviation contours are presented in Figs. 91, 92, and 93 for circle a, square d, and trapezoid g, respectively. The analyses from which the data were obtained used the nominal parameter values. The contours are shown for a incidence angle of 60° and a plane

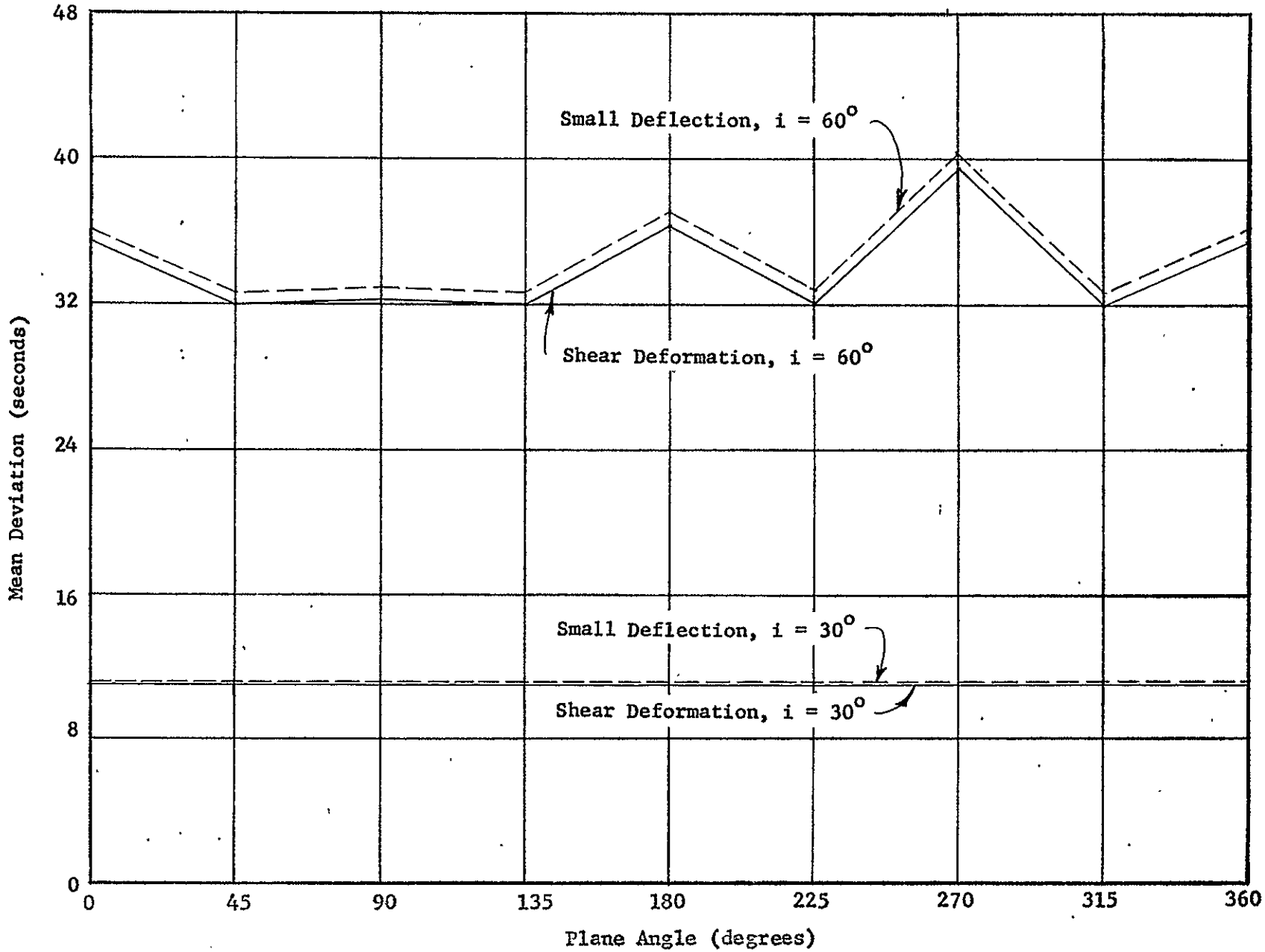

Figure 85. Mean of LOS Deviations - Variation of Deflection Prediction (Square d)

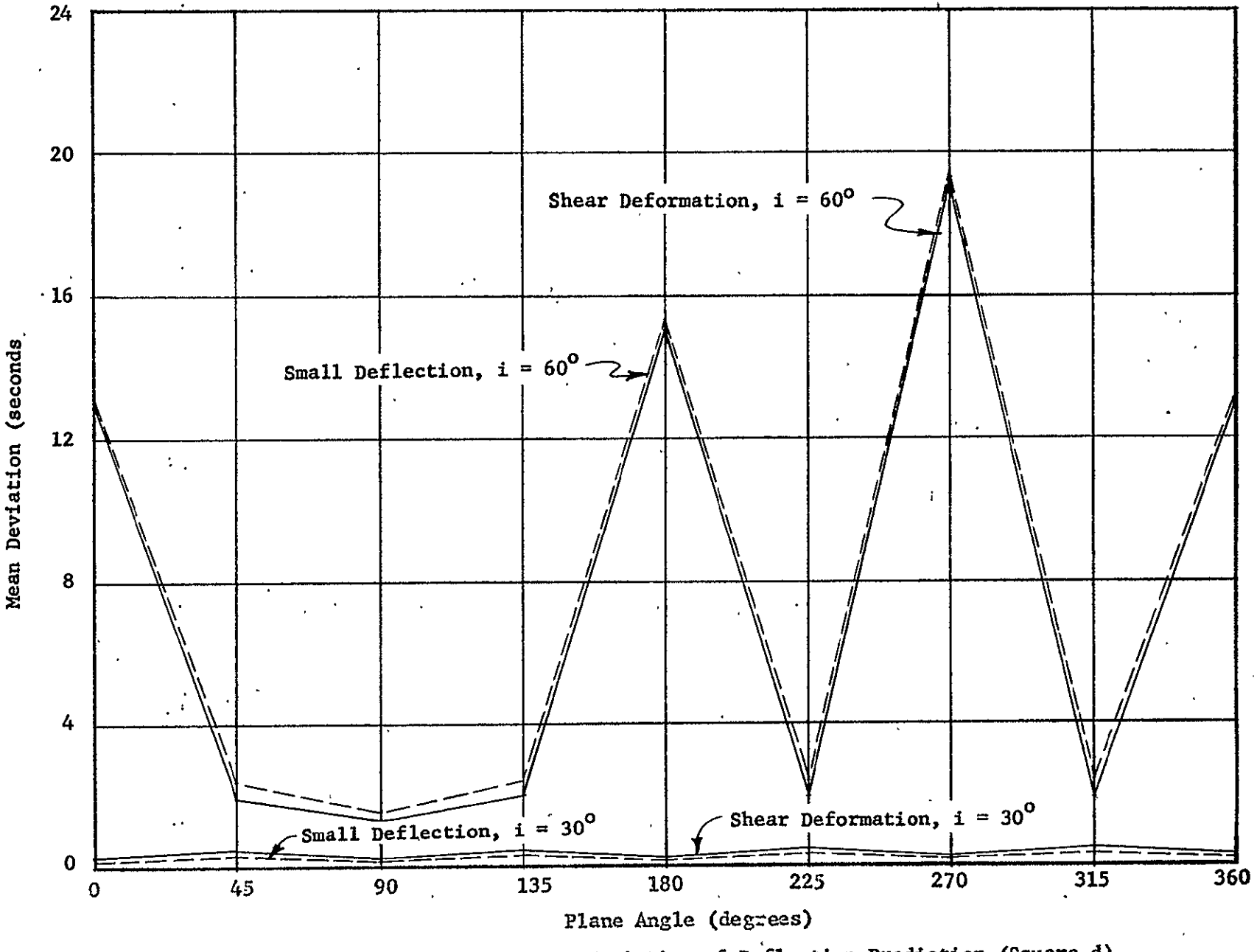

Figure 86. RMS of LOS Deviations - Variation of Deflection Prediction (Square d)

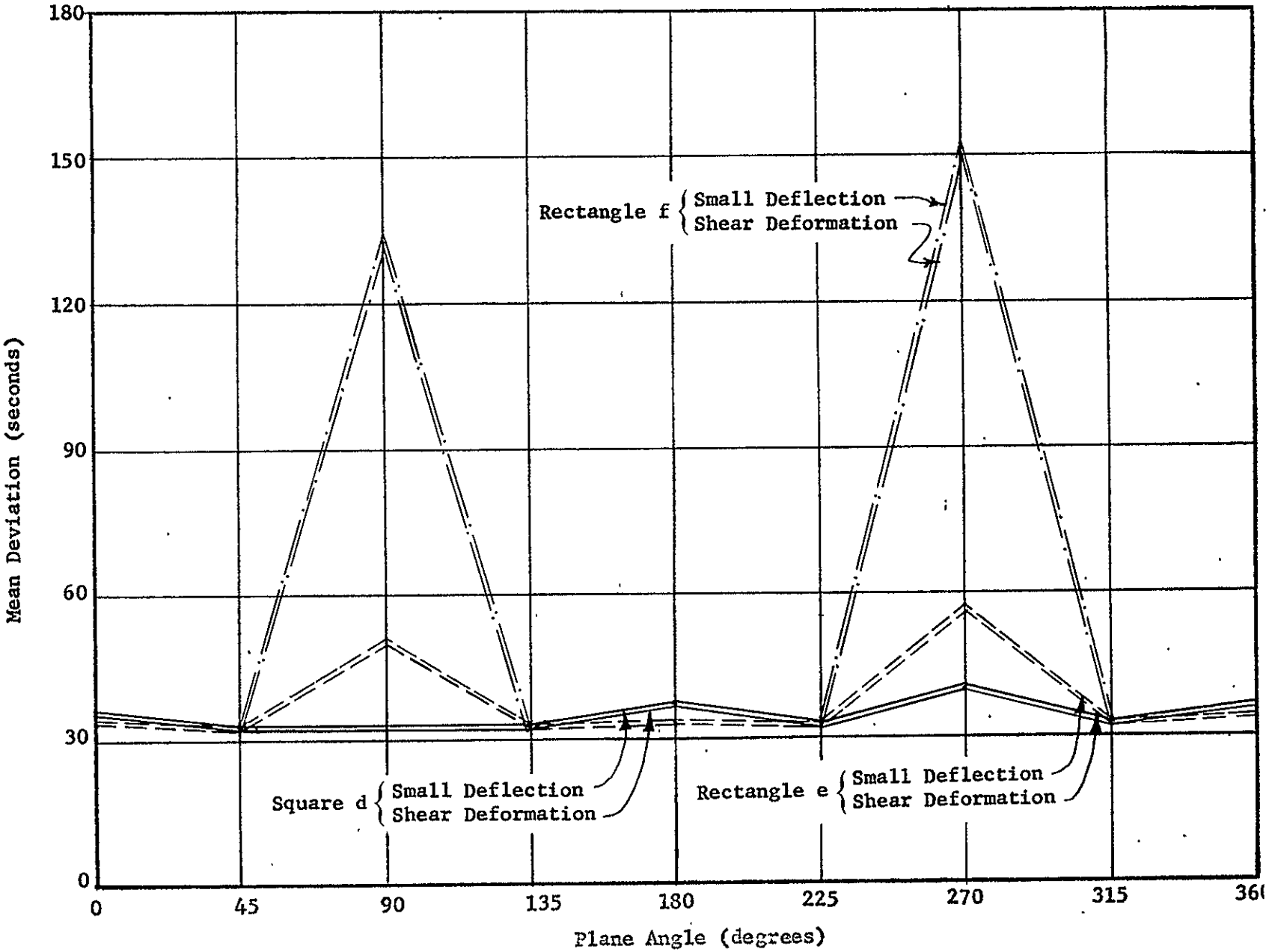

Figure 87. Mean of LOS Deviations - Variation of Deflection Prediction and Planform

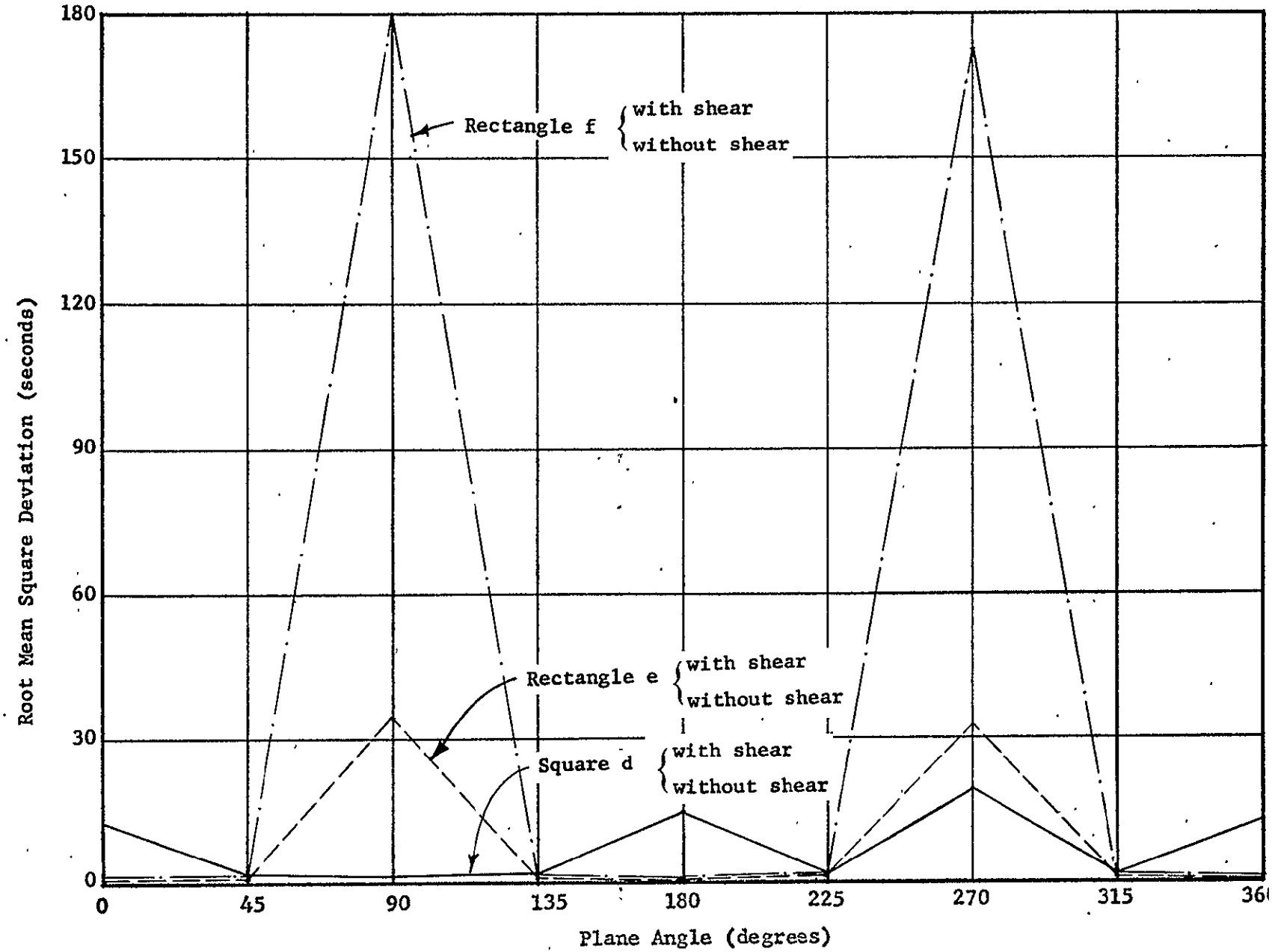

Figure 88. RMS of LOS Deviations - Variation of Deflection Prediction and Planform

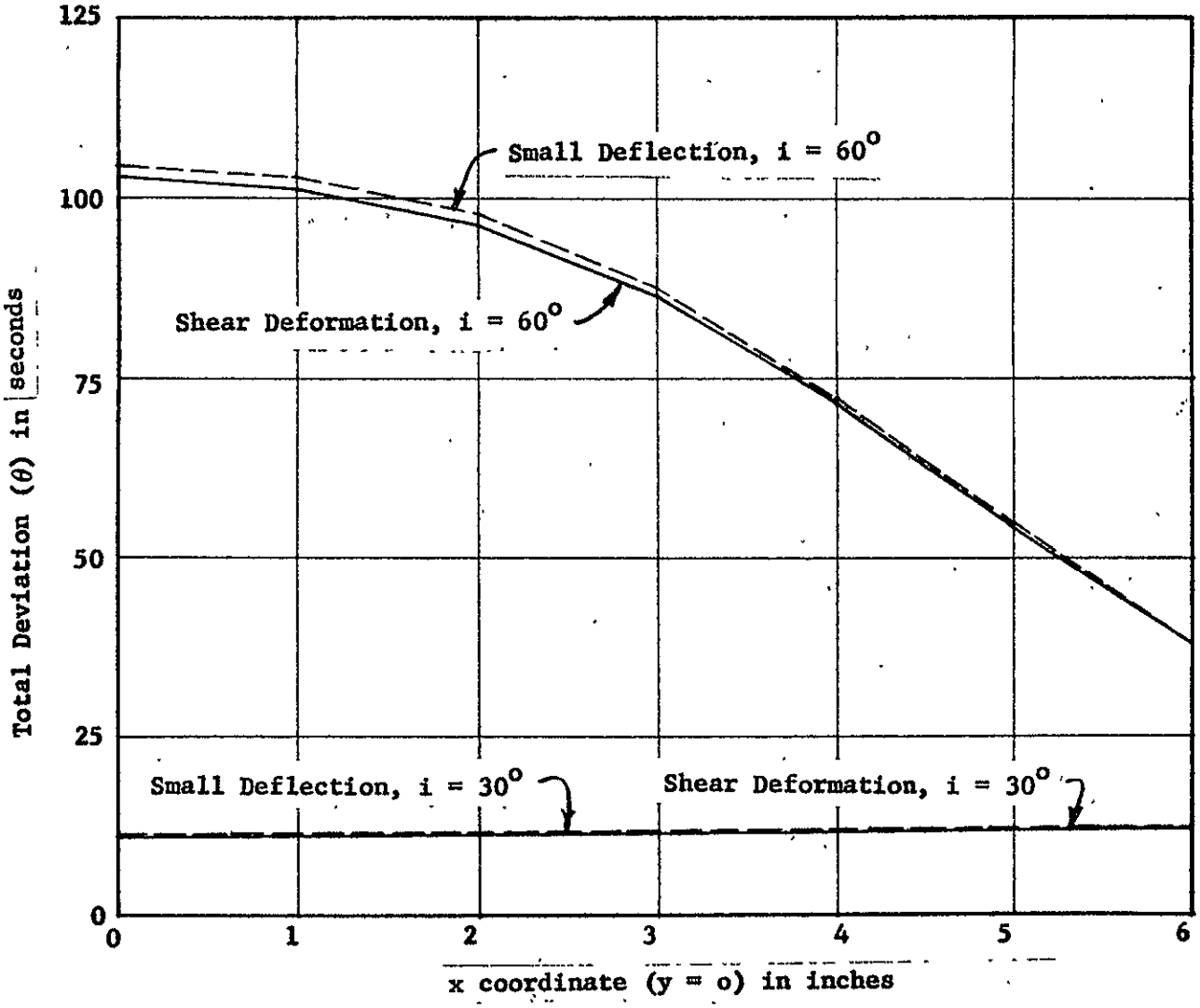

Figure 89. Total LOS Deviations Along x-axis (Shear and Small Deflection)

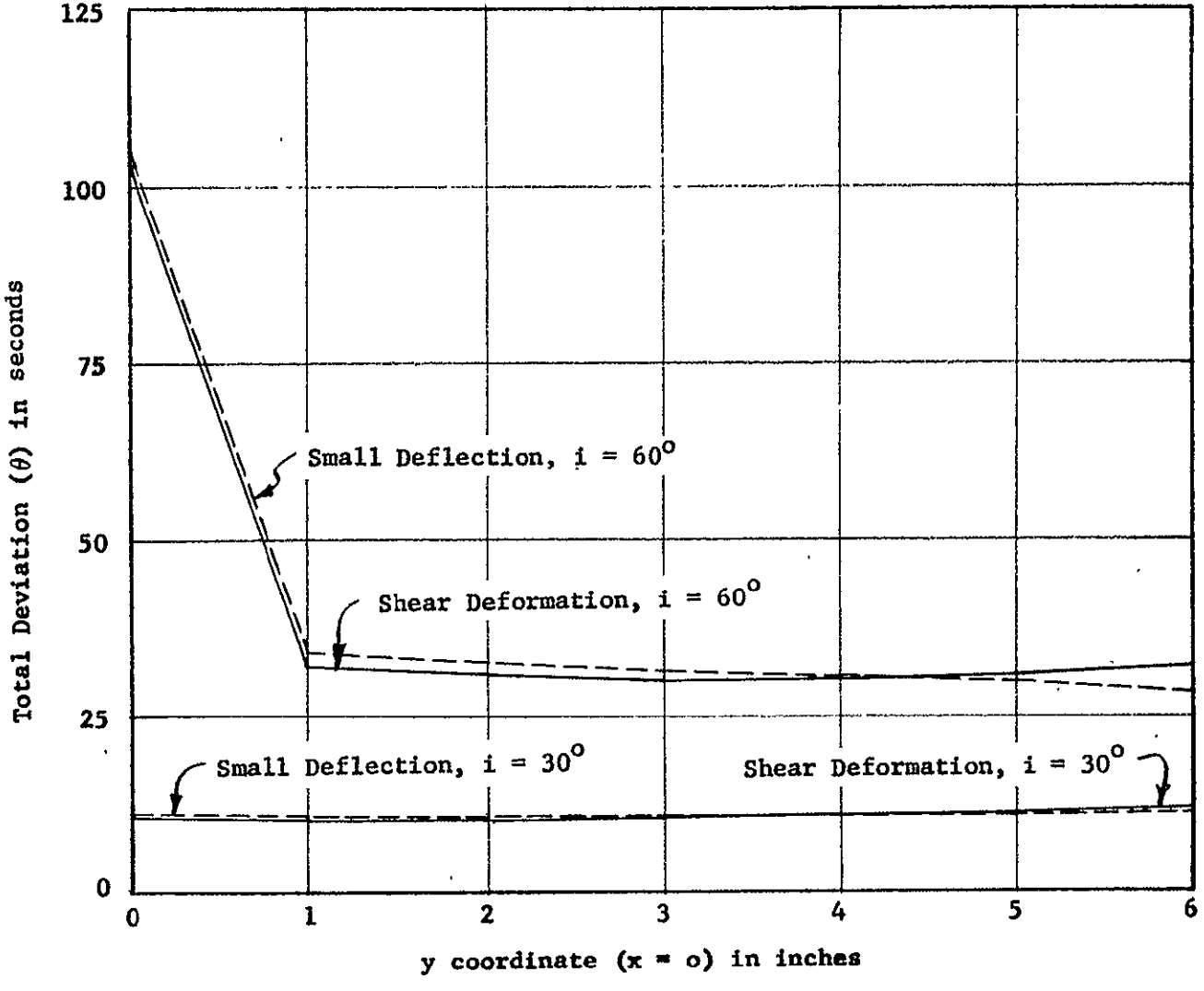

Figure 90. Total LOS Deviations Along y-axis (Shear and Small Deflection)

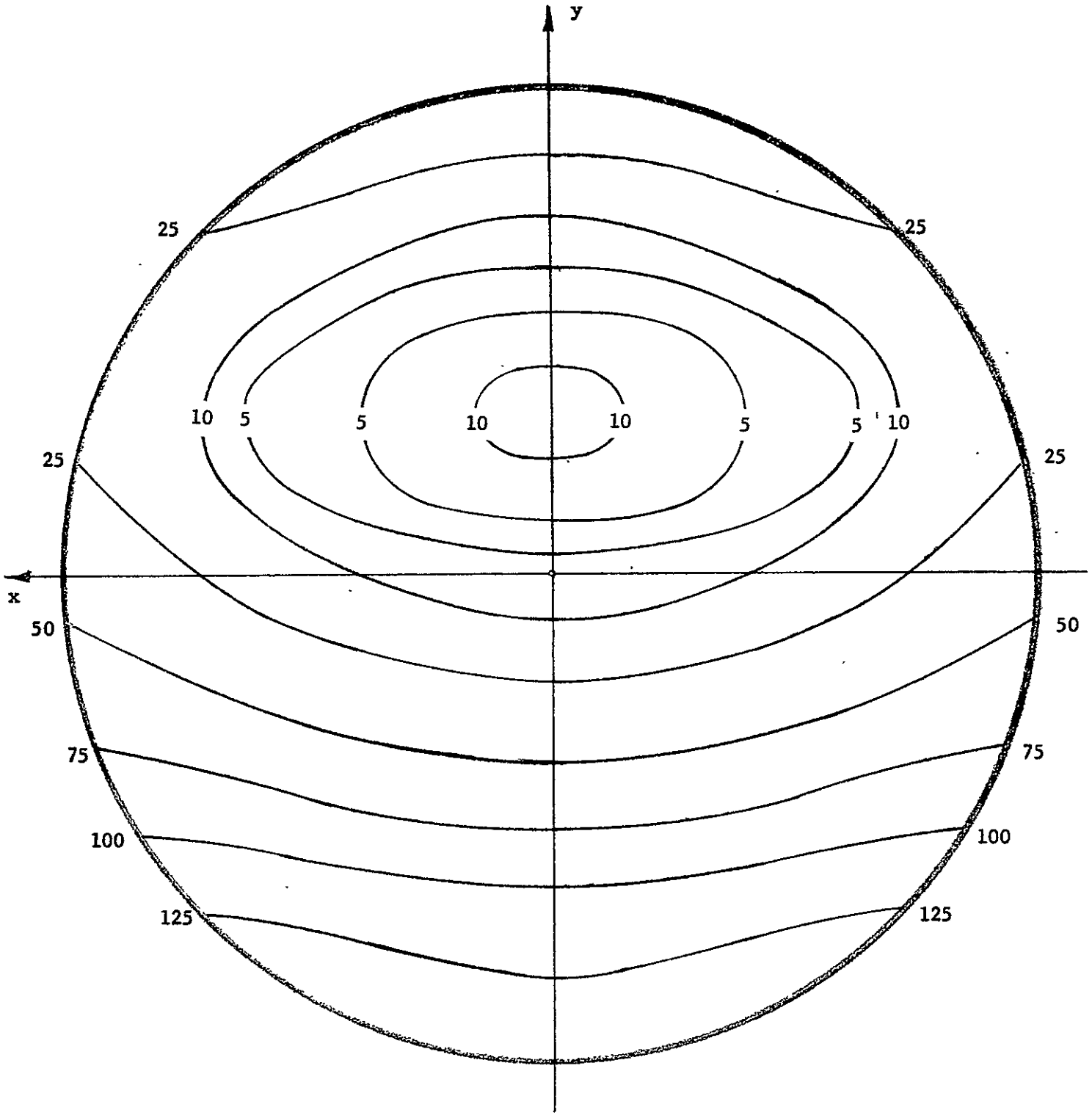

Figure 91. Constant LOS Deviation Contours - Circle a

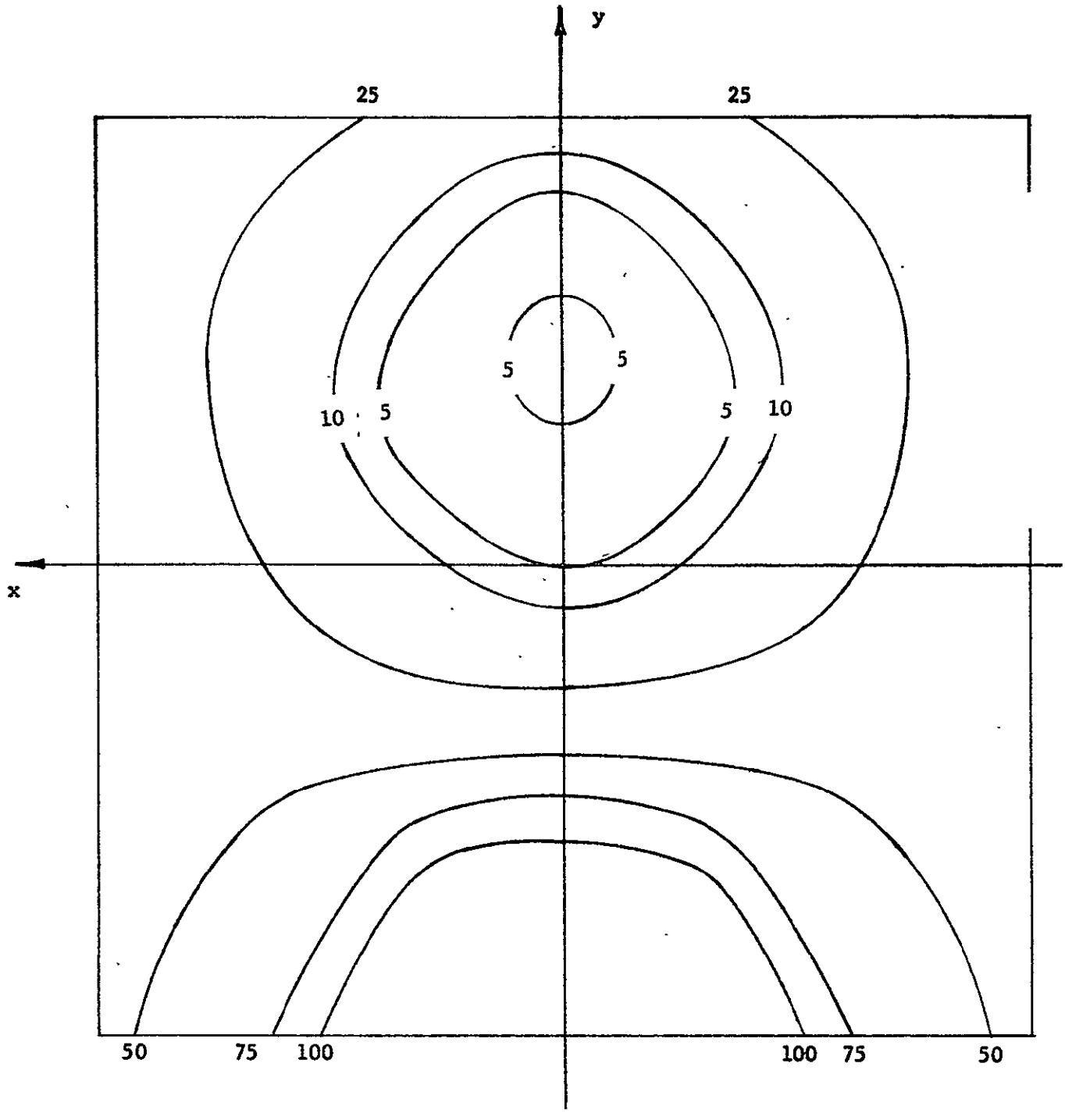

Figure 92. Constant LOS Deviation Contours - Square d

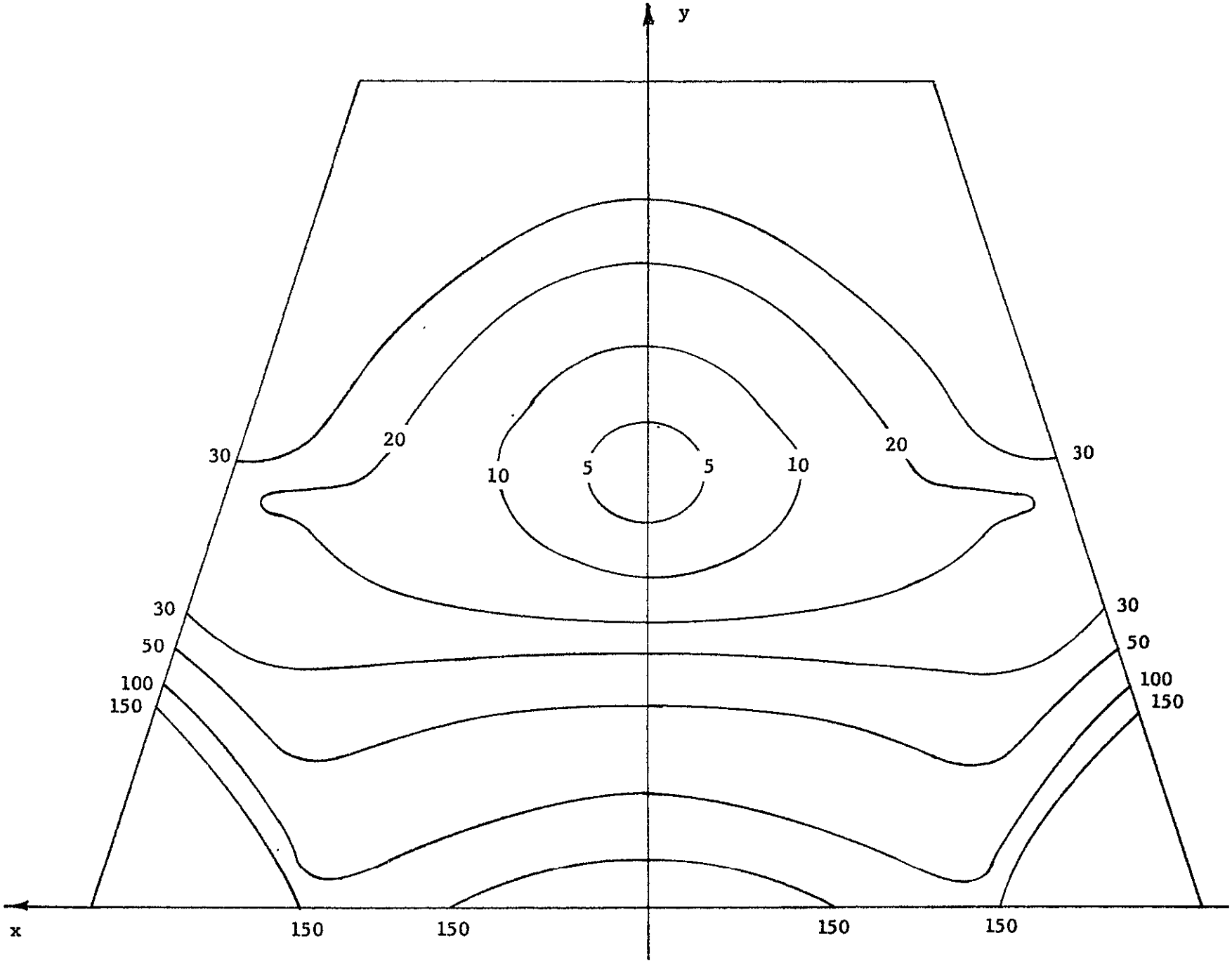

Figure 93. Constant LOS Deviation Contours - Trapezoid g

angle of 270°. The magnitudes of the contours are given in seconds of arc. These figures indicate the areas of the window through which observations can be made with least deviations of the line-of-sight (for a particular set of incidence and plane angles).

The area of best observation for circle a is an elliptical area centered at a point on the y-axis and about one-third the distance between the x-axis and the top of the window. For square d, the area is a circular ring centered at a point on the y-axis and about one-half the distance between the x-axis and the top edge of the window. The area of best observation for trapezoid g is a circular area about halfway between the top and bottom edges and centered on the y-axis.

Several general conclusions can be drawn from the studies of double-pane configurations:

1. Observations which are made at low incidence angles have the least deviations in the line-of-sight.

2. Of the configurations studied, an interstitial pressure of 7.5 psia, a pane separation distance of 0.25 inch and clamped edge conditions resulted in the best characteristics for circle a and square d.

3. For trapezoid g, the best characteristics were obtained for an interstitial pressure of 7.5 psia, a pane separation distance of 0.5 inch and simply supported edge conditions.

4. Considering large deflection effects in predicting deformations results in better window performance while the inclusion of shear deformation effects had no significant effect on window performance measures.

5. Of the pane shapes studied, circle a has the best characteristics.

Section 5

CONCLUDING REMARKS

This study provides the pressure deformation characteristics and line-of-sight deviations for a variety of window shapes and loadings. These data should assist in developing and evaluating window designs by defining the magnitudes of systematic line-of-sight errors associated with window deformations.

Spacecraft window surface deformations and line-of-sight deviations due to in-flight pressure environments are determined as a function of several configuration parameters. Variables include planform geometry (eight different shapes and three sizes), number of panes (one or two), pane thickness and spacing, pressure environment, and edge conditions. The effects of including large deflection and shear deformations in the prediction of deformations are also studied.

The data generated are preserved on microfilm cartridges and also on computer magnetic tapes. The data are classified as pressure deformations and single- and double-pane configuration ray trace deviations. Data from selected portions of each classification are presented and discussed.

Pressure deformation data for circle a, square d, and trapezoid g in single-pane configurations are presented in the form of contours of constant deflection and contours of maximum slope. These data show that maximum deflections and smallest maximum slopes occur near the center of each of the window. Thus, the area of best observation

lies near the center of the windows. Scaling laws are given for changes in pressure, window size and thickness, and window material stiffness.

A good window system is defined as the one for which corrections to the line-of-sight observations are small and constant over the surface of the window. The bases for determining whether or not a window is good are the mean and rms light ray deviations of all points on the window surface and how the mean deviation value varies as a function of the plane angle (the orientation of the plane in which the incidence angle is measured).

Single-pane configuration deviation data are presented for studies involving the variation of the following parameters: pane shape, pressure differential, dimensional scale, pane thickness, edge support condition, and incidence angle.

These data indicate that low incidence angles, small pressure differentials, small dimensional scales, large pane thicknesses, and clamped edge conditions result in the smallest LOS deviations. The last four parameters all tend to decrease the deflections of the window. The best planform shape of single-pane configurations is trapezoid h. In general, the trapezoidal shape is better than either of the other two shapes investigated.

Double-pane configuration deviation data are presented for studies involving the variation of the following parameters: pane shape, pressure environment, pane spacing, edge support condition, incidence angle, and the theory used in prediction of deformations.

Studies of these data indicate that observations made at low incidence angles have the least deviations in the line-of-sight. An interstitial pressure of 7.5 psia, a pane separation distance of 0.25 inch and clamped edge conditions result in the smallest LOS deviations for circle a and square d. For trapezoid g, the best results occur for an interstitial pressure of 7.5 psia, a pane separation distance of 0.5 inch and simply supported edge conditions.

The study shows the large deflection terms have a small effect in reducing the magnitude of the deflections of the window and result in better window performance characteristics. Including shear deformation effects has no significant effect on the prediction of deflections or on window performance measures.

Of the shapes studied in double-pane configurations, circle a has the best characteristics.

REFERENCES

1. Kelley, D. M. and Diether, P. A., "Computer Program to Predict Spacecraft Window Deformations and Compute Window Induced Angular Deviations of Light Rays," NASA CR 73477, Philco-Ford Corporation, Palo Alto, California, September 1970.

2. Melosh, R. J., Diether, P. A. and Brennen, M., "Structural Analysis and Matrix Interpretative System (SAMIS) Program Report," Jet Propulsion Laboratory, TM No. 33-307, Pasadena, California, December 1966.

3. Lang, T. E., "Structural Analysis and Matrix Interpretative System (SAMIS) User Report," Jet Propulsion Laboratory, TM No. 33-305, Pasadena, California, March 1967.

4. Melosh, R. J. and Christiansen, H. N., "Structural Analysis and Matrix Interpretative System (SAMIS) Program: Technical Report," Jet Prouplsion Laboratory, TM No. 33-311, Pasadena, California, November 1966.

5. White, K. C. and Gradeberg, B. L., "Methods for Predicting Spacecraft Window-Induced Line of Sight Deviations," NASA Ames Research Center, NASA TN D-4845, Moffett Field, California, July 1969.

6. Gradeberg, B. L. and White, K. C., "Theory of the Correction of Celestial Observation Made for Space Navigation or Testing," NASA Ames Research Center, NASA TN D-5239, Moffett Field, California, December 1969.

7. Ripperger, E. A., "Geometry" in Handbook of Engineering Mechanics edited by W. Flügge, McGraw-Hill, New York, 1962.